SYNTHESIS AND CHARACTERIZATION OF METAL COMPLEXES SUPPORTED BY BIS(ARYLIMINO)ACENAPHTHENE

Author

WANG JINGYI

Matriculation number

G1303290B

Supervisor: Dr. Felipe García

Co-supervisor: Dr. Soo Han Sen

DIVISION OF CHEMISTRY AND BIOLOGICAL CHEMISTRY
SCHOOL OF PHYSICAL & MATHEMATICAL SCIENCES

A thesis submitted to the Nanyang Technological University in fulfillment of the requirement for the degree of Doctor of Philosophy

January 2018

Acknowledgements

I would like to express my great appreciation to people who have supported and guided me throughout the four years of my PhD study.

In particular, I would like to thank Dr. Felipe García for first of all letting me to join his group and more importantly, for his guidance and supports not only on my project but also on other aspects of life. Also, thanks for being patient to all of us. I would also like to thank Dr. Soo Han Sen who have given me a lot of useful advices throughout my graduate study, and for letting me to share equipment and resources with his group.

Assistance on single crystal X-ray diffraction studies provided by Dr Rakesh Ganguly and Dr Li Yongxin was greatly appreciated. I would like to extend my acknowledgement to Miss Goh Ee Ling for her help on NMR studies, and Dr. Zhu Wenwei and Miss Pui Peng Yi for training me on mass spectroscopy and elemental analysis respectively.

Here, I would like to offer my special thanks to Dr. Jesús Díaz Álvarez who carried out computational studies for us in chapters 2 and 3, and Prof. Eli Zysman Colman who offered us a collaboration opportunity and provided us the iridium complexes in chapter 4. Also, thanks to Dr. Tan Teck Boon for proof reading this thesis.

Financial assistance was given Singapore International Graduate Award (SINGA) and it was greatly appreciated. Last but not least, I wish to thank my parents, my friends, and my labmates for their supports, understanding and encouragement throughout my graduate study.

Table of contents

Abstract

Abbreviations

Chapter 1: Introduction **1**

1.1 "*Non-innocent*" behavior in coordination complexes 2

1.2 Introduction to Bis(arylimino)acenaphthene (Ar-BIAN) ligand 3

1.2.1 General properties 3

1.2.1 Synthesis of Ar-BIAN ligands 5

1.3 Introduction to *p*-block elements 6

1.4 Transition metal complexes with Ar-BIAN ligands 7

1.5 Main group metal complexes with Ar-BIAN ligands 9

1.5.1 Group 13 complexes with Ar-BIAN ligands 9

1.5.2 Group 14 complexes with Ar-BIAN ligands 16

1.5.3 Group 15 complexes with Ar-BIAN ligands 19

1.6 Mechanochemical Synthesis 23

1.6.1 Introduction to mechanochemistry 23

1.6.2 Mechanochemical approaches to organometallics and coordination compounds 25

1.6.3 Mechanochemistry in catalysis 29

1.6.4 Mechanochemical approaches to main group inorganic and organometallic systems 32

1.7 Conclusion 34

Chapter 2: Mechanochemical route to indium(III) complexes **35**

2.1 Introduction 36

2.2 Results and discussion 38

*2.2.1 Synthesis of Ar-BIAN ligands and their indium(III) complexes (**2.1**-**2.4**)* 38

2.2.2 Spectroscopic and Crystallographic Studies 41

2.2.3 UV-vis and Electrochemical Studies 44

2.2.4 Computational Studies 47

2.3 Conclusions 49

2.4 Experimental and analytical techniques 50

2.4.1 General consideration 50

2.4.2 Mechanochemical synthesis of Ar-BIAN ligands 51

2.4.3 Mechanochemical synthesis of indium(III) complexes 53

2.4.4 "One-pot two step" mechanochemical synthesis of indium complexes 56

*2.4.5 X-ray data of indium(III) complexes **2.3** and **2.4*** 58

Chapter 3: Synthesis and the optical and electrochemical properties of indium(III) Ar-BIAN complexes 59

3.1 Introduction 60

3.2 Results and discussion 61

3.2.1 Synthesis of Ar-BIAN ligands and indium(III) complexes 61

3.2.2 Spectroscopic and Crystallographic Studies 65

3.2.3 UV-vis and Electrochemical Studies 67

3.2.4 Computational Studies 73

3.3 Conclusions 78

3.4 Experimental and analytical techniques 79

*3.4.1 Synthesis of Ar-BIAN ligands (**3.1a** – **3.4a**)* 79

*3.4.2 Synthesis of indium(III) complexes (**3.1b** – **3.5b**)* 83

3.4.3 Reduction of $[(p\text{-}MeOAr\text{-}BIAN)_2InCl_2]^+[InCl_4]^-$ 90

*3.4.4 X-ray data of indium(III) complexes **3.1b** – **3.5b*** 92

Chapter 4: Synthesis of modified Ar-BIAN ligand and the transient absorption studies of its Ir(III) complexes **94**

4.1 Introduction 95

4.1.1 Design of the functionalized Ar-BIAN ligand 96

4.1.2 General introduction to transient absorption spectroscopy 98

4.2 Results and discussion 100

*4.2.1 Synthesis of modified Ar-BIAN ligand ($CO_2Me\text{-}NMe_2Ar\text{-}BIAN$) (**4.1**)* 100

*4.2.2 Transient absorption spectroscopic study on iridium(III) complexes **4.3** and **4.4*** 102

4.3 Conclusions 108

4.4 Experimental and analytical techniques 108

4.4.1 General considerations 108

*4.4.2 Synthesis of compound **4.1*** 110

Chapter 5: Summary and outlook **117**

References **121**

Publication list **127**

Abstract

Although bis(arylimino)acenaphthene (Ar-BIAN) ligands have been recognized as robust ligands for metal complexes since the early 2000, most of its coordination chemistry was focused on transition metals with relatively little attention being paid to main group elements. In particular, the physicochemical properties of Ar-BIAN complexes, which is of interest to our group, still remain un-explored. On the other hand, in view of the growing interest in greener synthetic methods, solid state syntheses have become especially appealing to synthetic chemists. However, reports on mechanochemistry in molecular compounds, especially main group complexes, have been scarce, despite its appeal as a low-solvent, low-energy, and potentially atom-efficient synthetic method.

In this thesis, firstly, a mechanochemical grinding approach to the synthesis of Ar-BIAN ligands and its coordination complexes with heavy *p*-block element, indium, will be introduced (chapter 2). The atom-efficient, less time consuming, and low solvent aspects associated with this method will be highlighted. This is then followed by a more comprehensive description on the syntheses of a range of indium(III) Ar-BIAN complexes bearing different substituents at the aryl-diimine moiety (chapter 3). This chapter also concerns a systematic investigation on the optical and electrochemical properties of the as synthesized indium(III) Ar-BIAN complexes with the intention to explore their potential application as photosensitizers, and the effect of functionalization of the aryl-diimine moiety on such properties.

In chapter 4, a modified Ar-BIAN ligand design which includes an electron withdrawing group on the acenaphthene backbone will be presented. Besides, an improvement on the photoexcited lifetime of an iridium(III) complex bearing the modified Ar-BIAN ligand will be demonstrated using both steady state and time resolved spectroscopic measurements.

Abbreviations

Ar	aromatic
Ar-BIAN	bis(arylimino)acenaphthene
A	hyper-fine coupling constant
ACN	acetonitrile
BQA	bis(8-quinolinyl)amino
B3LYP	Becke, 3-parameter, Lee-Yang-Parr
^{t}Bu	tertiary butyl
bph	biphenyl
bpy	bipyridine
Cp’	*n*-propyltetramethylcyclopentadienyl
Cp*	pentamethylcyclopentadienyl
CV	cyclic voltammetry
CT	charge transfer
C^N	cyclometalated
CPCM	conductor-like polarizable continuum model
d	doublet
DAB	1,4-diaza-1,3-butadiene
Dipp	2,6-diisopropylphenyl
DSC	differential scanning calorimetry
DSSC	dye-sensitized solar cell
DCM	dichloromethane
DMF	*N*,*N*-dimethylformamide
DME	1,2-dimethoxyethane
dtb	di-*tert*-butyl
EPR	electron paramagnetic resonance
Et	ethyl
E_p	peak potential
Et_2O	diethyl ether
Fc	ferrocene

FMOs	frontier molecular orbitals
HR-MS	high resolution mass spectroscopy
ΔH	enthalpy change
ISC	intersystem crossing
ILCT	intra-ligand charge transfer
i_p	peak current
K_{eq}	equilibrium constant
LAG	liquid assisted grinding
LLCT	ligand to ligand charge transfer
LANL2DZ	Los Alamos National Laboratory 2-double-z
Me	methyl
Mes	2,4,6-trimethylphenyl
MAS NMR	magic angle spinning nuclear magnetic resonance spectroscopy
Mes	2,4,6-trimethylphenyl
$[M+1]^+$	parent ion bound to H^+
MLCT	metal to ligand charge transfer
m	multiplet
NHC	*N*-heterocyclic carbenes
NMR	nuclear Magnetic Resonance
NBS	N-Bromosuccinimide
OTf	trifluoromethanesulfonate
OD	optical density
OLEDs	organic light emitting diodes
o-CF_3	*ortho*-trifluoromethyl
Py	pyridine
PEG	polyethylene glycol
Phen	1,10-phenanthroline
PLLA	poly(L-lactide)
PL	photoluminescenece
Ph	phenyl
ppm	parts per million

p-MeO	*para*-methoxyphenyl
p-NMe_2	*para*-dimethylaminophenyl
p-Br	*para*-bromo
p-Cl	*para*-chloro
SCXRD	single crystal X-ray diffraction
ΔS	entropy change
s	singlet
TMS	trimethylsilyl
TEAB	tetraethylammonium bromide
TGA	thermogravimetric analysis
THF	tetrahydrofuran
TFAA	trifluoroacetic anhydride
TD-DFT	time-dependent density functional theory
TIP	tetrakis(imino)pyracene
τ	photoexcited state lifetime
VT-NMR	variable temperature NMR
λ	wavelength
δ	chemical shift

Chapter 1 Introduction

1.1 "*Non-innocent*" behavior in coordination complexes

Redox reactions play an important role in modern chemical transformations. The subject of redox active ligands together with their metal complexes and potential applications are of growing importance in coordination and organometallic chemistry since the 1960s.[1] The term "*innocent ligand*" was first introduced by Jørgensen in 1966, which refers to a ligand that allows the oxidation states of the central atoms to be unambiguously determined.[2] For instance, the Werner-type compound[3] such as *cis*-$[Co(NH_3)_4Cl_2]^+$ has a well-defined Co(III) metal center because the ligands are redox inactive (*innocent ligand*).[4] In contrast, "*non-innocent ligand*" implies an ambiguous assignment of oxidation states in metal complexes.[5] In 1962, Schrauzer and Mayweg reported the first example of a transition metal complex bearing a *non-innocent* ligand by reacting nickel disulfide with diphenylacetylene.[6] (Scheme 1.1) The resulting square planar nickel dithiolene complex has a magnetic property consistent with a Ni(II) metal center which, as proposed by the authors, would only be possible if the dithiobenzil ligands were reduced by one electron each.[6] Shortly thereafter, Gary and Maki reported the synthesis and characterization of many other transition metal complexes of the general Type I. (Figure 1.1a)[7] As illustrated in Figure 1.1b, these complexes can be considered as a M^{IV} complex with two dithiolates; as a M^{II} complex with two thiosemiquinones; or as a M^0 complex with two neutral dithioketones.[1b, 8] Consequently, the oxidation state cannot be determined precisely for either the central metal or the donor ligand. Therefore, "*non-innocence*" is more appropriately descried as a behavior for combinations of metal and ligands, rather than redox active ligands alone as stated in Jørgensen's original definition.[1b]

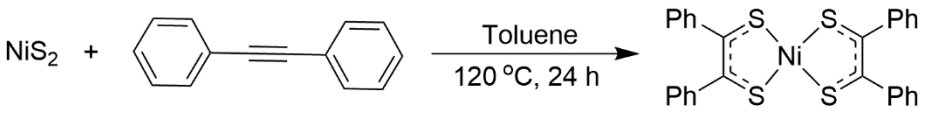

Scheme 1.1 *Synthesis of nickel dithiolate complex.*

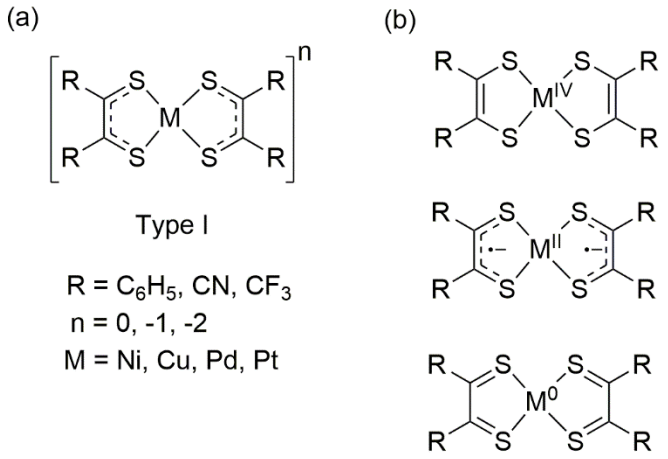

Figure 1.1 *(a) General structure of metal dithiolene complexes and (b) three possible structural representations corresponding to different oxidation states of the metal.*

1.2 Introduction to Bis(arylimino)acenaphthene (Ar-BIAN) ligand

1.2.1 General properties

Bis(arylimino)acenaphthene (Ar-BIAN) can be considered as a fusion product between a 1,4-diaza-1,3-butadiene (DAB) moiety and a naphthalene unit.[9] (Figure 1.2) The two imine functionalities are orthogonal to the naphthalene unit and therefore not in conjugation with the π-accepting framework.[10] In contrast to the uncoordinated R-DAB ligands in which the imine nitrogen atoms preferentially adopt the *s-trans* conformation, the rigid naphthalene backbone in Ar-BIAN ligands prevents rotation around the diimine C-C bond, locking it in a *s-cis* conformation which enables its chelation to metal centers.[9] (Figure 1.2) A comparison of the binding constants among a series of Ar-BIAN complexes with palladium(0) and (II) revealed that the chelating strength of the bidentate Ar-BIAN ligands falls between the acyclic Ph-DAB ligands (Ph-DAB = diphenyldiazabutadiene) and the more commonly known π-accepting ligands like phenanthroline and bipyridine.[11] The stabilities of metal complexes formed with Ar-BIAN ligands can be controlled by judicious choice of the substituents on the diimine moiety. In general, ligands with

more electron rich substituents on the imine bind more strongly to metal centers, and is more prominent with higher oxidation state metals.[11]

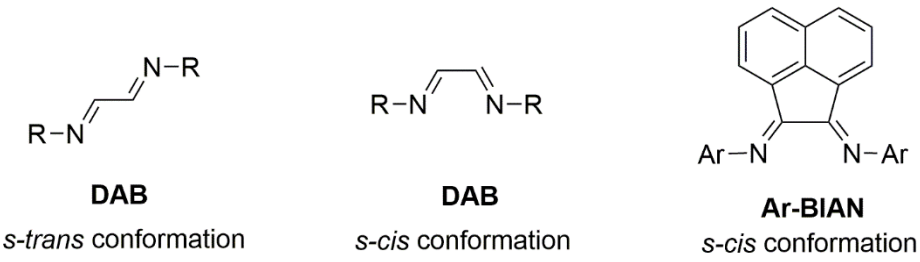

Figure 1.2 *Structural conformation of 1,4-diaza-1,3-butadiene (DAB) and Bis(arylimino)acenaphthene (Ar-BIAN)*

Another important feature of Ar-BIAN ligands is their ability to accept electrons. The good electron accepting property of Ar-BIAN ligand can be recognized from (i) the ability of α-diimines to stabilize a range of photochemically[12] and electrochemically[13] generated open shell complexes through delocalization of electron density into the antibonding orbitals, and (ii) the readily reducible naphthalene unit by alkali metals.[14] As illustrated in Figure 1.3, the reduction of Ar-BIAN ligand by the first electron produces a radical anion delocalized over the NCCN fragment. Second electron reduction results in formation of a dianion with a C=C double bond and two C-N single bonds. The third and fourth electron reduction of Ar-BIAN ligands places electron density into the naphthalene backbone. Fedushkin and co-workers carried out a synthetic study on the reduction of Dipp-BIAN (Dipp = 2,6-diisopropylphenyl) with sodium metal, and they have demonstrated that Ar-BIAN ligands can accept up to four electrons to form stable mono-, di-, tri, and tetra-anions.[15]

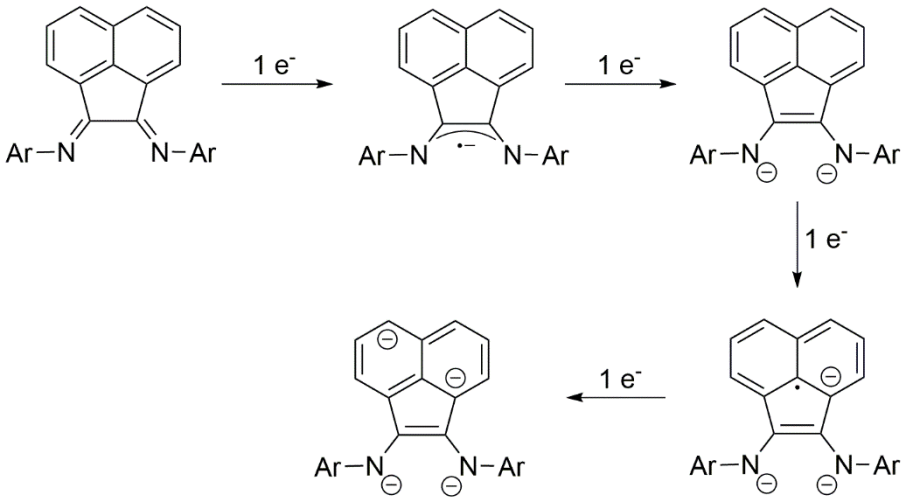

Figure 1.3 *Schematic representation of structural changes on Ar-BIAN upon reduction.*

1.2.2 Synthesis of Ar-BIAN ligands

In general, Ar-BIAN ligands are synthesized *via* condensation reactions between acenaphthoquinone and the corresponding aniline under acidic conditions. For example, Dipp-BIAN was synthesized by refluxing acenaphthoquinone with 2,6-diisopropylaniline in acetic acid for 1 h[10] while *o*-CF_3Ar-BIAN (*o*-CF_3 = *o*-trifluoromethyl) was formed by refluxing acenaphthoquinone with *o*-trifluoromethylaniline in a mixture of toluene and sulfuric acid for 3 days using a Dean-Stark trap.[16] In many other cases, complexation with either zinc chloride ($ZnCl_2$) or nickel bromide ($NiBr_2$) is necessary before removal of the metal ion to furnish the desired ligand.[10] (Scheme 1.2) For instance, *p*-MeOAr (*p*-methoxyphenyl), *p*-NMe_2Ar (*p*-dimethylaminophenyl), *p*-MeAr-BIAN (*p*-methylphenyl), *p*-BrAr (*p*-bromophenyl), and *p*-ClAr (*p*-chlorophenyl) were synthesized by refluxing acenaphthoquinone with two equivalents of the corresponding aniline in acetic acid in the presence of excess $ZnCl_2$ or $NiBr_2$, followed by de-metallation using potassium carbonate (K_2CO_3) or sodium oxalate ($Na_2C_2O_4$).[17] As indicated by Ragaini, the use of metal halide not only serves as a template around which Ar-BIAN is formed,

but also provides a driving force for the reaction by precipitation of the resulting metal Ar-BIAN complex due to its lower solubility in the reaction media as compared to the starting materials.[18]

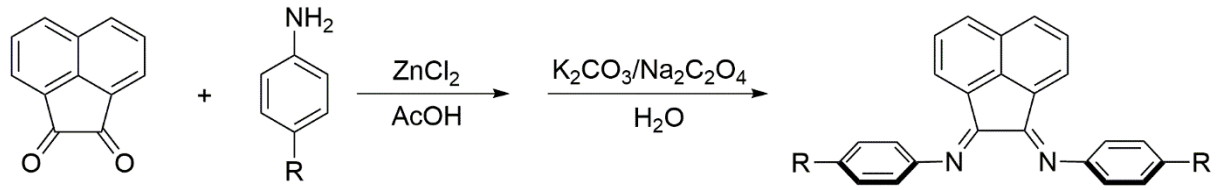

Scheme 1.2 *General synthetic route to Ar-BIAN.*

1.3 Introduction to *p*-block elements

Main group elements are characterized by the completion of their electron configurations using *s* and *p* electrons.[19] While the bonding in organometallic compounds with *s*-block elements is usually ionic in character, bonding in compounds with *p*-block elements is more covalent. This can be rationalized by the decrease in atomic size and increase in ionization energy as a result of the increase in effective nuclear charge across a period.[20]

On descending a typical *p*-block group (*e.g.* Group 13), there is an increase in metallic character from boron (B) to thallium (Tl), which can be recognized by the higher ionization energy of B as compared to Tl.[21] (Table 1.1) However, there are exceptions in this trend whereby gallium (Ga) and Tl exhibit slightly higher ionization energy than aluminum (Al) and indium (In) respectively. This phenomenon is attributed to *d*-block and lanthanide contraction. The *p*-block elements in period four are preceded by the first row transition metals, in which the *d* orbitals are being occupied. These orbitals have poor shielding properties and therefore the valence electrons in Ga experience a higher effective nuclear charge than expected, which in turn results in slightly higher ionization energy than Al. Similarly, the *p*-block elements in period six experience more attraction from the nucleus due to the poor shielding effect of the *f*-orbitals from the preceded lanthanides.[22]

Table 1.1 *1st ionization energy and standard reduction potential of group 13 elements*

Element	B	Al	Ga	In	Tl
1st ionisation energy / $kJmol^{-1}$	800.6	577.5	578.8	558.3	589.4
Standard reduction potential / V $M^{III}_{(aq)} + 2e^- \longrightarrow M^{I}_{(aq)}$	-	-2.7	-0.72	-0.44	+1.28

Apart from the trends in atomic parameters and variation in bonding across the period, another important difference between *s* and *p* block elements is the oxidation state. For *s*-block, only +1 (group 1) and +2 (group 2) oxidation states are known throughout the group. However, two (non zero) oxidation states are commonly known to *p*-block metals, the valence *n* oxidation state and the *n-2* oxidation state. The valence *n* oxidation state corresponds to the use of all outer shell *s* and *p* valence electrons and it is the oxidation state preferentially adopted by elements from the top of the group. However, heavier *p*-block elements also form compounds with the *n-2* oxidation state, which corresponds to the use of only *p* valence electrons for bonding. The *n-2* oxidation state becomes increasingly stable descending the group, as demonstrated by the standard reduction potential under aqueous conditions for group 13 elements .[21-22] (Table 1.1) The tendency of using only *p* electrons for bonding and retention of electrons in the *s* orbital is known as the "*inert pair*" effect, which stems from the thermodynamic balance between hybridization energy and bond energy.[20, 23]

1.4 Transition metal complexes with Ar-BIAN ligands

The study of bis(arylimino)acenaphthene ligands (Ar-BIAN) to form coordination complexes with palladium was initially carried out by Elsevier and co-workers in early 1990s.[10] Subsequently, dozens of transition metal complexes (*e.g.* palladium and zinc[24], copper and iron[25], cobalt and nickel[26]) based on this type of ligand have been described. Most of these complexes were

synthesized *via* simple reaction of Ar-BIAN ligand and the corresponding metal precursors either at room temperature or under refluxing conditions. Apart from the Pd(II) complex formed with Dipp-BIAN, all other aforementioned transition metal complexes with Ar-BIAN ligands adopt a distorted tetrahedral or square pyramidal (in the case of penta-coordination) geometry around the metal center. In the case of Dipp-BIAN complex with Pd(II), a square planar coordination was observed around the Pd metal center due to the energetically favored low spin arrangement for d^8 complexes.[24]

In addition to structural studies, the potential application of transition metal Ar-BIAN complexes as catalysts for organic transformation reactions has also been extensively studied. Elsevier and co-workers pioneered the investigation of the catalytic activity of Pd Ar-BIAN complexes. They found that these complexes exhibited remarkable catalytic activity towards C-C cross coupling reactions between organomagnesium, tin, and zinc reagents with organic halides.[27] It was reported that their reactions took place within several hours in tetrahydrofuran (THF) at ambient temperatures using only 1% catalyst loading, with isolated yields of 85-99%. Furthermore, it has been shown that zero valent Pd complexes with Ar-BIAN ligands are able to catalyze hydrogenation reactions of alkenes and alkynes.[28] Other examples of reactions catalyzed by transition metal Ar-BIAN complexes include olefin polymerizations catalyzed by Ni(II)-BIAN complexes,[29] allylic aminations of olefins,[30] and reduction of nitroarenes catalyzed by $Ru_3(CO)_{12}$/Ar-BIAN system,[31] and Suzuki-Miyaura cross coupling reactions catalyzed by Pd(II)/Ar-BIAN system.[32] The role of Ar-BIAN ligands in these reactions was determining. In the absence of Ar-BIAN ligand, low conversion and selectivity was found in the catalytic reduction of nitroarenes.[31c]

1.5 Main group metal complexes with Ar-BIAN ligands

The chemistry of Ar-BIAN ligands with transition metals is well-established, and many of the transition metal complexes with Ar-BIAN ligands have been studied as catalysts for important organic transformations. Comparatively, few reported studies were devoted to the chemistry of Ar-BIAN ligands with main group elements, and especially *p*-block elements. In fact, systematic investigation on the synthesis and structural properties of *p*-block Ar-BIAN complexes have only emerged in the early 2000s.

1.5.1 Group 13 complexes with Ar-BIAN ligands

The first group 13 complex of Ar-BIAN ligand was synthesized by Clyburne *et al.* in 2002.[33] They have reported the reaction of Dipp-BIAN with group 13 trihalides (BCl_3, $AlCl_3$, and $GaCl_3$) in a 1:2 ratio in dichloromethane (DCM). Three compounds with the general formula [(Dipp-BIAN)(ECl_2)][ECl_4] (Scheme 1.3) were isolated, [(Dipp-BIAN)(BCl_2)][BCl_4] (**1.1**), [(Dipp-BIAN)($AlCl_2$)][$AlCl_4$] (**1.2**), and [(Dipp-BIAN)($GaCl_2$)][$GaCl_4$] (**1.3**). Crystallographic studies on **1.1** and **1.3** revealed a cationic [(Dipp-BIAN)ECl_2]$^+$ (E = B or Ga) fragment which consists of a neutral Dipp-BIAN ligand coordinated to the metal center *via* a N-B or N-Ga dative bond. The counter anion [ECl_4]$^-$ is a tetrahedron with the E-Cl bond angles ranging from 100(1)° to 118(1)° in the case of B and from 106.54(9)° to 111.26(6)° in the case of Ga.[33] In contrast to Ar-BIAN ligands, the reaction of BCl_3 with the conventional 1,4-diaza-1,3-butadiene (DAB) ligand in hexane resulted in formation of two products. The first product was the expected diazaborolium complex [(Dipp-DAB)BCl_2]Cl (**1.4**) with two imine N atoms coordinating to the B center *via* dative bonds; while the other, as confirmed by single crystal X-ray diffraction, was a neutral diazaborolidine (**1.5**) with only a single chloride being bound to the B center.[34] (Scheme 1.4) Compound **1.5** was formed *via* a double chloroboration of Dipp-DAB, with the two Cl atoms being

added in an *anti* configuration to the C atoms on the DAB moiety. The authors proposed that the steric hinderance provided by the two diisopropylphenyl groups, makes the B atom not sustainable with tetra-coordination, and therefore facilitated the ejection of the Cl atoms.

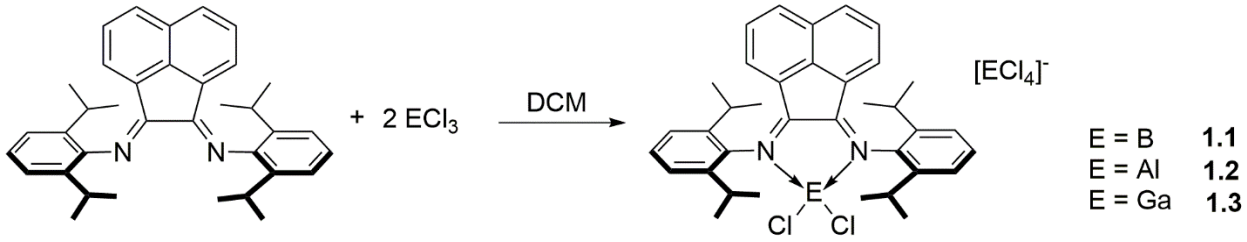

Scheme 1.3 *Formation of [(Dipp-BIAN)(ECl₂)][ECl₄] in DCM.*

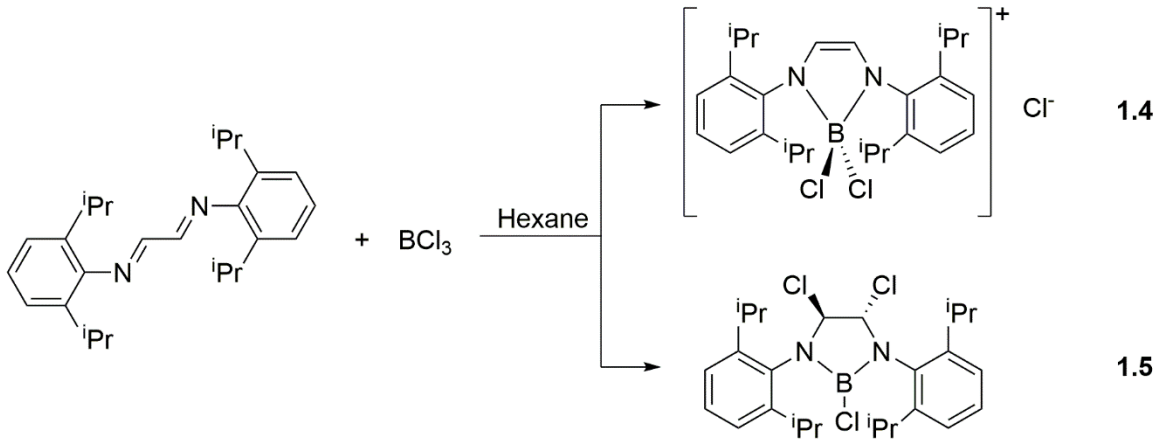

Scheme 1.4 *Formation of diazaborolidine (**1.5**) via double chloroboration of Dipp-DAB.*

A series of monomeric alkylaluminium complexes featuring Dipp-BIAN ligand was reported by Schumman and co-workers in 2005.[35] The compounds with a general formula [(Dipp-BIAN)AlR$_2$] where R = Me (methyl) (**1.6**) , Et (ethyl) (**1.7**) and ^{t}Bu (tert-butyl) (**1.8**) groups were prepared by metathesis of [(Dipp-BIAN)Na] with the respective alkylaluminium halide (R_2AlX) in diethyl ether (Et_2O) at room temperature. (Scheme 1.5) All three complexes possessed a tetrahedral coordination around the Al atom by their respective R groups and the two imine N atoms from the Dipp-BIAN ligand. In these complexes, the Dipp-BIAN ligand was reduced by one electron to form a radical anion. This was evidenced by Infra-red spectroscopy, whereby a bathochromic shift

of about 100 cm^{-1} for the *ν*(C=N) stretching frequency in **1.6**, **1.7**, and **1.8** was observed as compared to that of the free ligand. The radical anionic nature of the Dipp-BIAN ligand was further corroborated by electron paramagnetic resonance (EPR) spectroscopy.[35]

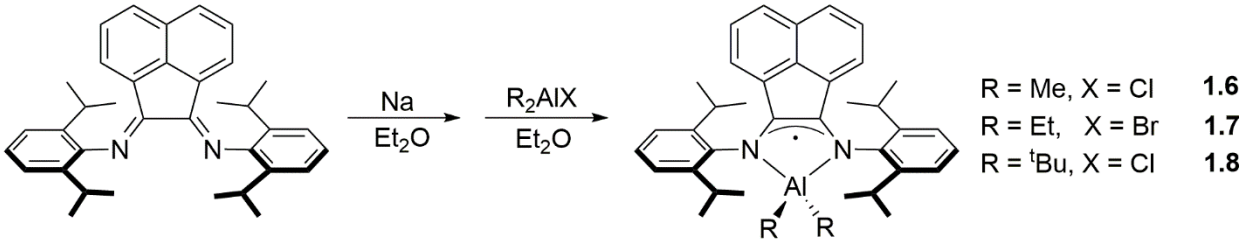

Scheme 1.5 *Formation of [(Dipp-BIAN)AlR₂] in Et₂O.*

Similarly, aluminum complexes with anionic Ar-BIAN ligands were also reported by simple reduction of Dipp-BIAN with excess aluminum metal in the presence of aluminum halide in toluene or Et_2O.[36] However, the nature of the product formed is solvent dependent. In toluene, the product obtained was a neutral complex [(Dipp-BIAN)$AlCl_2$] (**1.9**) supported by a radical anionic ligand, while in Et_2O, complex [(Dipp-BIAN)AlCl(Et_2O)] (**1.10**) bearing a dianionic ligand was formed. (Scheme 1.6) The formation of **1.10** is probably due to the oxophilic nature of Al which accepts electron density from Et_2O and therefore making the Al center prone to reduce the Ar-BIAN ligand. The difference between **1.9** and **1.10** can be easily recognized by a comparison of the C-N and C-C bond distances. The C-C bond length in **1.10** (ca. 1.390 Å) is shorter than that in **1.9** (ca. 1.431 Å) and has some C=C double bond character. Furthermore, the C-N bonds in **1.10** (1.394 Å and 1.418 Å) are significantly longer than those in **1.9** (1.346 Å and 1.341 Å), which suggests the formation of C-N single bonds. Other examples of Al complexes bearing a dianionic Ar-BIAN ligand are the monoalkyl aluminium complexes with general formula [(Dipp-BIAN)AlR(Et_2O)] (R = Me (**1.11**), Et (**1.12**)), which can be regarded as alkyl analogues of **1.10**.[37]

These were synthesized by reacting [(Dipp-BIAN)Na_2] with two equivalents of dialkylaluminium chloride R_2AlCl (R = Me, Et) in Et_2O at room temperature.

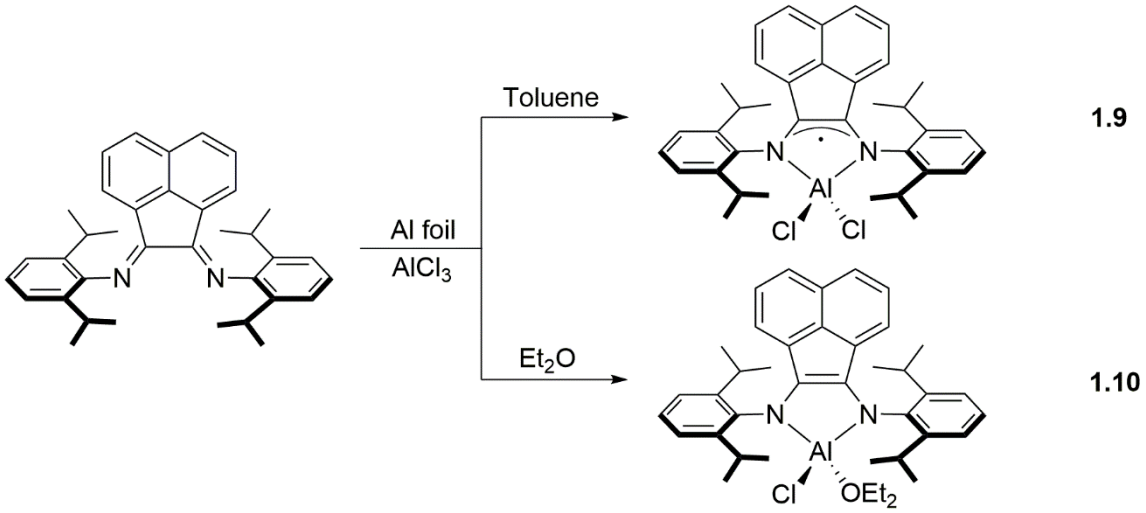

Scheme 1.6 *Formation of [(Dipp-BIAN)$AlCl_2$] (**1.9**) and [(Dipp-BIAN)AlCl(Et_2O)] (**1.10**).*

The reactivity of gallium(I) and indium(I) halide towards Ar-BIAN ligands was examined by Jones's group in 2003.[38] In the reaction of Dipp-BIAN with GaI in toluene, disproportionation occurred leading to formation of a paramagnetic Ga(III) species [(Dipp-BIAN)GaI_2] (**1.13**), which possesses similar N-Ga, C-N and C-C bond distances to the related DAB derivative [(Dipp-DAB)GaI_2].[39] In 2007, Fedushkin and co-workers reported the formation of a Dipp-BIAN chelated homobimetallic Ga-Ga and a heterometallic Ga-Zn compounds. Both complexes were characterized using single crystal X-ray diffraction (SCXRD) techniques.[40] The complex [(Dipp-BIAN)Ga-Ga(Dipp-BIAN)] (**1.14**) was synthesized by the reaction of [(Dipp-BIAN)K_3] with $GaCl_3$ in Et_2O/THF at room temperature. (Scheme 1.7) This compound is EPR silent which suggests the dianionic nature of both Dipp-BIAN ligands and thus the Ga atom in **1.14** has a +2 oxidation state. The related heterometallic compound [(Dipp-BIAN)Zn-Ga(Dipp-BIAN)] (**1.16**) was obtained by a one-pot reaction between [(Dipp-BIAN)Zn(μ-I)$_2$Zn(Dipp-BIAN)] (**1.15**), $GaCl_3$,

and [(Dipp-BIAN)K_4] in THF, among which **1.15** was synthesized from the reaction of Dipp-BIAN ligand with Zn metal in the presence of I_2.[41] (Scheme 1.8)

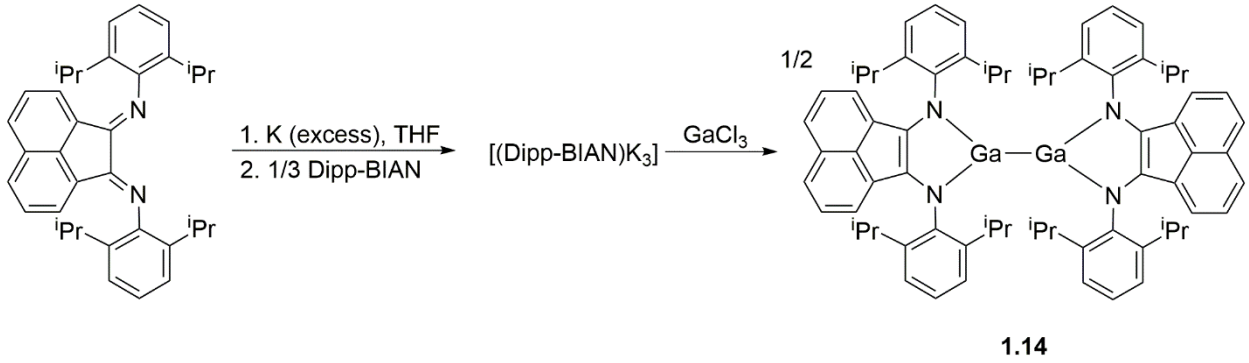

Scheme 1.7 *Formation of homobimetallic [(Dipp-BIAN)Ga-Ga(Dipp-BIAN)] (**1.14**).*

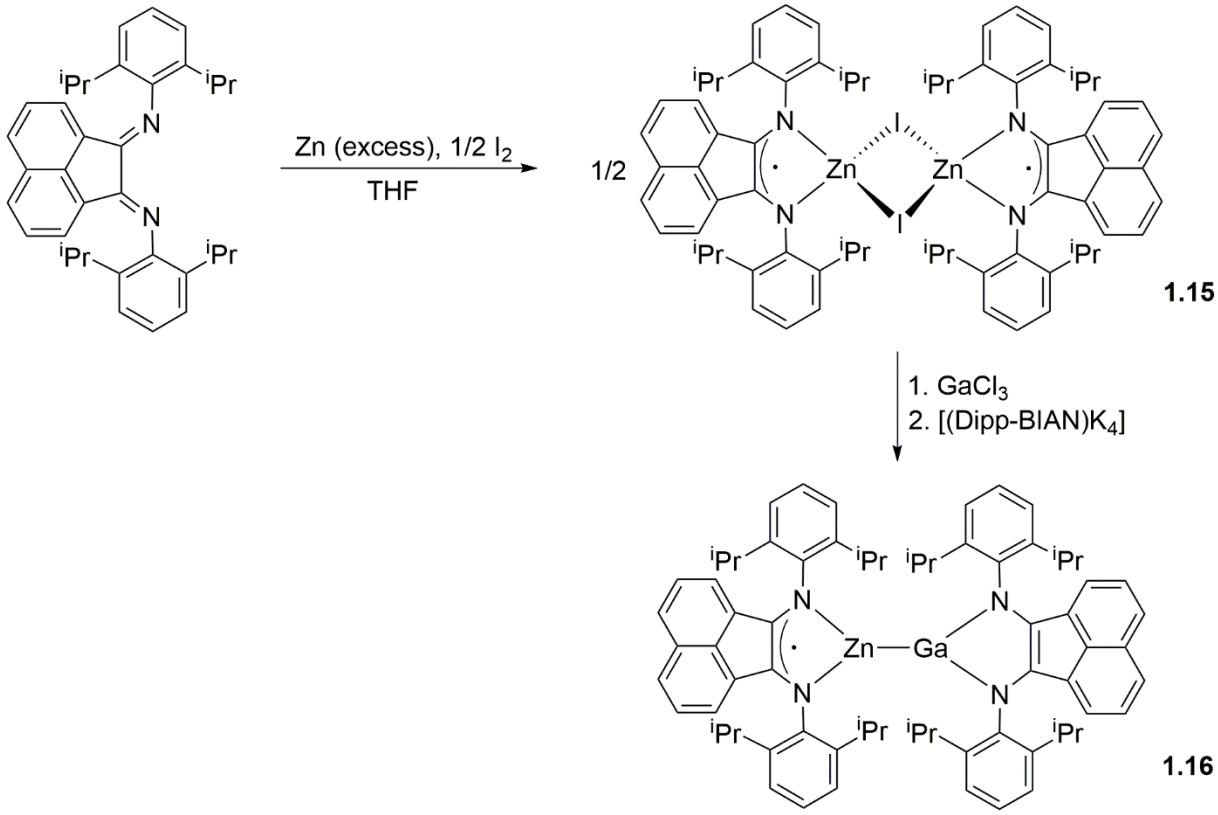

Scheme 1.8 *Formation of heterometallic [(Dipp-BIAN)Zn-Ga(Dipp-BIAN)] (**1.16**).*

An examination of the C-C and C-N bond distances within the N-C-C-N framework of **1.16** revealed a shortening of the C-N bonds and a lengthening of the C-C bonds when compared to

those of the homobimetallic derivative **1.14**. (Table 1.2) In fact, the respective bond distances in **1.16** fall in between those observed from the Zn-Zn homometallic species [(Dipp-BIAN)Zn-Zn(Dipp-BIAN)] (**1.17**) supported by two radical anionic Dipp-BIAN ligands[42] and **1.14** which was held by two dianionic Dipp-BIAN ligands. This suggests that the Dipp-BIAN ligands in **1.16** are neither radical anions nor dianions alone. The most plausible explanation to this given by the authors is a possible disorder between the Zn and Ga atom which makes them indistinguishable based on crystallographic data.[40] This was further supported by the EPR spectrum of **1.16** which showed hyperfine coupling of the Zn atom to only two but not four N atoms.

Table 1.2 *Comparison of the average C-N and C-C bond distances between* ***1.14***, ***1.16***, *and* ***1.17***.

Compound	**1.14**	**1.16**	**1.17**
C-N	1.388 Å	1.354 Å	1.329 Å
C-C	1.377 Å	1.410 Å	1.443 Å

The scope of **1.14** was further developed by Fedushkin's group based on its reactivity towards transition metals, *e.g.* molybdenum (Mo).[43] It was demonstrated that the reaction of **1.14** with $[Mo(CO)_6]$ and $[CpMo(CO)_3]_2$ resulted in formation of paramagnetic [(Dipp-BIAN)Ga-$Mo(CO)_5$] (**1.18**) and diamagnetic [(Dipp-BIAN)Ga–$MoCp(CO)_3$] (**1.19**) respectively. (Scheme 1.9) Crystallographic data for **1.19** revealed the presence of a C=C bond and two C-N bonds around the diimine framework. However, in **1.18**, the C-C bond distance around the diimine framework is slightly longer than that in **1.19**, whereas its average C-N bond distance is slightly shorter. Therefore, the diimine C-C and C-N bonds in **1.18** possess single bond and double bond character respectively, which distinguished it from complex **1.19**. In **1.18**, the Ga carbenoid acts as a neutral σ-donor towards the Mo(0) center while in **1.19**, it acts as an anionic ligand towards the Mo(II) center. It was anticipated by the authors that this adaptive behavior of the Ga carbenoid species would allow the reactivity at the transition metal center to be tuned. Furthermore, it was found that

facile cycloaddition occurred when **1.14** was treated with alkynes, resulting in formation of a C-C and a C-Ga bonds in the addition product.[44] This unique reactivity has promoted the examination of such complexes as catalysts for hydroamination of alkynes[45] with anilines and it was demonstrated that their catalytic activity is comparable to those of transition metal based systems.[46]

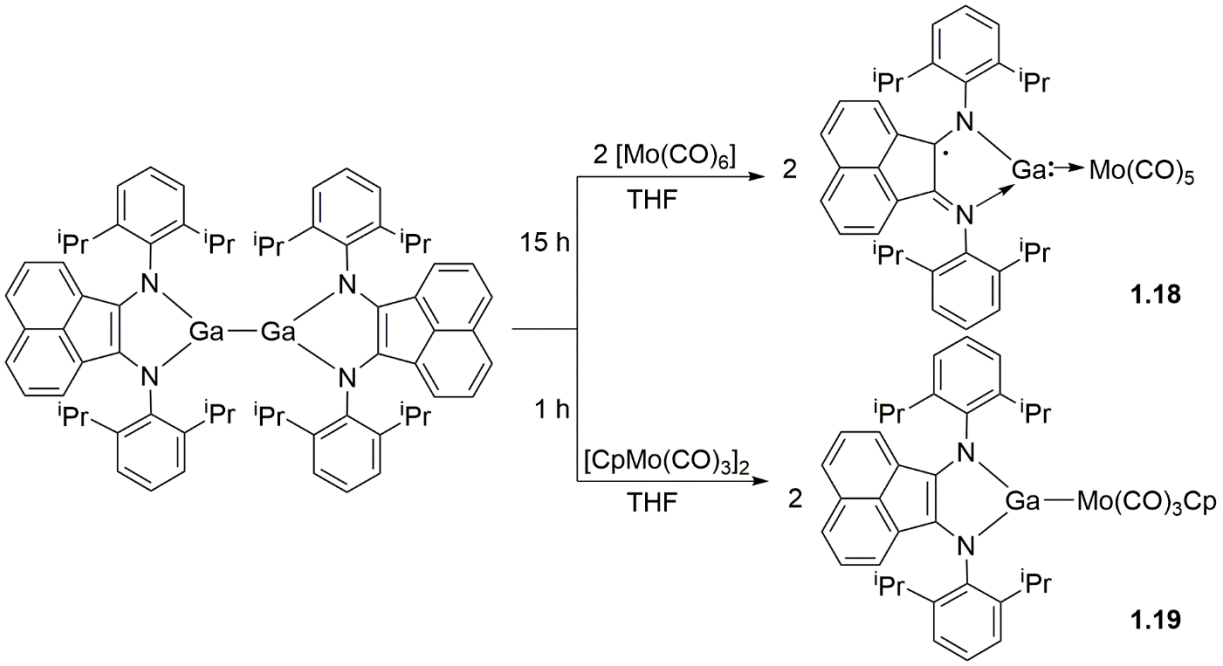

Scheme 1.9 *Synthesis of [(Dipp-BIAN)Ga-Mo(CO)$_5$] and [(Dipp-BIAN)Ga–MoCp(CO)$_3$].*

The complexation of Ar-BIAN ligands to heavier group 13 elements is less extensively reported as compared to the lighter analogs. There has been only one crystallographically reported example of Ar-BIAN ligand coordinated to an indium(III) metal center. Treatment of Mes-BIAN (Mes = 2,4,6-trimethylphenyl) with indium trichloride ($InCl_3$) in THF resulted in formation of the corresponding indium complex [(Mes-BIAN)$InCl_3$(THF)] (**1.20**).[47] (Scheme 1.10) It was crystallized as a mononuclear complex consisting of a neutral Mes-BIAN ligand chelated to an $InCl_3$. This was confirmed by an examination of the C-C (*ca*. 1.526 Å) and C-N (*av*. 1.279 Å) bond distances within the N-C-C-N framework, which were the typical values of C-C and C=N bonds.[47] The reaction of Mes-BIAN ligand with Thallium(I) hexafluorophosphate ($TlPF_6$) produced

[Tl(Mes-BIAN)$_2$][PF$_6$] (**1.21**). It consists of a Tl atom linked to four imine N atoms from two Mes-BIAN ligands, forming a distorted square pyramidal geometry with the Tl atom being placed at the vertex of the square pyramid.[47] The Tl atom is located at 0.772 Å above the plane defined by the N(1)-C(1)-C(12)-N(2) framework. (Figure 1.4) Also, the Tl-N bond distances (2.783 and 2.838 Å) are significantly longer than those measured in a related Tl(I) amido complex[Tl][BQA] (*ca*. 2.689 Å and 2.802 Å) (BQA = bis(8-quinolinyl)amino), suggesting a weaker bond.[48] Nevertheless, **1.21** represents the first example of a structurally authenticated Tl(I) complex of a neutral α-diimine ligand.

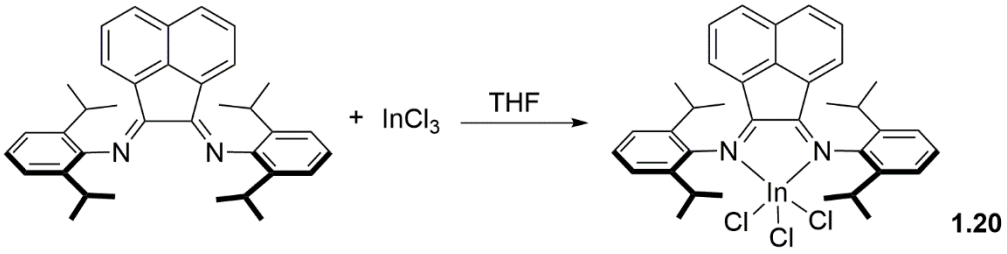

Scheme 1.10 *Synthesis of [(Mes-BIAN)InCl$_3$(THF)] (**1.20**).*

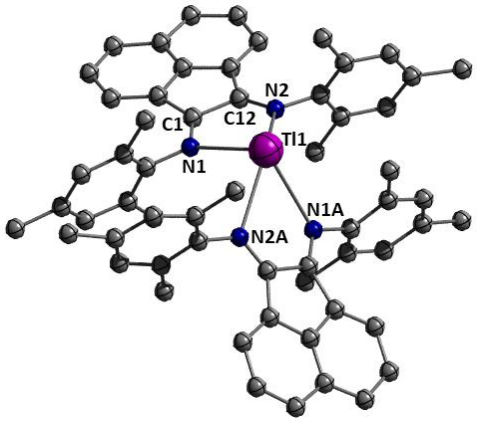

Figure 1.4 *Ball and stick representation of [(Mes-BIAN)$_2$Tl]$^+$ from **1.21**.*[47]

1.5.2 Group 14 complexes with Ar-BIAN ligands

The complexation of group 14 metals with Ar-BIAN ligands were mainly studied by the Fedushkin group. In 2004, they reported the formation of three germylenes, [(Dipp-BIAN)Ge] (**1.22**), [(dtb-

BIAN)Ge] (dtb = di-*tert*-butyl) (**1.23**), and [(bph-BIAN)Ge] (bph = biphenyl) (**1.24**) from metal exchange reactions of the respective magnesium Ar-BIAN complexes with $GeCl_2$.[49] (Scheme 1.11) Compound **1.22** can also be synthesized from the reaction of $GeCl_4$ with [(Dipp-BIAN)Na_4], obtained from Dipp-BIAN and Na (excess). A broadening of signals was observed from the ^1H NMR spectrum of **1.23** recorded in C_6D_6, suggesting the presence of both *syn* and *anti*-isomers in solution. In contrast, **1.24** exists as only one isomer with *anti*-configuration in both solid and solution.

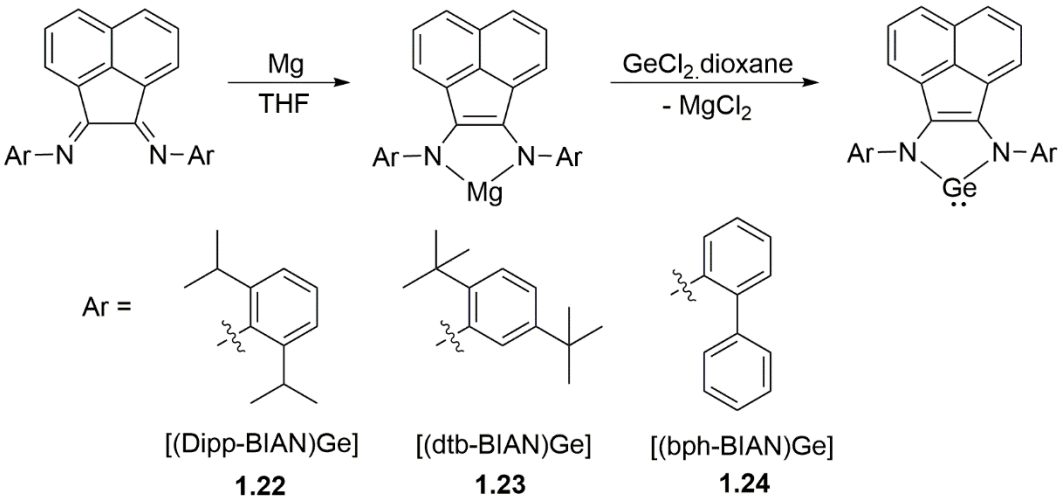

Scheme 1.11 *Formation of three germylenes*.

While all of the aforementioned germylenes **1.22**, **1.23**, and **1.24** possess a dianionic Ar-BIAN ligand with a Ge(II) metal center, a related [(Dipp-BIAN)GeCl] (**1.25**) Ge(II) compound bearing a radical anionic Ar-BIAN ligand can be prepared either by reacting the free Dipp-BIAN ligand with 2 equivalents of $GeCl_2$ or by metathesis of [(Dipp-BIAN)Na] with $GeCl_2$.[50] Compound **1.25** exhibits a slightly distorted trigonal pyramidal geometry with the germanium atom being positioned at its apex. (Figure 1.5a) Similar to the Dipp-BIAN ligand, dtb-BIAN also reacts with $GeCl_2$ to form [(dtb-BIAN)GeCl] (**1.26**) in which the ligand formed a radical anion.[51] The EPR spectrum for both **1.25** and **1.26** revealed coupling between the unpaired electron and the Ge, Cl

and N nuclei. However the ^{73}Ge, ^{35}Cl, and ^{37}Cl hyper-fine coupling constants in **1.25** (A_{Ge} = 0.96, $A_{Cl(35)}$ = 0.78, $A_{Cl(37)}$ = 0.65) and **1.26** (A_{Ge} = 0.63, $A_{Cl(35)}$ = 0.47, $A_{Cl(37)}$ = 0.39) are significantly different despite their structural similarity. This disparity was attributed to the difference in contribution of the germanium *s* and *p* orbitals to the Ge-Cl bond. The larger the contribution of the *s* orbital to the Ge-Cl bond, the larger the Ge and Cl hyper fine coupling constants. This interpretation is also in agreement with the larger N-Ge-Cl angle observed in **1.25** (195.3°) as compared to that in **1.26** (189.1°).[51] (Figure 1.5b)

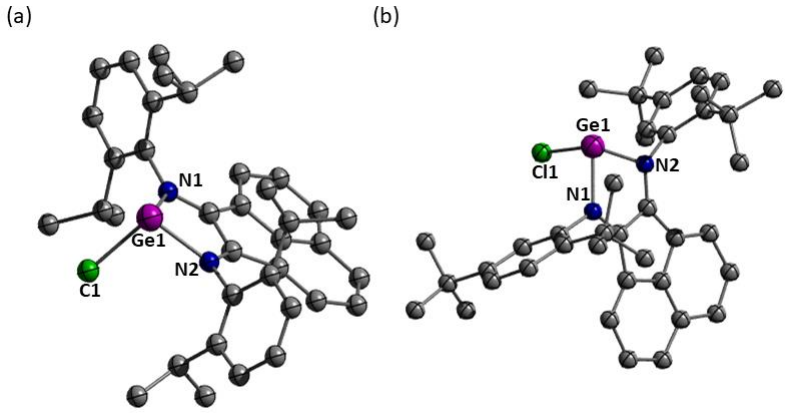

Figure 1.5 *Ball and stick representation of (a) [(Dipp-BIAN)GeCl] (**1.25**)[50] and (b) [(dtb-BIAN)GeCl] (**1.26**),[51] as determined by SCXRD.*

With the aim of synthesizing tin analogs of the germylenes, metathesis reaction of $SnCl_2$ with the disodium salt of Dipp-BIAN ligand [(dipp-BIAN)Na_2] was studied.[51] However, this reaction only led to formation of elemental tin and free Dipp-BIAN ligand. On the other hand, reaction of $SnCl_2$ with the Mes-BIAN ligand resulted in disproportionation of the metal center, forming the Sn(IV) compound [(Mes-BIAN)$SnCl_4$] (**1.27**) and tin metal.[52] (Scheme 1.12) Compound **1.27** consists of a neutral Mes-BIAN ligand forming two dative bonds with the $SnCl_4$ unit, which features the same coordination environment as [(Dipp-BIAN)$SnCl_4$] (**1.28**) formed by treating Dipp-BIAN directly with $SnCl_4$.[47] In contrast to the Mes-BIAN ligand, the reaction of $SnCl_2$ with dtb-BIAN ligand did

not lead to disproportionation of the metal center but gave the corresponding Sn(II) complex [(dtb-BIAN)$SnCl_2$] (**1.29**) instead.[51] (Scheme 1.13) X-ray crystallographic analysis on **1.29** revealed that the $SnCl_2$ is coordinated to only one N atom from the dtb-BIAN ligand. However, its ^1H NMR spectrum in C_6D_6 suggested the presence of a mirror plane bisecting the N-C-C-N framework since the *tert-butyl* groups on each diimine moiety appeared to be magnetically equivalent. This suggests that the $SnCl_2$ fragment exchanges rapidly between the two diimine N atoms in solution on the timescale of the experiment.

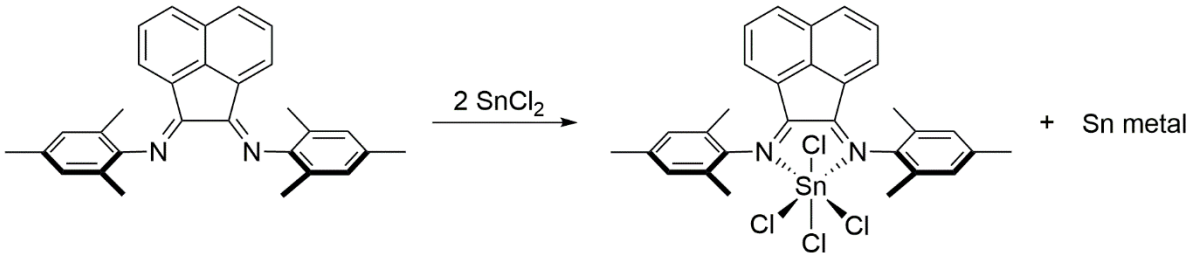

1.27

Scheme 1.12 *Formation of [(Mes-BIAN)$SnCl_4$] (**1.27**) from the reaction of Mes-BIAN with $SnCl_2$.*

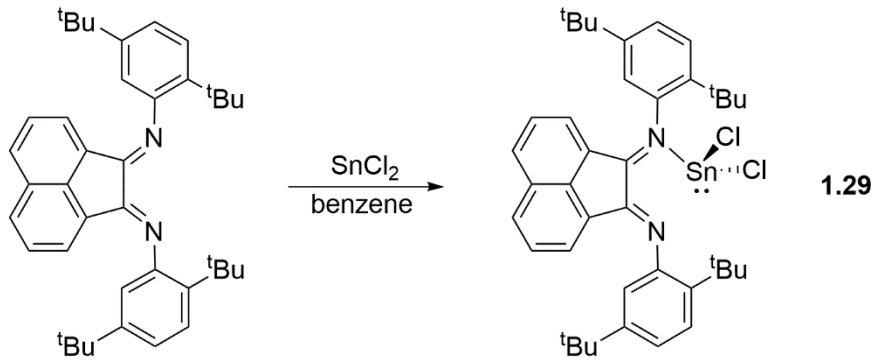

1.29

Scheme 1.13 *Formation of [(dtb-BIAN)$SnCl_2$] (**1.29**).*

1.5.3 Group 15 complexes with Ar-BIAN ligands

The chemistry of Ar-BIAN ligands with Pnicogens was much less studied as compared to groups 13 and 14. Cowley and co-workers reported the first application of Ar-BIAN ligand in the context of group 15 chemistry, which focused on the reaction of PCl_3 or $AsCl_3$ with Dipp-BIAN ligand.[53]

They demonstrated that the reduction of PCl_3 with $SnCl_2$ in the presence of bis(phosphine) ligands resulted in the formation of cyclic triphosphenium ion (**1.30**).[54] (Scheme 1.14) It was proposed that in this reaction, an initial formation of 'PCl" and $SnCl_4$ occurred *via* reduction of PCl_3 with $SnCl_2$. The "PCl" species was then coordinated to the bis(phosphine) ligand concomitant with or prior to a halide abstraction by $SnCl_4$. Inspired by these findings, Cowley and co-workers investigated the result of trapping the "PCl" species with ligands other than phosphines, *e.g.* the Ar-BIAN ligands.[53] Treatment of Dipp-BIAN with one equivalent of PCl_3 and $SnCl_2$ afforded the phosphenium salt [(Dipp-BIAN)P][$SnCl_5$·THF] (**1.31**). The related arsenium salt [(Dipp-BIAN)As][$SnCl_5$·THF] (**1.32**) can also be obtained with $AsCl_3$ using the same protocol. (Scheme 1.15) X-ray structural analysis of **1.31** and **1.32** both revealed a PN_2C_2 ring with the C-C and C-N bond distances corresponding to a C=C double bond and C-N single bond respectively. Hence, the Dipp-BIAN ligand was reduced by two electrons, while the oxidation state of the P or As metal center remained as +3. This was further supported by the ^{31}P chemical shift of +232 ppm, which is in the range previously reported for phosphenium cations.[55] The authors also investigated the reaction of Dipp-BIAN with PI_3 and without $SnCl_2$ as the reducing agent. This reaction resulted in quantitative formation of the phosphenium triiodide salt [(Dipp-BIAN)P][I_3] (**1.33**), which also possessed a phosphenium cation as indicated by ^{31}P NMR data.

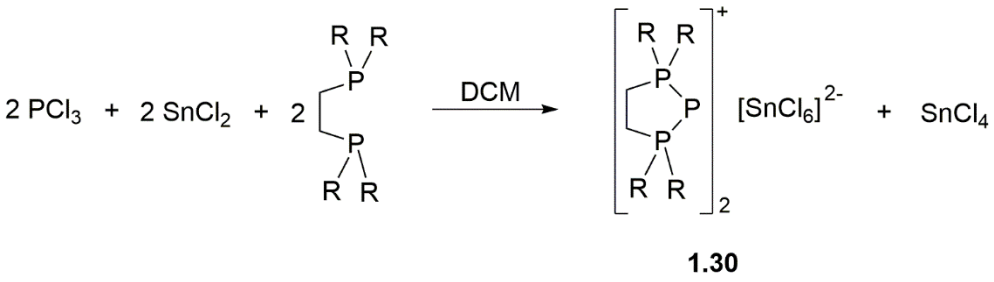

1.30

Scheme 1.14 *Formation of cyclic triphosphenium ion (**1.30**) via reduction of PCl_3.*

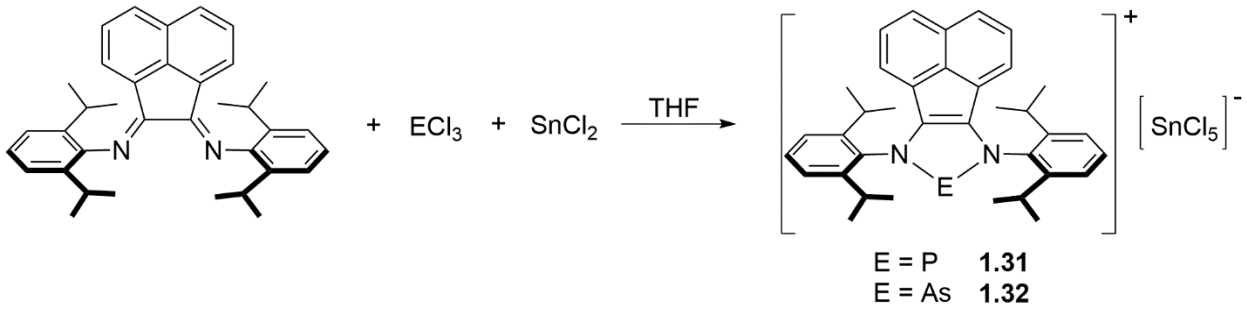

Scheme 1.15 *Formation of [(Dipp-BIAN)P][$SnCl_5$·THF] (**1.31**) and [(Dipp-BIAN)As][$SnCl_5$·THF] (**1.32**).*

The antimony (Sb) and bismuth (Bi) complexes supported by Ar-BIAN ligands were obtained from the reaction of Ar-BIAN directly with the halide salts of the corresponding Pnictogen. For example, treatment of Dipp-BIAN with an equimolar $SbCl_3$ in DCM furnished the expected Sb(III) complex [(Dipp-BIAN)$SbCl_3$] (**1.34**).[47] Based on the X-ray crystallographic analysis, the Sb(III) metal center exhibits a distorted square-pyramidal geometry, in which the vacant equatorial position is occupied by the lone pair of non-bonding electrons on Sb. The C-C bond distance (*ca.* 1.526 Å) in **1.34** are indicative of a single bond while the two C-N bond distances (*ca.* 1.266 Å and 1.298 Å) fall in the range of C=N double bonds. Therefore, **1.34** contained a neutral Dipp-BIAN ligand coordinating to the $SbCl_3$ metal center through two dative N-Sb bonds. It is important to note that the two N-Sb bond distances are very different (2.617 Å and 2.846 Å) and both are significantly longer than those reported for the related Sb(III) diimine complexes, [^{t}Bu-DAB($SbCl_3$)$_2$] (**1.35**) (2.460 Å and 2.418 Å)[56] and [(bpy)$SbCl_3$] (bpy = bipyridine) (**1.36**) (2.317 Å and 2.245 Å).[57] This suggests that despite its facile formation, the N-Sb bonds in **1.34** are relatively weak as compared to those of other Sb(III) complexes supported by diimine ligands. Recently, Suter and co-workers reported the synthesis of cationic coordination complexes of Sb with Dipp-BIAN ligand.[58] Reactions of $SbF(OTf)_2$ or $SbF_2(OTf)$ (OTf = trifluoromethanesulfonate) with Dipp-BIAN in DCM resulted in the formation of Sb(III) complexes [SbF(Dipp-BIAN)](OTf)$_2$

(**1.37**) and [SbF_2(Dipp-BIAN)](OTf) (**1.38**) respectively. Further treatment of **1.37** with trimethylsilyl cyanide (TMS-CN) or azidotrimethylsilane (TMS-N_3) gave the corresponding cyano-Sb(III) complex [Sb(CN)(Dipp-BIAN)](OTf)$_2$ (**1.39**) and azido-Sb(III) complex [SbN_3(Dipp-BIAN)](OTf)$_2$ (**1.40**) respectively. (Scheme 1.16) These reactions represent an example of using Ar-BIAN ligands to support cations involving fluoro, azido and cyano-antimony moieties.

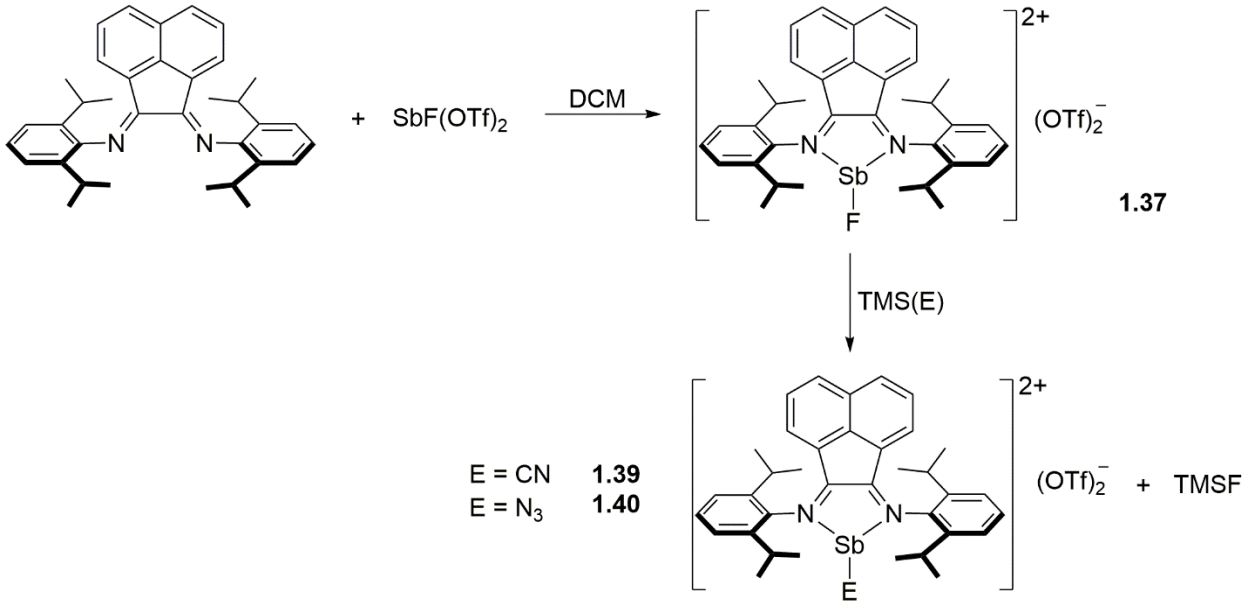

Scheme 1.16 *Formation of [SbF(Dipp-BIAN)](OTf)$_2$ (**1.37**) and its substitution reactions.*

Similar to the preparation of Sb(III) Ar-BIAN complexes, the Bi(III) Ar-BIAN complexes [(Dipp-BIAN)$BiCl_3$] (**1.41**) and [(Mes-BIAN)$BiCl_3$] (**1.42**) were synthesized by reaction of the corresponding Ar-BIAN ligand with $BiCl_3$.[47] However, diffraction quality crystals were only obtained for **1.42**. In contrast to the antimony derivatives discussed above, the solid state structure of **1.42** is a μ-Cl bridged dimer, *i.e.* each of the two Bi atoms are bridged by Cl^- anions. The N-Bi bond distances (*ca*. 2.606 Å and 2.708 Å) are longer than those observed in the related binuclear,

octahedral Bi(III) complexes, *e.g.* [(bipy)$BiBr_3$] (2.417 Å and 2.516 Å), indicating weaker N-Bi bonds.

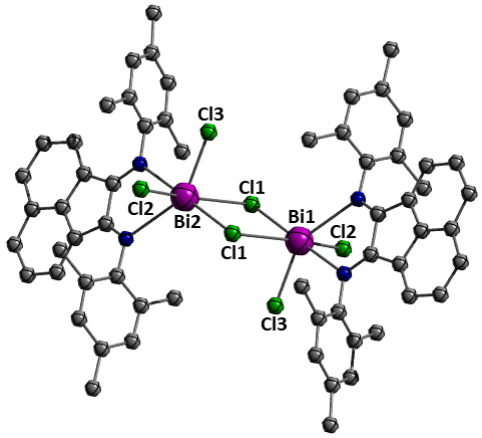

Figure 1.6 Ball and stick representation *of [(Mes-BIAN)$BiCl_3$]$_2$.*

1.6 Mechanochemical Synthesis

1.6.1 Introduction to mechanochemistry

Based on the International Union of Pure and Applied Chemistry's definition, "mechanochemical reaction" refers to a chemical reaction that is induced by direct absorption of mechanical energy, which can be generated through many means such as compression, shearing, grinding, rubbing, etc.[59] The application of mechanochemistry dates back to prehistoric times when mortar and pestle are used predominantly for size reduction.[60] In the late 19th century, M. Carey Lea described the difference between mechanochemically induced reactions and thermochemical reactions. He reported that both silver chloride (AgCl) and mercury chloride ($HgCl_2$) undergo decomposition when triturated in a mortar. However, when only heat was applied, $HgCl_2$ sublimed while AgCl melted without decomposition.[61] These findings have demonstrated that mechanical action could induce unique chemical changes which cannot be achieved thermally. This important discovery

led to the creation of mechanochemistry as an independent branch of chemistry, and according to Takacs,[62] Lea was recognized as “the father of mechanochemistry”.

There are different ways in which mechanical energy could be harnessed for chemical transformations. One of the most commonly employed methods in laboratory research is grinding. This can be conducted either manually using a pestle and mortar or automatically using ball mills. As the force exerted by experimentalists in manual grinding varies from person to person, it is difficult to achieve quantitative consistency between experiments, hence mortar and pestle grinding techniques are generally used for qualitative investigation of mechanochemical reactions.[63] For a more systematic and more reproducible investigation of chemical processes, ball mills are usually employed as it enables greater control over the reaction conditions, such as duration and frequency.[64] There are several types of commercially available automated mills, such as shaker and planetary ball mills, automated mortar grinder, and twin screw extruders. Among these, the shaker and planetary mills are more commonly employed for laboratory scale reactions. (Figure 1.7) In shaker mills, the reaction vessel, containing the required substrates and ball bearings, typically made of stainless steel, are rapidly shaken at a specific frequency. Similarly, in planetary mills, each reaction vessel spins axially in a circular motion, while the jar moves in the opposite direction, thus allowing for the balls inside the vessel to effectively mix and grind the solids together. In order to systematically investigate a mechanochemical reaction, several parameters need to be taken into account, which includes the milling duration, speed or frequency, mass of the balls and ball-to-powder ratios.

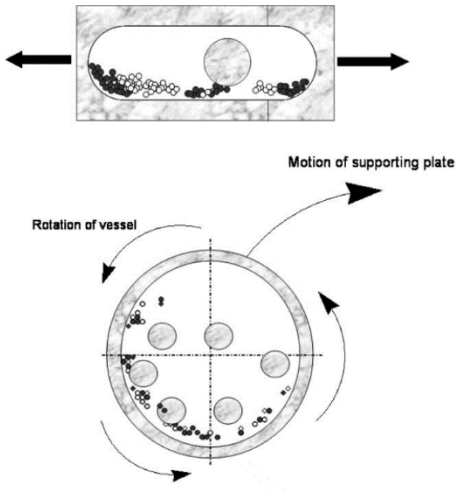

Figure 1.7 *Schematic representation of motion inside shaker mill and planetary mill.*[64]

Recently, the use of mechanochemistry for synthetic chemistry has gained popularity and ball milling can be applied for the synthesis of a variety of compounds, (*e.g.* organic,[65] organometallics,[66] polymers,[67] nanocomposites,[68] alloy systems[69] *etc.*) and finds a wide range of applications from pharmaceuticals[70] to catalysis,[71] minerals processing,[72] and even geology.[73] Although it is not possible to discuss all of them in this thesis, many good review articles and books have been published that discuss the history and development of mechanochemistry, and highlights their application in these areas in detail.[60, 63-64, 71b, 74]

1.6.2 Mechanochemical approaches to organometallics and coordination compounds

Although mechanochemical synthesis has attracted increasing interest in the field of synthetic chemistry, organometallic compounds synthesized mechanochemically represent only a small but growing amount. In 1999, Makhaev and co-workers reported the mechanochemical synthesis of ferrocene *via* reactions between iron(II) chloride ($FeCl_2$) and cyclopentadienides of sodium (Na), potassium (K), and thallium (Tl).[75] More recently, the application of mechanochemical synthesis on organogold compounds with *N*-heterocyclic carbenes (NHC) as ancillary ligands was also reported. The conventional synthesis of [Au(NHC)(R)] (R = alkyl) complexes involves firstly the

preparation of the hydroxide derivatives, which are air and moisture stable, from the corresponding halide complexes. This is followed by reaction with organic acids (R-H) to afford the desired [Au(NHC)(R)] complex.[76] Generally, the reaction works with both strong acids (bearing low pK_a and electron withdrawing groups) and weak acids (bearing high pK_a and electron donating groups). Inspired by Maier and co-workers who synthesized a [Au(NHC)(OH)] complex by grinding [Au(NHC)(Cl)] with KOH and a small amount of benzene,[77] Nolan's group reported a solid-state synthesis of [Au(Dipp-NHC)(OPh)] (**1.43**) directly from the [Au(Dipp-NHC)(Cl)] complex without going through the hydroxide derivative.[78] (Scheme 1.17) The ^{1}H NMR spectrum of the crude reaction mixture suggested almost complete conversion with only 5 min of neat grinding. The scope of this reaction was explored with many different organic phenols. However, to the author's surprise, this methodology did not work well with the most acidic phenol they have screened, pentafluorophenol. Instead, a significant amount of [Au(Dipp-NHC)(OH)] (**1.44**) was formed. Nevertheless, the reported one-pot grinding protocol provides a significant improvement on the reaction time as compared to the solution based synthesis.

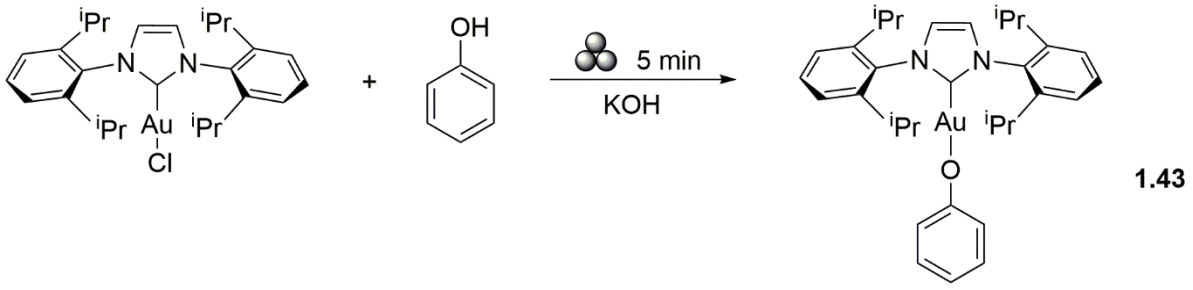

Scheme 1.17 *"One pot" mechanochemical synthesis of [Au(Dipp-NHC)(OPh)]* ***(1.43)****.*

To show how mechanochemistry is used for fundamental organometallic transformations, Friščić and co-workers have conducted a "*proof of concept*" oxidative halogenation of $[CpRe(CO)_3]$ using MX (M = Na, Cu, X = Cl, Br, I) and oxone ($2KHSO_5{\cdot}KHSO_4{\cdot}K_2SO_4$) as a solid oxidant.[79]

Conventional synthesis of [CpRe(CO)$_2$Br$_2$] (**1.45**) involves the use of Br$_2$ in trifluoroacetic acid or AlCl$_3$, which produces a mixture of *lat* and *diag*-isomers in 13% and 38% yield respectively. In comparison, oxidative addition induced by mechanochemistry produced **1.45** in excellent yield with a *lat* and *diag*-isomer ratio of 53:47 when LiBr was employed as the bromide source. (Scheme 1.18) It is also interesting to note that the selectivity between *diag*- and *lat*- isomers can be tuned by varying the bromide source. The use of NaBr afforded exclusively *diag*-**1.45** while CuBr gave mainly the *lat*-**1.45**. Although the as described oxidative addition of halogens to metals is a conceptually simple and well-established reaction, it represents the first example of fundamental organometallic transformations achieved in the solid-state *via* mechanochemical method.

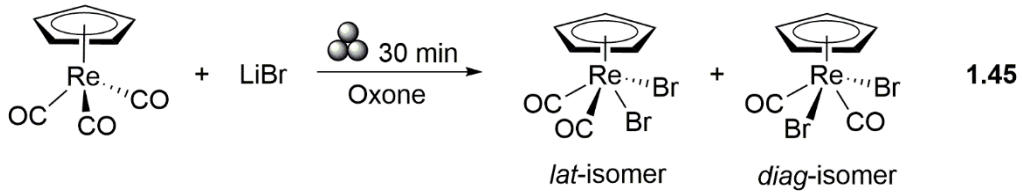

Scheme 1.18 *Oxidative halogenation of [CpFe(CO)$_3$] via mechanochemistry.*

The same group of authors have also established a multi-step, multi-component mechanochemical strategy that couples oxidative halogenation and ligand exchange reaction together. In addition, they have demonstrated that these two reactions can be mutually orthogonal.[80] Firstly the oxidative addition of Re$_2$(CO)$_{10}$ was carried out mechanochemically in the presence of NaBr and oxone. This reaction has gone to completion after 5 min milling process which was confirmed by powder X-ray diffraction. Subsequent work up with acetone afforded the addition product Re(CO)$_5$Br (**1.46**) in excellent yields (86-95% depending on the halide). (Scheme 1.19a) The authors then evaluated the mechanochemical ligand exchange reaction of **1.46** by reacting it with 2.5 equivalents of tetraethylammonium bromide (TEAB). After 3 h milling, [TEA]$_2$[Re(CO)$_3$Br$_3$] (**1.47**) was obtained in 82 % yield. (Scheme 1.19b) The promising results obtained from the

mechanochemical strategies for both oxidative halogenation and ligand exchange reaction have enabled the design of a multi-step mechanochemical route (one-pot sequential manner) to yield **1.47** directly. This was conducted by the synthesis of **1.46**, followed by direct addition of TEAB and further milling for 3 h without prior purification and isolation. This procedure produced **1.47** in 78% yield. An even more simplified procedure (one-pot multi-component) involved milling all reactants, $Re_2(CO)_{10}$, Oxone and TEAB together in one grinding vessel for 3 h. This strategy afforded **1.47** in 84% yield. (Scheme 1.19c)

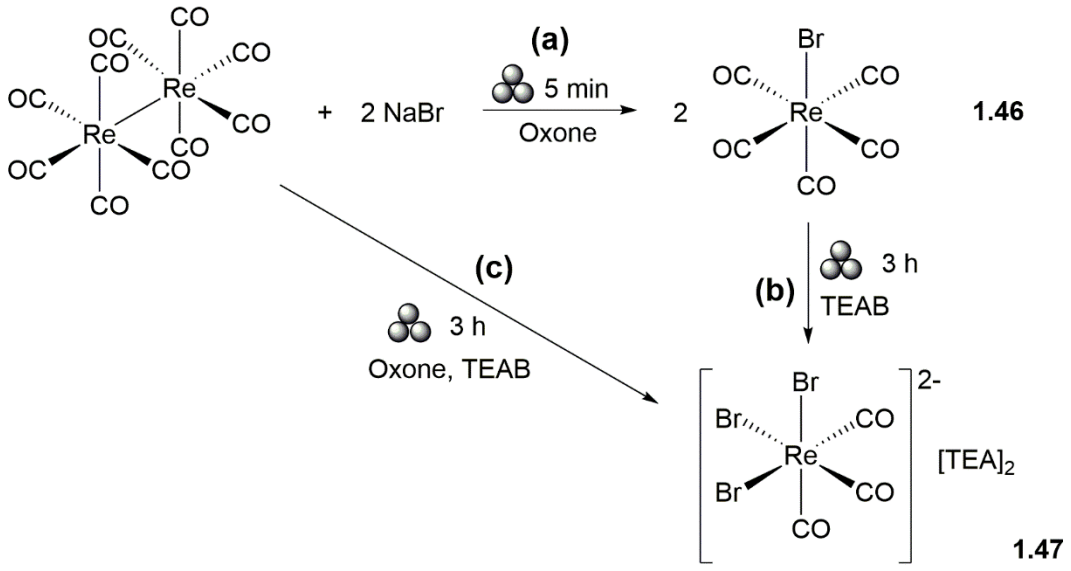

Scheme 1.19 *Mechanochemical synthesis of $[TEA]_2[Re(CO)_3Br_3]$ through one pot sequential manner (a and b) and one pot multi-component manner (c).*

It has been shown that first row transition metal salts react readily with chelating ligands under mechanochemical conditions. For example, manual grinding of nickel (II) nitrate $[Ni(NO_3)_2.6H_2O]$ with 1,10-phenanthroline (phen) for only 2 min resulted in the formation of $[Ni(phen)_3(NO_3)_2]$ (**1.48**) accompanied by a clear color change to red.[81] Further, a series of nickel(II) and cobalt(II) complexes supported by neutral diimine ligands were reported by Duarte and co-workers.[82] On the other hand, substitution reactions at platinum (II) metal centers are generally slower than at

divalent first row transition metals centers. Nevertheless, Balema and Pecharsky described the solid-state synthesis of *cis*-[$(PPh_3)_2PtCl_2$] (**1.49**) from balling milling of polycrystalline $PtCl_2$ with two equivalents of PPh_3. Further treatment of **1.49** with K_2CO_3 produced *cis*-[$(PPh_3)_2Pt(CO_3)$] (**1.50**) in high yields.[83] (Scheme 1.20) Based on ^{31}P MAS NMR spectrum, the formation of **1.49** was completed after 1 h. The completion of this reaction was also confirmed by differential scanning calorimetry (DSC) coupled with thermogravimetric analysis (TGA), indicated by the absence of endothermic processes originated from melting of PPh_3.

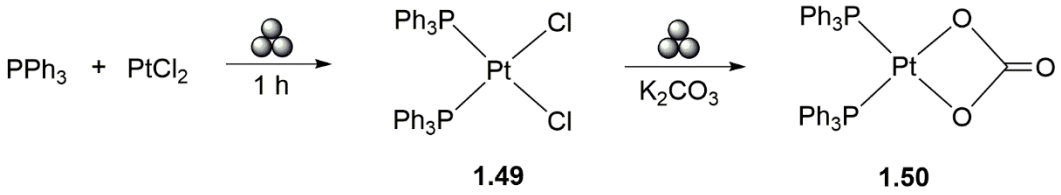

Scheme 1.20 *Mechanochemical synthesis of cis-[$(PPh_3)_2PtCl_2$] (**1.49**) and cis-[$(PPh_3)_2Pt(CO_3)$] (**1.50**).*

1.6.3 Mechanochemistry in catalysis

Other than the synthesis of organometallic complexes, mechanochemistry has also been extensively explored in catalysis. For instance, a mechanochemical approach for Ru-catalyzed cross-metathesis and ring closing metathesis of liquid and solid olefins was developed by Do *et al.*[84] The reactions were conducted using two Teflon milling jars equipped with one stainless steel ball bearing. A difference in reactivity was observed between solid and liquid olefins. Reactions with liquid olefins like styrene proceed much more readily (within 30 min) than reactions with high melting solid olefins like 4-vinylbenzoic acid (no reaction even after 5 h). However, with a small amount of THF (up to 100 μL) as an additive, the reactivity of the later can be greatly improved. A palladium-catalyzed Mizoroki-Heck reaction was also reported using mechanochemistry, in which cinnamate was produced quantitatively when phenyl iodide was treated with *tert*-butyl acrylate using PEG (polyethylene glycol) as a reducing agent.[85] (Scheme

1.21) In 2015, Bolm and co-workers explored the mechanochemically induced C-H bond functionalization catalyzed by [(Cp*$RhCl_2$)$_2$] (Cp* = pentamethylcyclopentadienyl) (**1.51**).[86] (Scheme 1.22) In a later publication, the authors developed a mechanochemical procedure of synthesizing **1.51**, starting from rhodium trichloride ($RhCl_3$) and pentamethylcyclopentadiene (Cp*H) with MeOH as an additive for liquid assisted grinding (LAG), in which microliter scale solvent is added to the reaction mixture to provide better molecular mobility.[87] After 3 h milling, **1.51** was produced in 74% yield. The synthesized Rh(III) catalyst (**1.51**) was then used in the mechanochemical C-H bond halogenation of 2-phenylpyridine (Scheme 1.23), with N-bromosuccinimide (NBS) as the brominating agent, affording the desired product **1.52** in 84% yield. Recently, Bolm's group has also studied the related mechanochemical C-H bond amidation reactions of arenes catalyzed by both Rh(III) catalyst,[88] and Ir(III) catalyst.[89]

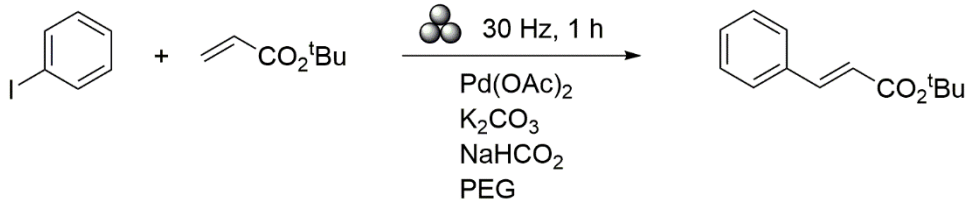

Scheme 1.21 *Mechanochemical Mizoroki-Heck arylation.*

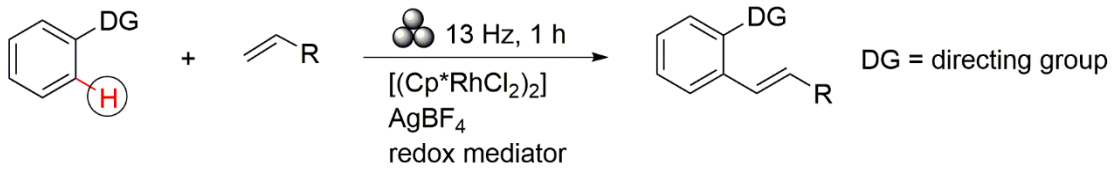

Scheme 1.22 *Mechanochemical oxidative Heck reaction.*

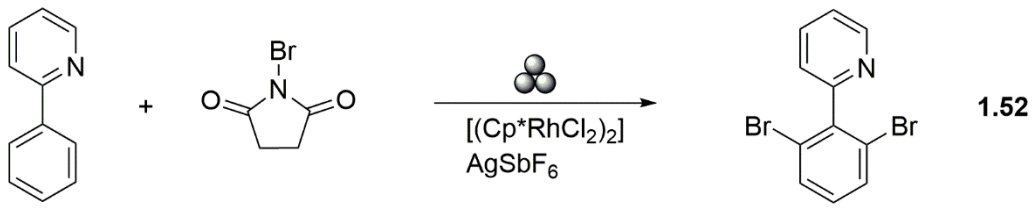

Scheme 1.23 *Mechanochemical Rh(III)-catalyzed halogenation of 2-phenylpyridine.*

A palladium-mediated C-H bond activation in an asymmetrically substituted azobenzene ligand was achieved using a mechanochemical ball milling approach.[90] The reaction was carried out with LAG by treating 4'-(N,N-dimethylamino)-4-nitroazobenzene (**1.53**) with $Pd(OAc)_2$ in the presence of glacial acetic acid. (Scheme 1.24) This resulted in the formation of mono (**1.54**) (when 1 equivalent of Pd(II) was added) and di-cyclopalladated complexes (**1.55**) (when 2 equivalents of Pd(II) were added). The reaction was monitored by ^{1}H NMR every 90 min and it has demonstrated that **1.55** was formed through **1.54** which acted as an intermediate. This finding was also confirmed by *in situ* Raman spectroscopic technique.

Significant progress has also been made in other mechanochemically promoted organic transformations. For example, in C-C bond formation processes like Sonogashira,[91] Suzuki reactions;[92] coupling reactions of alkynes;[93] cross-dehydrogenative coupling reactions;[94] and some C-N bond formation reactions.[95]

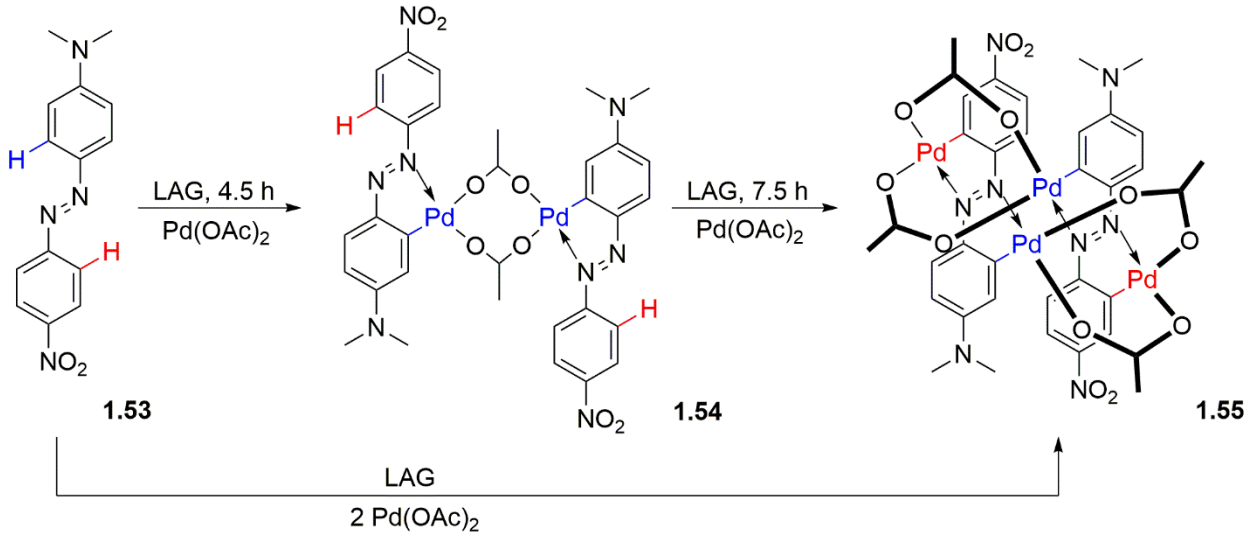

Scheme 1.24 *Mechanochemical C-H bond activation in 4'-(N,N-dimethylamino)-4-nitroazobenzene.*

1.6.4 Mechanochemical approaches to main group inorganic and organometallic systems

The application of mechanochemical synthesis in organometallic systems has been greatly focused on transition metal complexes.[82, 96] However, not much progress has been made in the synthesis of main-group inorganic and organometallic systems using mechanochemistry. The first example of a crystallographically characterized main group complex synthesized *via* mechanochemistry was reported by Hanusa and co-workers, in which a tris(allyl)aluminum complex was formed and characterized.[97] (Scheme 1.25) In this reaction, a 1,3-bis(trimethylsilyl)allyl (A') aluminum complex (**1.56**) was synthesized by simply grinding AlX_3 (X = Cl, Br, I) with 3 equivalents of K(A') for 1-2 h, followed by extraction with hexane. On the contrary, solution phase synthesis carried out in THF or Et_2O (diethyl ether) only gave unidentifiable mixtures of products.

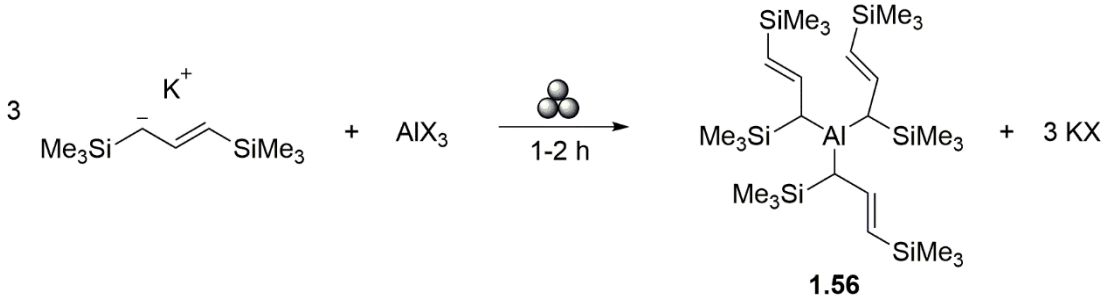

Scheme 1.25 *Mechanochemical synthesis of unsolvated tri(allyl)aluminum complex.*

Another important reaction in the field of main group organometallic compounds is the large scale synthesis of bis(*n*-propyltetramethylcyclopentadienyl)strontium complex [$SrCp'_2(OEt_2)$] (Cp' = *n*-propyltetramethylcyclopentadienyl) (**1.57**), a good liquid precursor for deposition methods like chemical vapor or atomic layer deposition.[98] Typical small scale synthesis of $SrCp'_2$ involves a salt metathesis reaction between alkali metal cyclopentadienides (*e.g.* KCp') with strontium halides (*e.g.* SrI_2). However, on larger scale synthesis, the effectiveness of this reaction is limited by the poor solubility of SrI_2 in any aprotic organic solvents. Therefore, a mechanochemical synthesis of $SrCp'_2$ was attempted using KCp' and SrI_2. (Scheme 1.26) It was shown that LAG

produced **1.57** in 88% yield and the reaction can be sped up by up to six times on the preparative scale.

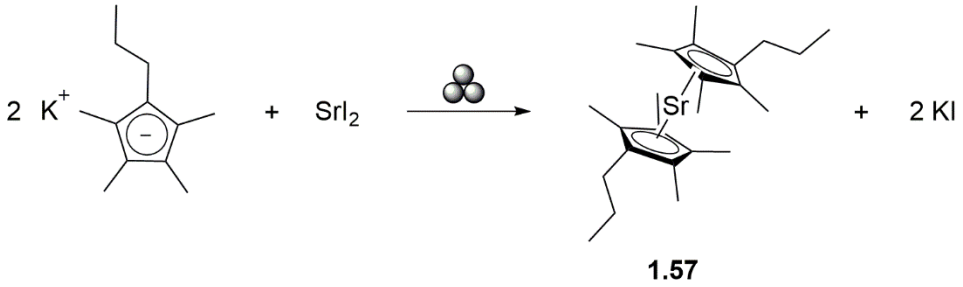

Scheme 1.26 *Mechanochemical synthesis of SrCp'₂.*

More recently, Glavinovic *et al.* described a chlorine-free protocol for the synthesis of organogermanes (GeR_4), which bypassed the generation of moisture sensitive and corrosive $GeCl_4$ intermediate.[99] Inspired by the mild and selective oxidizing power of quinones, the authors evaluated the oxidation of Ge(0) by 3,5-di-tert-butylbenzoquinone under ball milling conditions in the presence of pyridine (py). (Scheme 1.27) After 3 h grinding of the reactants with a 1:1 mixture of toluene/H_2O as an additive for LAG, the corresponding Ge(IV) catecholate complex **1.58** was generated with 83% yield. This protocol can be extended to the reaction of GeO_2 and 3,5-di-tert-butylcatechol under identical conditions, producing **1.58** in 84% yield. After the synthesis of **1.58**, it was then reacted with an excess amount of alkyl magnesium chlorides (R-MgCl) to afford GeR_4. Overall, substitution reactions using the Ge(IV) catecholate complexes present advantages over the conventional method in terms of the milder reaction conditions and the higher isolated yield of the organogermanes synthesized.

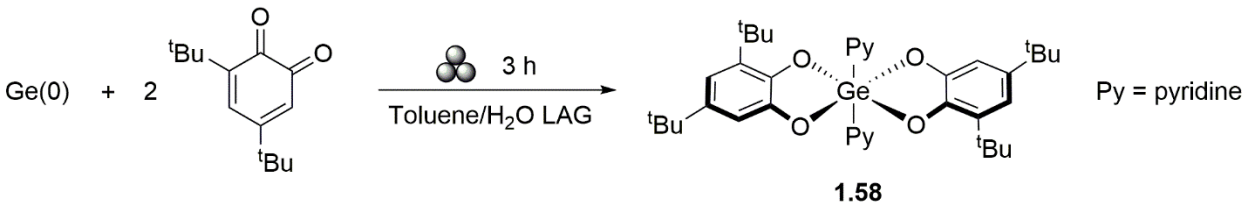

1.58

Scheme 1.27 *Mechanochemical synthesis of $Py_2Ge(IV)$ catecholate (**1.58**).*

1.7 Conclusion

In this introductory chapter, a literature review on (i) main group metal complexes supported by Ar-BIAN ligands and (ii) mechanochemical methods towards main group inorganic compounds has been presented. From these discussions, it can be inferred that although Ar-BIAN ligands are recognized as robust ligands for transition metal complexes, its coordination chemistry towards main group elements are comparatively less well-studied and the physicochemical investigation of such complexes are still in its infancy. In addition, much attention had been focused on the structural studies of the as synthesized main group Ar-BIAN complexes, but little was done to explore their photophysical properties. Therefore, in this thesis, the synthesis of main group, and more specifically, indium Ar-BIAN complexes *via* both solution state method and solid-state mechanochemical method will be discussed. Also, systematic investigation on the photophysical properties of metal Ar-BIAN complexes will be reported to explore their potential application as photosensitizers.

Chapter 2
Mechanochemical route to indium(III) complexes

2.1 Introduction

Polypyridyl complexes of heavy transition metals (*e.g.* ruthenium) have been widely investigated as photosensitizers because of their significant absorption in the visible light region of the electromagnetic spectrum ($\varepsilon \sim 20000$ to $25000\ M^{-1}cm^{-1}$) and long lived photoexcited state ($\tau \sim 1\ \mu s$).[100] The intense visible light absorption in Ru(II) polypyridyl complexes originates from the metal to ligand charge transfer (MLCT) transitions from the filled metal based *d* orbitals to the empty ligand based π^* orbitals, which are both spin and Laporte allowed transitions.[22] Furthermore, heavy atom effect exhibited by Ru can enhance the rate of intersystem crossing (ISC) from the photoexcited singlet to triplet state, resulting in long excited state lifetimes.[101]

With respect to the investigation of main group metal complexes as potential photosensitizers, indium complexes are attractive targets because of their low toxicity, relatively low reduction potential,[102] and their ability to mediate or catalyze organic reactions.[103] Macdonald and co-workers have demonstrated that the frontier orbitals of a 1,3-diazabutadiene ($^{Ph}DAB^{H}$, Ph = phenyl) complex of In(I) is consistent with the presence of an indium-based HOMO and a ligand-based LUMO.[104] (Figure 2.1) Therefore, upon absorption of a photon with energy that exceeds its HOMO-LUMO gap, electronic transitions *via* MLCT may occur, which mimics the class of electronic transitions responsible for visible light absorption in known $Ru^{II}(bpy)_3$ complexes.[100a, 105]

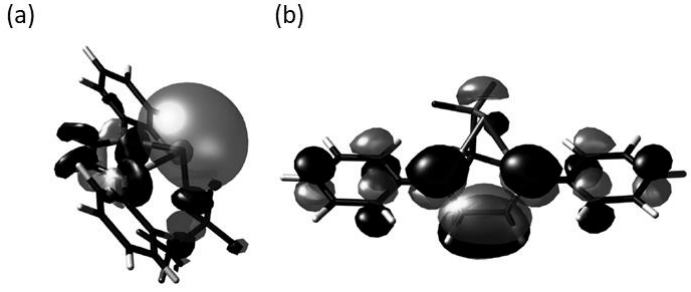

Figure 2.1 *The electron density distribution of (a) HOMO and (b) LUMO in* $^{Ph}DAB^{H}$*·InOTf.*[104]

Bis(arylimino)acenaphthene (Ar-BIAN) ligands are more rigid derivatives of the aforementioned diazabutadiene ligands and have been shown to form robust complexes with transition metal centers.[11] In addition, functionalization on Ar-BIAN ligands are synthetically more accessible than in polypyridine compounds.[17] The ease of their synthesis, coupled with the customizable π-acceptor scaffolds provided by its extensive π-system on the acenaphthene backbone, have made Ar-BIAN ligands versatile diimine alternatives to the frequently employed polypyridine ligands as molecular photosensitizers. Henceforth, we hypothesized that coordination complexes formed between Ar-BIAN ligands and In(I) may exhibit interesting photophysical properties that might have potential applications as main group photosensitizers.

The use of mechanochemistry for the synthesis of molecular inorganic compounds has been explored extensively for transition metal complexes. However, such studies on main group inorganic and organometallics systems remain rare, with the exception of previously discussed examples in section 1.6.4. With the increase in demand for chemical industries to find more environmentally-benign and sustainable strategies for the bulk synthesis of high value chemicals, the use of mechanochemistry has become particularly attractive due to its rapid, solvent-independent, and high yielding characteristics. The inherent advantages of mechanochemistry have been previously discussed, and thus present a good opportunity to utilize such solid-state techniques for the synthesis of main group BIAN complexes.

As discussed in section 1.2.2, Ar-BIAN are generally synthesized by condensation of acenaphthoquinone with the corresponding aniline (usually in the presence of $ZnCl_2$ or $NiBr_2$), followed by demetallation. In the following sections, a mechanochemical milling approach will be introduced for the preparation of Ar-BIAN ligands and the subsequent formation of the corresponding indium(III) complexes. These reactions were performed with anilines bearing both

electron-donating and electron-withdrawing groups to demonstrate their compatibility with different electronic properties. These compounds were further characterized by UV-vis spectroscopy and cyclic voltammetry (CV) to establish their absorption profile and reduction potentials for future investigations as photosensitizers.

2.2 Results and discussion

2.2.1 Synthesis of Ar-BIAN ligands and their indium(III) complexes (2.1-2.4)

Two Ar-BIAN ligands with *para*-methoxy (*p*-MeOAr-BIAN **2.1**) and *para*-bromo (*p*-BrAr-BIAN **2.2**) substituents on the diimine moiety were synthesized in high yields *via* ball milling of acenaphthoquinone with the corresponding aniline in the presence of acid catalyst and Na_2SO_4 for 3 h. (Scheme 2.1) For **2.1**, a small amount of acetic acid (AcOH) was added to catalyze the reaction while trifluoroacetic anhydride (TFAA) was used for the synthesis of **2.2**. Such mechanochemical protocol avoids the formation of Ar-BIAN Zn(II) complexes and therefore circumvents the subsequent demetallation step. For compound **2.1**, the crude ^{1}H NMR spectrum obtained directly after the ball milling process showed relatively pure sample with only a small amount of *p*-anisidine which can be easily removed by washing the sample with Et_2O. (Figure 2.2) However, the crude ^{1}H NMR spectrum obtained directly from ball milling for the synthesis of **2.2** revealed unreacted *p*-bromoaniline and undesired side products from mono-condensation as well as the desired ligand from double-condensation. (Figure 2.3) In this case, the unreacted *p*-bromoaniline can be washed away with Et_2O and analytically pure sample can be obtained after recrystallizing the remaining solid with a combination of DCM/pentane. Although one extra recrystallization step is necessary, the solid state mechanochemical process still presented greatly improved reaction time and simplified work up procedure for the synthesis of both **2.1** and **2.2**. To exclude the

possibility of thermally induced reactions, control experiments were performed in which all reactants were placed in the reaction vessel and heated at 60 °C and 180 °C for 4 h without milling. Based on the ^{1}H NMR spectrum, the former showed some product formation together with unreacted aniline and other unidentifiable side products, whereas the later resulted in decomposition of both **2.1** and **2.2**.

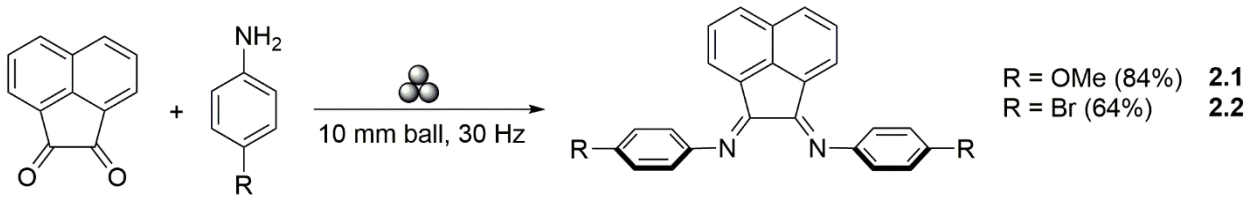

Scheme 2.1 *Mechanochemical synthesis of p-MeOAr-BIAN (**2.1**) and p-BrAr-BIAN (**2.2**).*

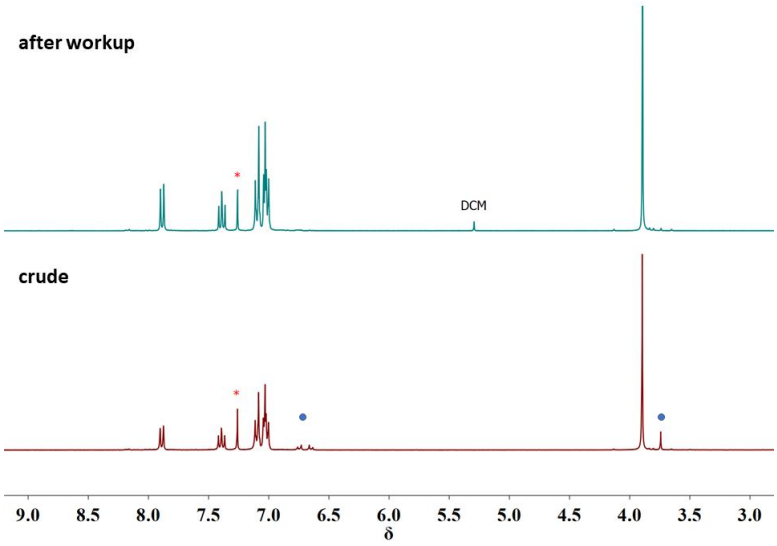

Figure 2.2 *The ^{1}H NMR spectrum of **2.1** recorded in $CDCl_3$ before and after purification. Blue circles indicate unreacted p-anisidine.*

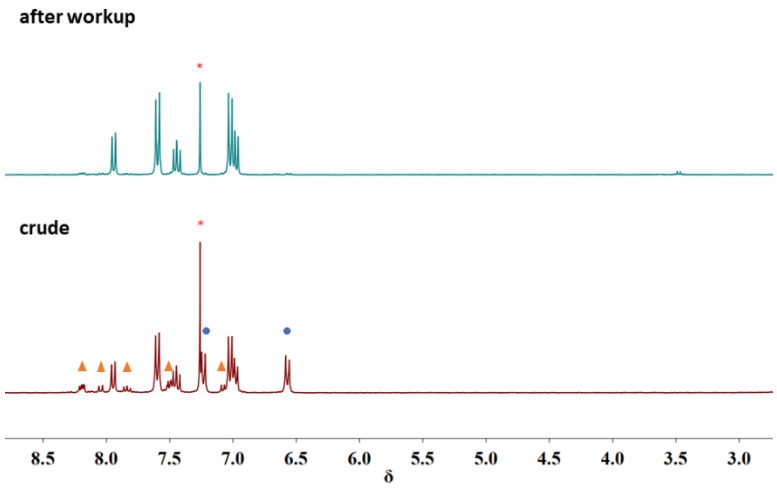

Figure 2.3 *The ^{1}H NMR spectrum of* ***2.2*** *recorded in $CDCl_3$ before and after purification. Blue circles indicate unreacted p-bromoaniline and orange triangles indicate mono-imine side products.*

The indium(III) Ar-BIAN complexes *p*-MeOAr-BIAN-$InCl_3$ (**2.3**) and *p*-BrAr-BIAN-$InCl_3$ (**2.4**) were prepared from ball milling of **2.1** and **2.2** with $InCl_3$ for 40 min and 2 h respectively. (Scheme 2.2) Analytically pure samples can be obtained by recrystallization from acetonitrile (ACN) and Et_2O for **2.3** and (*N*,*N*-dimethylformamide) DMF and Et_2O for **2.4**. Furthermore, direct formation of the indium(III) Ar-BIAN complexes was attempted by milling the crude products from mechanochemical ligand synthesis with $InCl_3$. This "two-step one-pot" process resulted in isolation of **2.3** with 57 % yield after recrystallization. However, the formation of **2.4** was not so successful using this method. Although single crystal X-ray data showed that **2.4** was obtained, the ^{1}H NMR spectrum of the crude reaction mixture revealed many other unidentifiable products. In light of the results obtained from the "two-step one pot", a "one-step one pot" reaction was attempted in which acenaphthoquinone was grinded with $InCl_3$, and *p*-anisidine (for the synthesis of **2.3**) and *p*-bromoaniline (for the synthesis of **2.4**) respectively for 2 h. This protocol showed successful application on the synthesis of **2.3** but failed to produce compound **2.4**. Nevertheless,

these “one pot” reactions further demonstrated the orthogonality of multi-step mechanochemical synthesis, parallel with the strategies reported by Hernández *et al.* in 2014.[80]

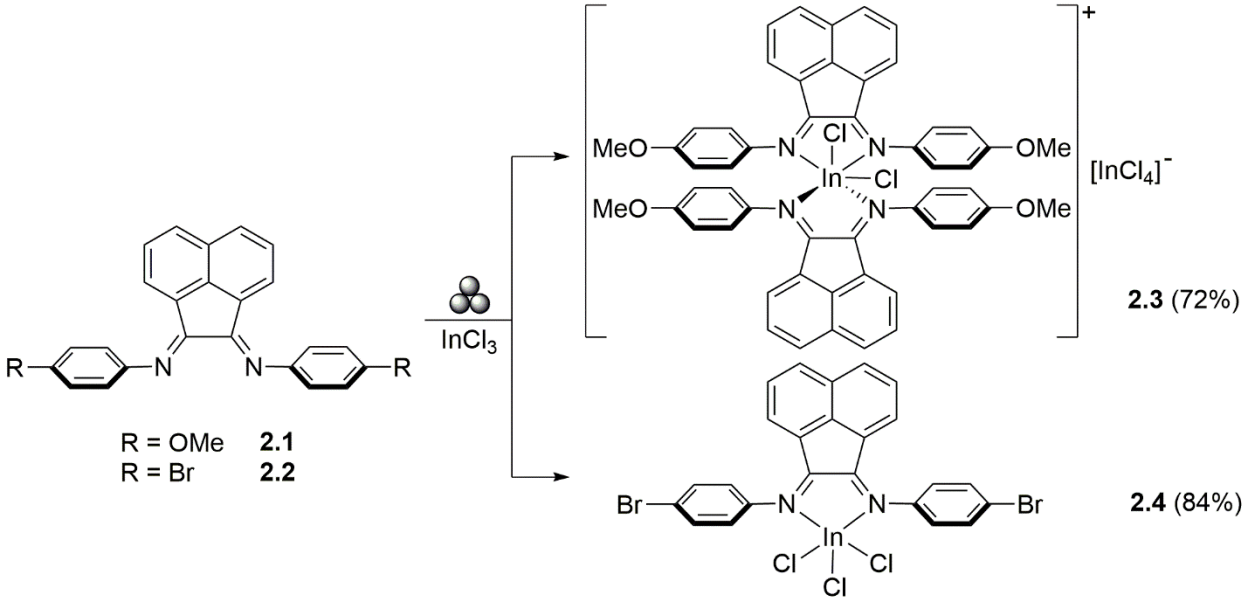

Scheme 2.2 *Mechanochemical synthesis of p-MeOAr-BIAN-$InCl_3$ (**2.3**) and p-BrAr-BIAN-$InCl_3$ (**2.4**).*

2.2.2 Spectroscopic and Crystallographic Studies

Crystals with good quality for single crystal X-ray diffraction analysis were grown for both **2.3** and **2.4**. Both indium(III) complexes possess a distorted octahedral geometry at the metal center. Compound **2.4** consists of a single bidentate Ar-BIAN ligand with a DMF molecule coordinated to the In(III) metal center, forming the octahedral complex. In contrast, compound **2.3** crystallized out as a bis(BIAN) complex with $[InCl_4]^-$ as the counter anion. (Figure 2.4) For both **2.3** and **2.4**, the C-C and average C-N bond distances within the diimine framework are consistent with the previously reported C-C single bond and C=N double bond distances in related Ar-BIAN complexes.[47] Therefore, the In(III) Ar-BIAN complexes synthesized herein can be considered as donor acceptor complexes between neutral Ar-BIAN ligands and In(III) metal centers. Due to the different number of ligands coordinated to the In center in **2.3** and **2.4**, and the fact that **2.3** is a

cationic complexes while **2.4** being a neutral complex, direct comparison between the binding strength of **2.1** and **2.2** in their resulting complex cannot be made even though the average In-N bond distance in **2.3** (2.31 Å) is slightly shorter than the respective bond distances in **2.4** (2.35 Å). The average In-Cl bond distance in the bis(BIAN) cation of compound **2.3** is 2.40 Å while that for compound **2.4** is 2.43 Å, both of which are similar to those measured in a hexacoordinated $InCl_3(THF)_3$ complex (2.42 Å).[106]

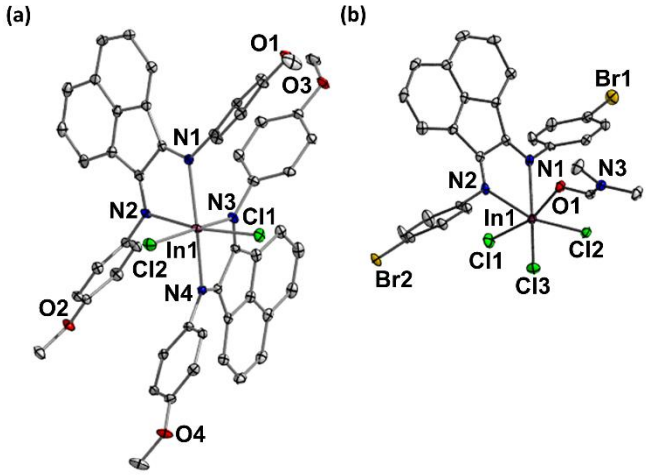

Figure 2.4 *Thermal ellipsoid plots (50%) of (a) $[(p\text{-}MeOAr\text{-}BIAN)_2InCl_2]^+$ and (b) $[(p\text{-}BrAr\text{-}BIAN)InCl_3]$ respectively. Hydrogen atoms have been omitted for clarity. Selected bond lengths (Å): (a) In1-N1 2.296(2), In1-N2 2.324(2), In1-N3 2.311(2), In1-N4 2.323(2), In1-Cl1 2.413(5), In1-Cl2 2.396(5). (b) In1-N1 2.390(3), In1-N2 2.301(3), In1-Cl1 2.434(9), In1-Cl2 2.419(9), In1-Cl3 2.429(9), In1- O1 2.258(2).*

Compounds **2.1** to **2.4** have been fully characterized by ^1H and ^{13}C NMR spectroscopy, high resolution mass spectroscopy (HR-MS) and elemental analysis. (see section 2.4) It was observed that at room temperature, the ^1H NMR spectrum of **2.3** displayed broadened signals in the aromatic region. This may be a result of *cis-trans* isomerization in solution on the time scale of the experiment. To understand the behavior of **2.3** in solution, variable temperature NMR (VT-NMR) spectroscopy was performed in acetone-d_6, which was chosen because of its low melting point (-

95 °C). As shown in Figure 2.5, the isomerization process slowed down when the temperature was decreased since the broadened signals started to be resolved. Below -70 °C, three singlets were observed at around 4 ppm with an intensity ratio of 1:1:1. These signals correspond to the three proton environments of the methoxy groups in the *trans*- and *cis*-isomers, with one singlet being assigned to the *trans*-isomer and two to the *cis*-isomer. In the aromatic region, two sets of signals, one from each isomer, could be vaguely identified at temperatures below -60 °C. The ratio between the *trans* and *cis* isomer varies with temperature. At -15˚C, the *trans*- and *cis*-isomers were present in a 0.95:1 ratio. As the temperature was lowered to -35˚C, this ratio changed to 0.54:1 and appeared to level off as 0.50:1 at -75˚C. The thermodynamic parameters for the *cis*-*trans* equilibrium process of **2.3** were estimated by fitting the experimental data with the Van't Hoff equation $\ln(K_{eq}) = [(-\Delta H/RT) + (\Delta S/R)]$. A plot of ln(Keq) *vs.* 1/T revealed a linear dependence of equilibrium constant (K_{eq}) with temperature (T). (Figure 2.6) The equilibrium constants at different temperatures were obtained as a ratio between the concentration of the *trans* isomer and the *cis* isomer, which was determined from the relative integration of peaks belonging to each isomer (marked peaks in Figure 2.5). An enthalpy change of $\Delta H = +20$ kJ mol^{-1} and an entropy change of +75 J mol^{-1} K^{-1} for this isomerization process were determined based on the gradient and y-intercept of the linear fit line respectively. A positive ΔH implies an endothermic process which suggests that heat was absorbed going from the *cis* to the *trans* isomer. The enthalpic change is comparable to a similar *cis*-*trans* isomerization process in an octahedral azole ruthenium−nitrosyl complex reported by Gavriluta *et al*.[107]

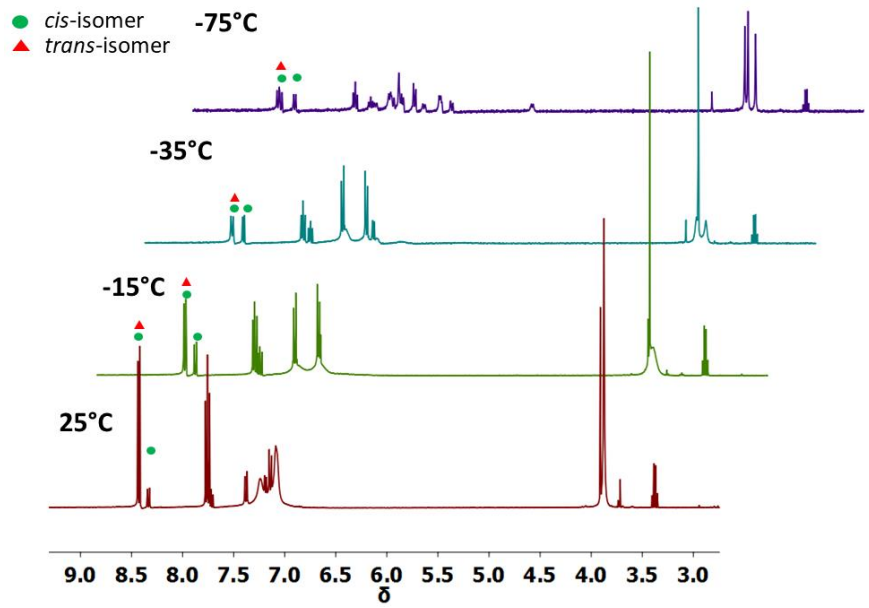

Figure 2.5 *^{1}H NMR spectra of* ***2.3*** *recorded in acetone-d_6 at 25 ˚C, -15 ˚C, -35 ˚C and -75 ˚C. (Marked peaks were used to calculate the equilibrium constants K_{eq} at different temperatures).*

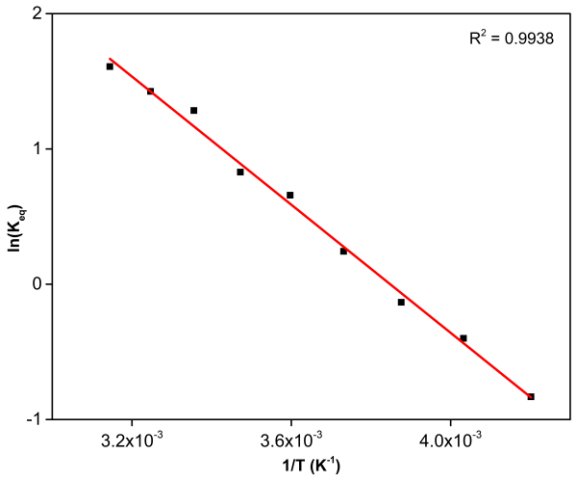

Figure 2.6 *Van't Hoff plots for* ***2.3*** *recorded in acetone-d_6 from -35 °C to 45 °C (ln K_{eq} = –2368/T + 9).*

2.2.3 UV-vis and Electrochemical Studies

To establish the absorption profile of the indium(III) Ar-BIAN complexes, UV-vis spectra for compounds **2.3** and **2.4** were recorded at 298 K. The UV-vis spectra for Ar-BIAN ligands **2.1** and **2.2** were also obtained for comparative purposes. (Figure 2.7) In general, the extinction coefficient is lower for **2.4** with an electron-withdrawing bromo-group than that of **2.3** with an electron-

donating methoxy-group. The same trend was observed when comparing the ligands **2.1** and **2.2**, which was consistent with similar observation as reported by Hasan and co-workers.[17] The higher energy bands below 350 nm and the lower energy bands above 400 nm may be assigned to the π-π* ligand centered transitions from both the diimine and the acenaphthene and between the diimine and acenaphthene respectively, similar to the assignments reported in the literature for related Ar-BIAN systems.[108] (*vide infra*)

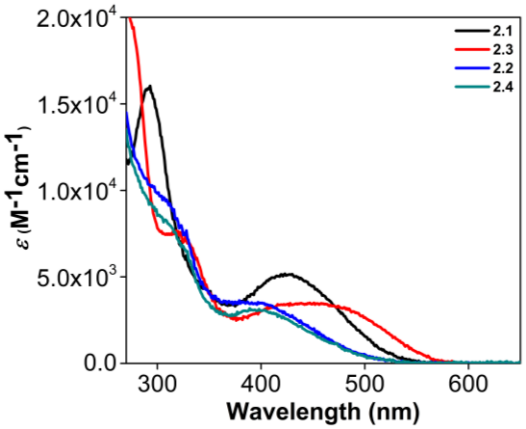

Figure 2.7 *UV-vis spectra for **2.1** and **2.3** in ACN, and **2.2** and **2.4** in DMF.*

The electrochemical behavior of the indium(III) Ar-BIAN complexes **2.3** and **2.4** were also studied by cyclic voltammetry (CV). The voltammogram for **2.3** was recorded in ACN while that for **2.4** was recorded in DMF. (Figure 2.8) During the cathodic scan of **2.3**, a total of six reduction waves were observed. The first reduction at E_p^{red} = -0.8 V is chemically reversible because ΔE_p = 60 mV and the ratio of the cathodic and anodic peak currents stays around one regardless of the scan rate. (Figure 2.9a) This was further confirmed by a linear fit of oxidation peak current (where E_p^{oxi} = +0.74 V) plotted against the square root of scan rate. (Figure 2.9b) In contrast, no chemically reversible processes were identified in the case of **2.4**, with only two quasi-reversible reduction waves observed between E_p^{red} = -1.0 V and E_p^{red} = -2.2 V. We propose that these two reduction waves arise from the reduction of In(III) metal center in **2.4**. When the metal is reduced, one of

the Cl^- dissociates which may cause some structural changes to the molecule. This in turn renders its re-oxidation process to occur at a different potential. Subsequent reduction processes observed in **2.4** are probably due to ligand reduction. The anodic waves occurring between E_p^{oxi} = -1.2 V and E_p^{oxi} = +0.1 V may be attributed to the re-oxidation of any intermediate products formed after reduction. The fact that reduction waves attributed to the reduction of In(III) metal center appeared to be electrochemically reversible for **2.3** but not in the case of **2.4** suggested an increased stability of the putative $[(p\text{-MeOAr-BIAN})_2InCl_3]^-$ as compared to $[(p\text{-(BrAr-BIAN})InCl_3]^-$.

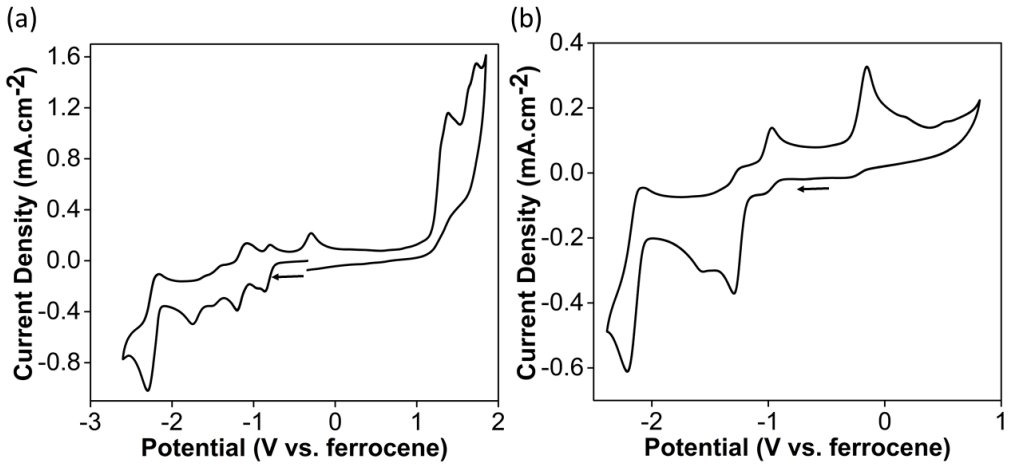

Figure 2.8 *Cyclic voltammograms for (a)* ***2.3*** *in ACN solution and (b)* ***2.4*** *in DMF solution with 0.10 M* $(nBu_4N)PF_6$ *as the supporting electrolyte and glassy carbon (3 mm in diameter) as the working electrode. All potentials reported are referenced to* Fc^+/Fc*. Scan rate: 100 mV* s^{-1}.

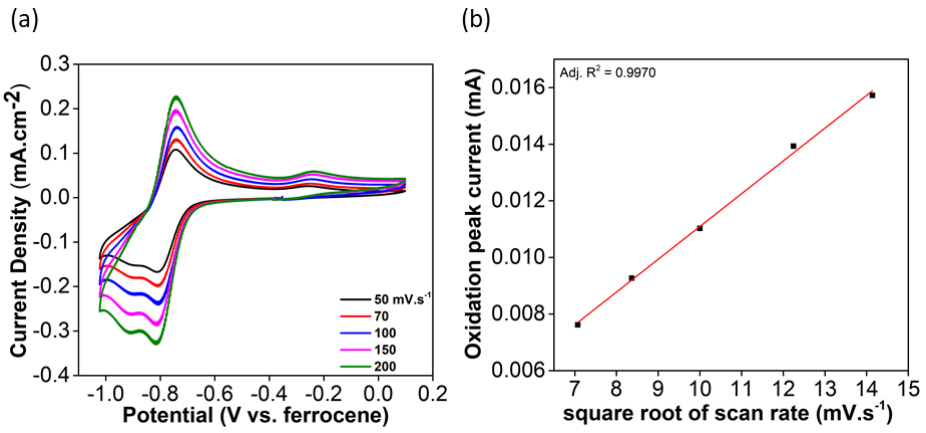

Figure 2.9 (a)*The 1st and 2nd reduction waves of* ***2.3*** *at different scan rates. All potentials reported are referenced to* Fc^+/Fc. *(b) A plot of peak current at* $E_p^{oxi} = +0.74$ *V versus square root of scan rate.*

2.2.4 Computational Studies

Time-dependent density functional theory (TD-DFT) calculations were used to predict the electronic absorption spectra of the In(III) Ar-BIAN complexes **2.3** and **2.4**. The energy and geometry optimization were carried out at the B3LYP level with the 6-31+G* Pople basis set for non-metal atoms, and LANL2DZ basis set for heavier In, Br, and Cl atoms. Furthermore, the spectra have been calculated either in vacuum or with the polarizable continuum model to account for solvent effects. The experimental and theoretical spectra for **2.3** and **2.4** are shown in Figure 2.10. In general, the experimentally determined absorption profiles match well with the theoretical ones, despite some minor discrepancies on the lower energy end of the absorption spectra. In addition, the theoretical absorption spectra obtained, by taking into account solvent effects, is a better match to the experimental absorption spectra and therefore it is necessary to include solvation in our theoretical studies. The calculated predominant contributions to the lower energy absorption maximum for **2.3** (λ_{max} = 460 nm) corresponds to electronic transitions from HOMO→LUMO and HOMO-2→LUMO. (Table 2.1) On the other hand, the lower energy absorption maximum for **2.4** (λ_{max} = 395 nm) corresponds exclusively to the HOMO→LUMO transition. (Table 2.2)

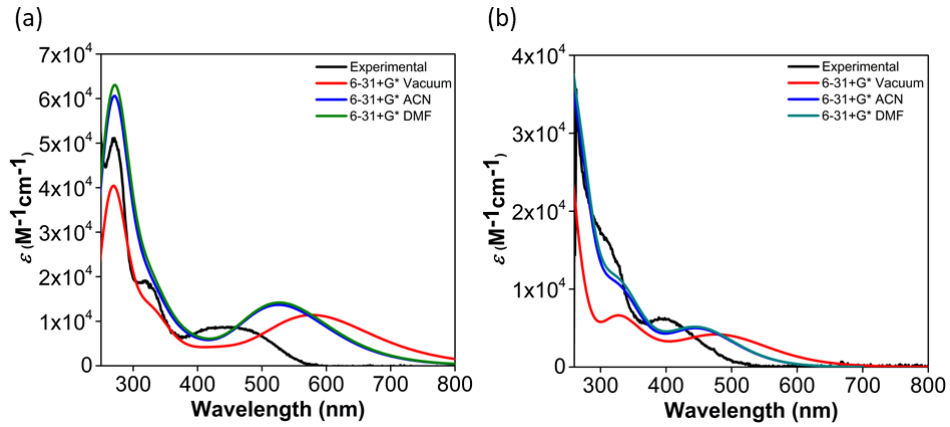

Figure 2.10 *Calculated and experimental absorption spectra for (a)* ***2.3*** *and (b)* ***2.4****.*

Table 2.1 *Orbital contributions to the electronic absorption transitions of* ***2.3*** *using a B3LYP/6-31+G* level of theory; only transitions with oscillator strengths >0.03 have been taken into account.*

Transition	λ_{max} (nm)	*f*	Orbital contributions (%)
HOMO-3 →LUMO+1			2.30
HOMO-2 →LUMO			66.70
HOMO-1 →LUMO	525	0.1332	2.69
HOMO-1 →LUMO+1			19.95
HOMO →LUMO			5.17
HOMO-2 →LUMO			10.87
HOMO-1 →LUMO			4.98
HOMO-1 →LUMO+1	570	0.0468	3.29
HOMO →LUMO			72.02
HOMO →LUMO+1			5.94

Table 2.2 *Orbital contributions to the electronic absorption transitions of* ***2.4*** *using a B3LYP/6-31+G* level of theory; only transitions with oscillator strengths >0.03 have been taken into account.*

Transition	λ_{max} (nm)	*f*	Orbital contributions (%)
HOMO → LUMO	466	0.0856	98
HOMO-1 → LUMO	427	0.0298	97
HOMO-2 → LUMO	413	0.0273	96

Based on the calculated electron density distributions, the HOMO of **2.4** is largely contributed by the arylimino moiety, whereas the LUMO is mainly delocalized over the acenaphthene framework.

(Figure 2.11) Therefore a HOMO-LUMO transition corresponds to transitions between the diimine and the acenaphthene moiety, which is in agreement with our assignments of the UV-vis spectral bands.

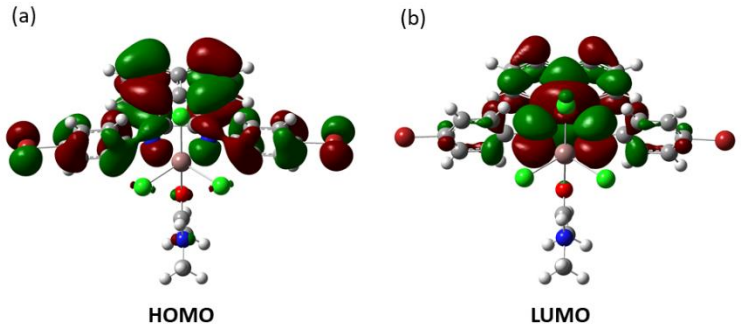

Figure 2.11 *Electron density distributions of (a) HOMO and (b) LUMO for* ***2.4*** *calculated at the B3LYP/6-31+G(d) level of theory.*

2.3 Conclusions

In this chapter, an atom-efficient and essentially solvent-free route to the synthesis of Ar-BIAN ligands (**2.1** and **2.2**) and their corresponding indium(III) complexes (**2.3** and **2.4**) using a mechanochemical milling approach was presented. This methodology circumvents the use of transition metal halides as the templating agent, and reduced the reaction time for the synthesis of both the Ar-BIAN ligands and the indium(III) complexes. Furthermore, this protocol can be generalized to electron-donating and electron-withdrawing variants of the Ar-BIAN ligands and their complexes. Both indium(III) BIAN complexes absorb in the UV-vis region with compound **2.3** absorbing closer to 700 nm due to the presence of electron-donating methoxy groups. The electrochemical behavior of **2.3** and **2.4** was established by cyclic voltammetry, demonstrating the feasibility of electrochemical reduction to their indium(I) derivatives, which may serve for potential application as photosensitizers.

2.4 Experimental and analytical techniques

2.4.1 General considerations

All reactions were carried out in a stainless steel grinder jar using a Retsch Mixer Mill MM400. The recrystallization of products was performed under a dry and inert atmosphere by using a combination of standard Schlenk line techniques and a Vacuum Atmospheres N_2 glovebox. Solvents including tetrahydrofuran (THF), Et_2O and pentane were distilled over Na/benzophenone and degassed using freeze-pump-thaw cycles prior to use. Anhydrous ACN were collected from a PURE SOLV MD-5 solvent purification system and stored in a glovebox. Anhydrous 1,2-dimethoxyethane (DME) and DCM were distilled over calcium hydride (CaH_2) and stored in a glovebox. Anhydrous DMF in a Sure-Seal bottle was purchased from Sigma-Aldrich and used as received. Deuterated chloroform ($CDCl_3$) and acetone (acetone-d_6) were distilled over CaH_2 and potassium carbonate (K_2CO_3) respectively. All reagents were purchased from commercial sources and were used without further purification.

The ^1H and $^{13}C\{^1H\}$ NMR spectra were recorded at 298 K on a Bruker Advanced DPX400 and DPX300 spectrometers. The chemical shift values were reported in parts per million (ppm) relative to TMS, using residual protonated solvents as the internal standards (^1H: $\delta = 7.26$ for $CDCl_3$ and $\delta = 2.05$ for acetone-d_6; ^{13}C: $\delta = 77.2$ for $CDCl_3$). UV-Vis absorption measurements were carried out on a Shimadzu UV-3600 spectrophotometer. Cyclic voltammetry (CV) experiments were conducted in a glovebox with N_2 atmosphere, using a Biologic SP-300 potentiostat with 1.0 mM solutions of each sample and 0.10 M of tetrabutylammonium hexafluorophosphate (n-Bu_4NPF_6) as the electrolyte. Crystallographic data were recorded on a Bruker X8 CCD diffractometer. High-resolution ESI mass spectra were obtained using a Waters Q-Tof Premier.

2.4.2 Mechanochemical synthesis of Ar-BIAN ligands

*Synthesis of p-MeOAr-BIAN (**2.1**)*

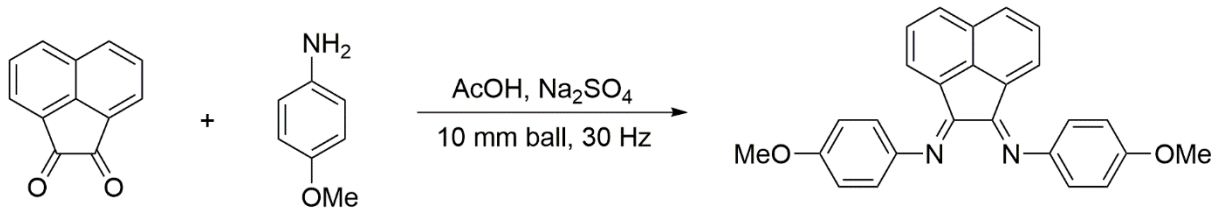

***Scheme 2.3** Mechanochemical synthesis of p-MeOAr-BIAN (**2.1**).*

A stainless steel grinder jar was dried in an oven at 120 ºC overnight prior to use. The grinder jar was charged with acenaphthoquinone (0.073 g, 0.40 mmol), *p*-anisidine (0.099 g, 0.80 mmol), acetic acid (5.7 µL, 0.10 mmol, 25 mol%), and Na_2SO_4 (0.014 g, 0.10 mmol, 25 mol%), and equipped with a 10 mm stainless steel ball. The jar was then grinded for 3.5 h at 30 Hz. The resultant red powder was dissolved in dichloromethane (DCM), filtered, and the filtrate was concentrated and washed with pentane. The crude product was recrystallized by layering a THF solution of the product beneath pentane and the isolated yield was 0.13 g (84%). ^{1}H NMR (400 MHz, $CDCl_3$): δ = 3.90 (s, 6 H), 7.01 - 7.04 (m, 6 H), 7.09 - 7.11 (m, 4 H), 7.39 (t, J = 8.0 Hz, 2 H), 7.89 (d, J = 8.4 Hz, 2 H). ^{13}C{^{1}H} NMR (100 MHz, $CDCl_3$): δ = 55.7, 114.8, 119.9, 123.8, 127.7, 128.9, 129.0, 131.4, 141.8, 145.1, 157.1, 161.7. HRMS (ESI+, m/z) calculated for $C_{26}H_{21}N_2O_2$ $[M + H]^+$ m/z = 393.1603, found 393.1595.

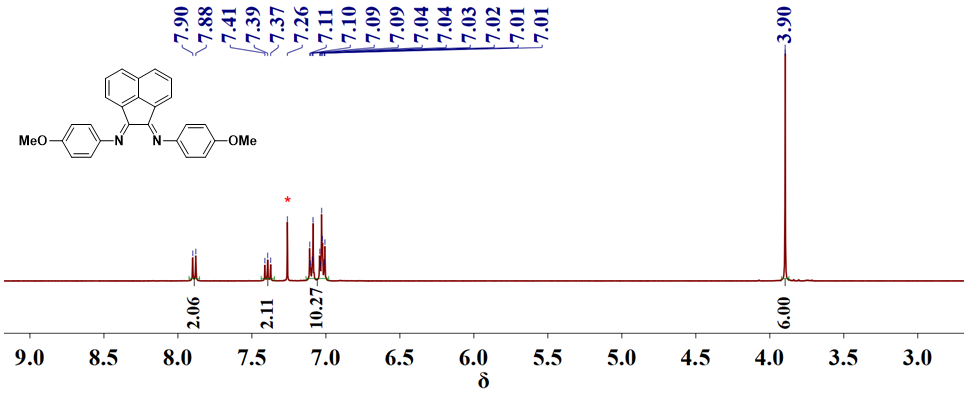

Figure 2.12 *The ^{1}H NMR spectrum of* ***2.1*** *recorded in $CDCl_3$.*

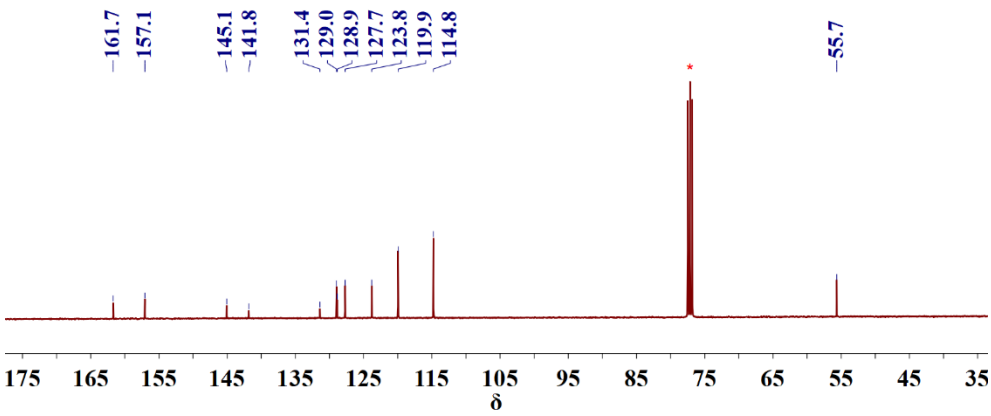

Figure 2.13 *The ^{13}C NMR spectrum of* ***2.1*** *recorded in $CDCl_3$.*

*Synthesis of p-BrAr-BIAN (**2.2**)*

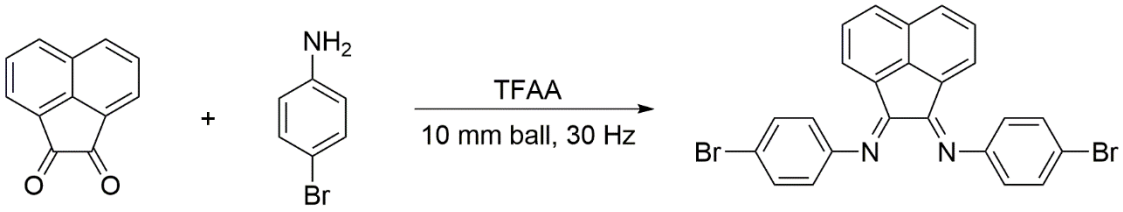

Scheme 2.4 *Mechanochemical synthesis of p-BrAr-BIAN (**2.2**).*

A stainless steel grinder jar was dried in an oven at 120 ºC overnight prior to use. The grinder jar was charged with acenaphthoquinone (0.073 g, 0.40 mmol), *p*-bromoaniline (0.17 g, 1.0 mmol), trifluoroacetic anhydride (14.1 µL, 0.10 mmol, 25 mol%), and equipped with a 10 mm stainless steel ball. The jar was then grinded for 3 h at 30 Hz. The resultant yellow solid was washed with Et_2O. The crude product was recrystallized by layering a DCM solution of the product beneath pentane and the isolated yield was 0.13 g (64%). ^{1}H NMR (300 MHz, $CDCl_3$): δ = 6.96 - 7.05 (m, 6 H), 7.45 (t, J = 7.5 Hz, 2 H), 7.60 (d, J = 8.7 Hz, 4 H), 7.94 (d, J = 8.1 Hz, 2 H). $^{13}C\{^{1}H\}$ NMR (100 MHz, $CDCl_3$): δ = 117.7, 120.3, 124.2, 127.9, 128.3, 129.6, 131.4, 132.7, 142.1, 150.6, 161.6. HRMS (ESI+, m/z) calculated for $C_{24}H_{15}N_2{}^{79}Br^{81}Br$ $[M + H]^+$ m/z = 490.9581, found 490.9574.

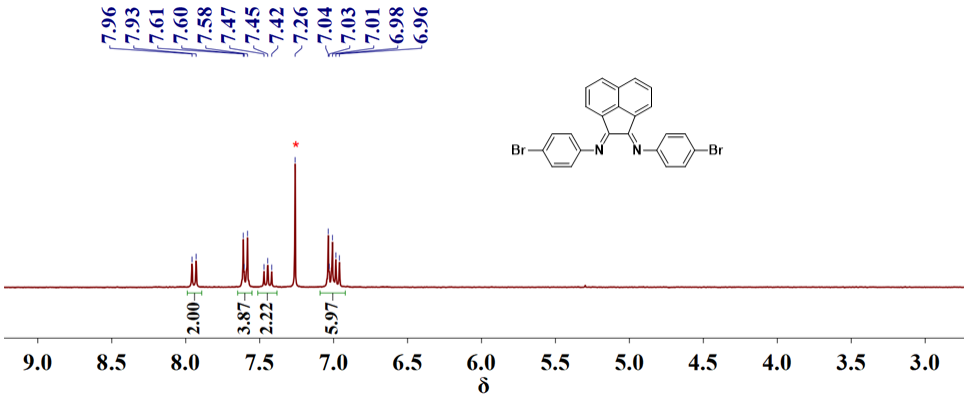

Figure 2.14 *The ^{1}H NMR spectrum of* ***2.2*** *recorded in $CDCl_3$.*

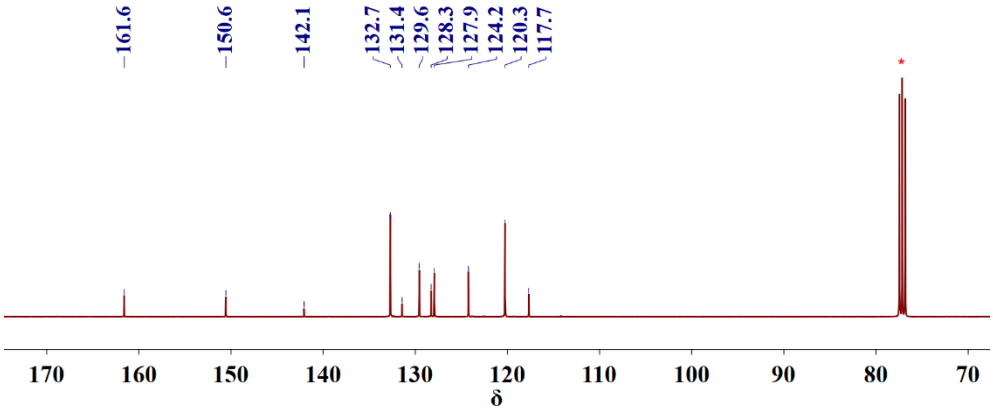

Figure 2.15 *The ^{13}C NMR spectrum of* ***2.2*** *recorded in $CDCl_3$.*

2.4.3 Mechanochemical synthesis of indium(III) complexes

Synthesis of [(p-MeOAr-BIAN)$_2$InCl$_2$][InCl$_4$] ***(2.3)***

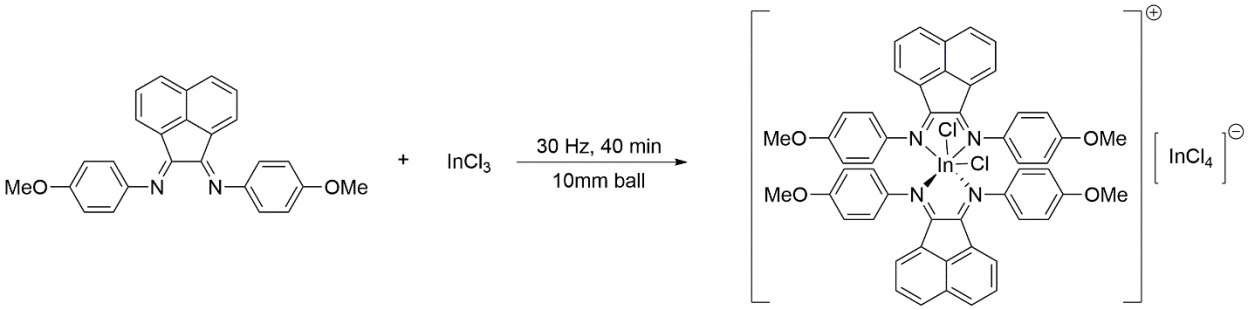

Scheme 2.5 *Mechanochemical synthesis of [(p-MeOAr-BIAN)$_2$InCl$_2$][InCl$_4$]* ***(2.3)****.*

A stainless steel grinder jar was dried in an oven at 120 ºC overnight prior to use. The grinder jar was charged with *p*-MeOAr-BIAN (0.039 g, 0.10 mmol) and $InCl_3$ (0.022 g, 0.10 mmol), and

equipped with a 10 mm stainless steel ball. The jar was then grinded for 40 min at 30 Hz. The resultant red solid was purified by washing with Et_2O and the isolated yield was 0.044 g (72%). The purity of the product was confirmed by elemental analysis. (Anal. Calcd. for $C_{26}H_{20}N_2O_2InCl_3$: C, 50.89; H, 3.29; N, 4.57. Found: C, 50.78; H, 3.45; N, 4.44.) Recrystallization by vapor diffusion of Et_2O into an ACN solution of the red solid resulted in single crystals suitable for single crystal X-ray analysis. ^1H NMR (400 MHz, acetone-d_6, -75 °C, trans-isomer): δ = 3.90 (s, 12 H), 6.0 (d, J = 8.2 Hz, 4 H), 7.05 (d, J = 8.8 Hz, 4 H), 7.25-7.29 (m, 16 H), 8.45 (d, J = 8.4 Hz, 4 H). $^{13}C\{^1H\}$ NMR (100 MHz, acetone-d_6, 25 °C): δ = 56.2, 56.4, 115.7, 116.4 (broad, may have peaks overlapping), 124.5 (broad, may have peaks overlapping), 124.7, 126.1, 127.2, 127.4, 128.2, 130.0, 130.3, 132.3, 133.4, 134.6, 137.1, 138.5, 146.0, 160.7, 161.4, 162.7. HRMS (ESI+, m/z) calculated for $C_{52}H_{40}N_4O_4InCl_2$ $[M]^+$ m/z = 969.1465, found 969.1418. Anal. Calcd. for $C_{26}H_{20}N_2O_2InCl_3$: C, 50.89; H, 3.29; N, 4.57. Found: C, 50.59; H, 3.09; N, 4.57.

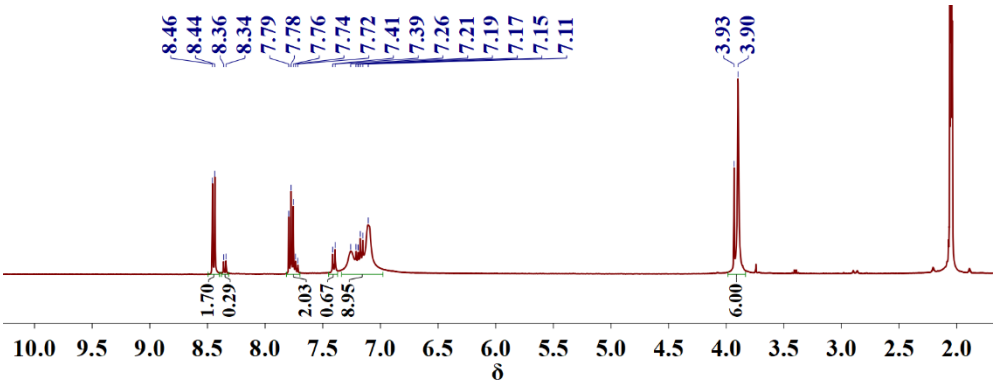

Figure 2.16 *The ^1H NMR spectrum of* ***2.3*** *recorded in Acetone-d_6 at 25 °C.*

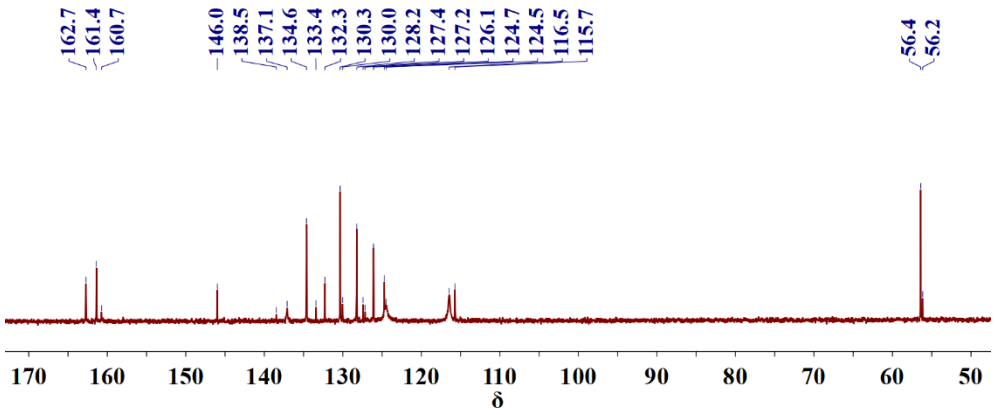

Figure 2.17 *The ^{13}C NMR spectrum of* ***2.3*** *recorded in Acetone-d_6 at 25 °C.*

*Synthesis of [(p-BrAr-BIAN)$InCl_3$]•DMF (**2.4**)*

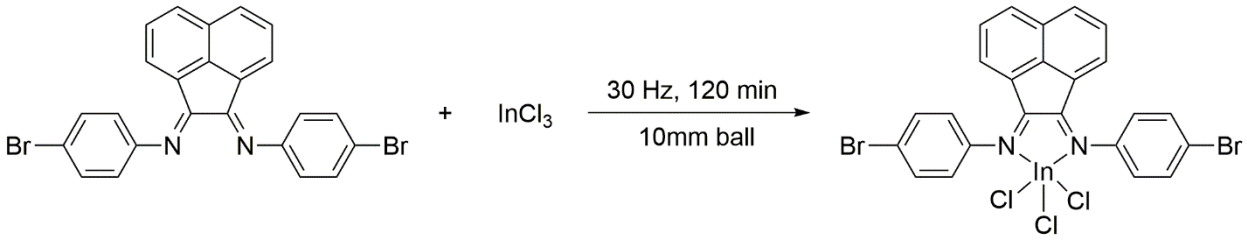

Scheme 2.6 *Mechanochemical synthesis of [(p-BrAr-BIAN)$InCl_3$]•DMF (**2.4**).*

A stainless steel grinder jar was dried in an oven at 120 ºC overnight prior to use. The grinder jar was charged with *p*-BrAr-BIAN (0.049 g, 0.10 mmol), $InCl_3$ (0.022 g, 0.10 mmol), and equipped with a 10 mm stainless steel ball. The jar was then grinded under argon atmosphere for 120 min at 30 Hz. The resultant yellow solid was purified by washing with DCM and the isolated yield was 84%. The purity of the product was confirmed by elemental analysis. (Anal. Calcd. for $C_{24}H_{14}Br_2Cl_3InN_2 \cdot H_2O$: C, 39.52; H, 2.21; N, 3.84. Found: C, 39.40; H, 2.17; N, 3.69.) Recrystallization by vapor diffusion of Et_2O into a DMF solution of the yellow solid resulted in single crystals suitable for single crystal X-ray analysis. ^1H NMR (400 MHz, acetone-d_6, -25 °C): δ = 7.16 (s, broad, 2 H), 7.43 (m. 4 H), 7.78 (t, J = 8.0 Hz, 2 H), 7.83 (d, J = 7.6 Hz, 4 H), 8.40 (d, J = 8.4 Hz, 2 H). The $^{13}C\{^1H\}$ NMR could not be obtained due to the poor solubility of **2.4** in most of the deuterated solvents. HRMS (ESI+, m/z) calculated for $C_{24}H_{15}N_2{}^{81}Br_2{}^{113}InCl_3$ $[M+H]^+$ m/z

= 710.7667, found 710.7686. Anal. Calcd. for $C_{24}H_{14}Br_2Cl_3InN_2 \cdot 2DMF$: C, 42.02; H, 3.29; N, 6.53. Found: C, 42.04; H, 3.15; N, 6.19.

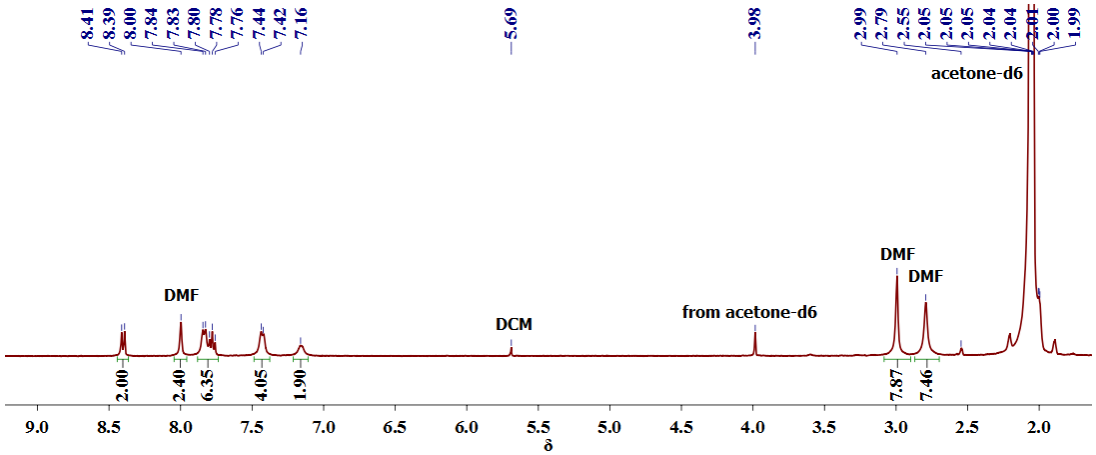

Figure 2.18 *The ^{1}H NMR spectrum of **2.4** recorded in Acetone-d_6 at -25 °C.*

2.4.4 "One-pot two step" mechanochemical synthesis of indium complexes

*<u>One pot synthesis of [(p-MeOAr-BIAN)$_2$InCl$_2$][InCl$_4$] (**2.3**)</u>*

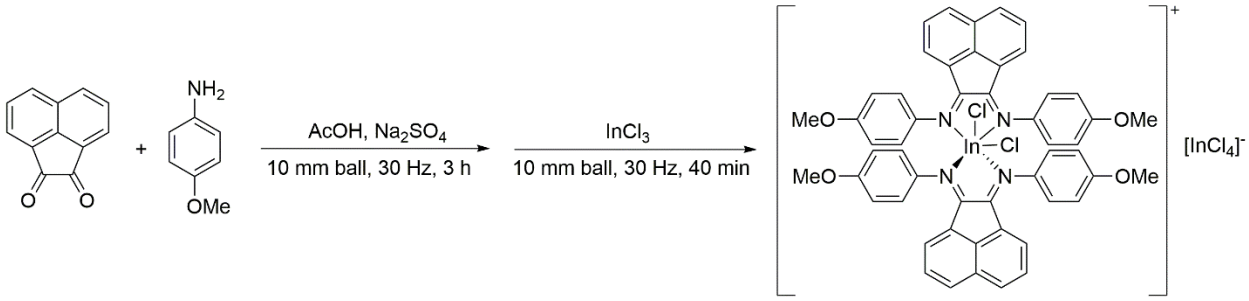

Scheme 2.7 *"One-pot two-step" mechanochemical synthesis of **2.3**.*

A stainless steel grinder jar was dried in an oven at 120 ºC overnight prior to use. The grinder jar was charged with acenaphthoquinone (0.036 g, 0.20 mmol), *p*-anisidine (0.049 g, 0.20 mmol), acetic acid (2.9 µL, 0.050 mmol, 25 mol%), and Na_2SO_4 (0.0071 g, 0.05 mmol, 25 mol%), and equipped with a 10 mm stainless steel ball. The jar was then grinded for 3 h at 30 Hz. To the resultant red powder, $InCl_3$ (0.044 g, 0.20 mmol) was added in the glovebox and the mixture was further grinded for 40 min. The resultant red solid was recrystallized by vapor diffusion of Et_2O

into an ACN solution of the crude product and the isolated yield was 0.048 g (57%). A unit cell measurement was performed on a single crystal grown from this reaction and it was found to be indistinguishable from those obtained by isolating **2.1** first.

*One pot synthesis of [(p-BrAr-BIAN)$InCl_3$] (**2.4**)*

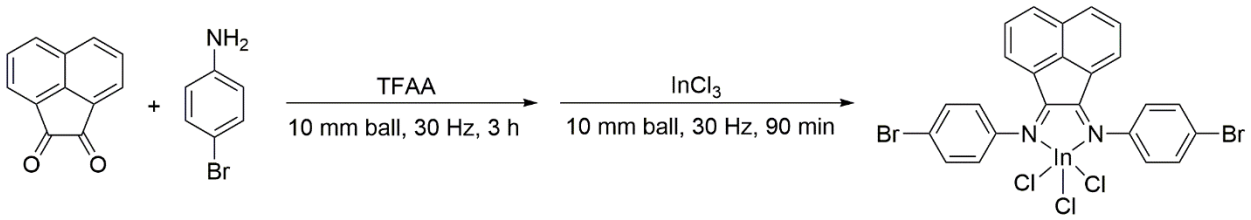

Scheme 2.8 *One pot mechanochemical synthesis of [(p-BrAr-BIAN)$InCl_3$] **2.4**.*

A stainless steel grinder jar was dried in an oven at 120 ºC overnight prior to use. The grinder jar was charged with acenaphthoquinone (0.036 g, 0.20 mmol), *p*-bromoaniline (0.069 g, 0.20 mmol), and trifluoroacetic anhydride (7.1 μL, 0.050 mmol, 25 mol%), and equipped with a 10 mm stainless steel ball. The jar was then grinded for 3 h at 30 Hz. To the resultant khaki powder, $InCl_3$ (0.044 g, 0.20 mmol) was added in the glovebox and the mixture was further grinded for 90 min. The resultant orange solid was recrystallized by vapor diffusion of Et_2O into a DMF solution of the crude product. The product formed was confirmed by single crystal X-ray data. A unit cell measurement was performed on a single crystal grown from this reaction and it was found to be indistinguishable from those obtained by isolating **2.2** first.

2.4.5 X-ray data of indium(III) complexes 2.3 and 2.4

Table 2.3 *X-Ray data of compounds [(p-MeOAr-BIAN)$_2$$InCl_2$][$InCl_4$] (**2.3**) and (p-BrAr-BIAN)$InCl_3$ (**2.4**)*

	2.3	**2.4**
Chemical formula	$C_{52}H_{40}Cl_6In_2N_4O_4$	$C_{30}H_{28}Br_2Cl_3InN_4O_2$
Formula weight/ $gmol^{-1}$	1227.25	857.55
Temperature/ K	103(2)	103(2)
Wavelength/ Å	0.71073	0.71073
Crystal size	0.320 x 0.360 x 0.420	0.060 x 0.140 x 0.200

Crystal habit	Red block	Orange plate
Crystal system	triclinic	monoclinic
Space group	P -1	P 1 21/c 1
a/ Å	9.6102(4)	12.4120(10)
b/ Å	15.9145(7)	19.7758(15)
c/ Å	17.2004(8)	13.5227(10)
α/°	79.7863(13)	90
β/°	76.3618(14)	107.797(3)
γ/°	74.1154(12)	90
Volume/ $Å^3$	2440.90(19)	3160.4(4)
Z	4	4
ρ (Calc)/$mg.m^{-3}$	1.670	1.802
Absorp. Coeff./ mm^{-1}	1.324	3.565
F(000)	1224	1688
Θ range/ °	2.94 to 31.11°	1.72 to 31.11°
Index range	-13<=h<=13, -23<=k<=23, -24<=l<=24	-18<=h<=18, -28<=k<=28, -19<=l<=17
Refl. collected	72379	77866
Indep. Refns. (R_{int})	15605 (0.0547)	10081 (0.0980)
Coverage of independent reflections	99.4%	99.2%
Max., min., transmission	0.6770 and 0.6060	0.8150 and 0.5360
Data/ restraint/parameters	15605 / 0 / 617	10081 / 0 / 383
Goodness-of-fit on F^2	1.024	1.058
Final R indices [I>2σ(I)]	R1 = 0.0321, wR2 = 0.0605	R1 = 0.0388, wR2 = 0.0905
R indices (all data)	R1 = 0.0469, wR2 = 0.0663	R1 = 0.0686, wR2 = 0.1151
Largest diff. peak and hole/ e. $Å^{-3}$	0.728 and -0.557	1.246 and -0.961
Refinement method: Full-matrix least-squares on F^2		

Chapter 3

Synthesis and the optical and electrochemical properties of indium(III) Ar-BIAN complexes

3.1 Introduction

As discussed in section 1.1 and 1.2, "*non-innocent ligand*" refer to ligands in metal complexes where the oxidation states are ambiguous and need to be experimentally determined. Aryl bis(imino)acenaphthenes (Ar-BIAN) are examples of such ligands. Although many transition metal coordination complexes supported by Ar-BIAN ligands have been described, their main

group and lanthanide counterparts are comparatively poorly explored, with the majority being constituted by groups 1 and 2 Ar-BIAN complexes. In these systems, the Ar-BIAN ligands typically undergo facile reduction by groups 1 and 2 metals that are dependent on the stoichiometry of the reaction. Most of this work was described by Fedushkin and co-workers.[15, 109] For example, an investigation on the reaction of Dipp-BIAN with Na or Li revealed a step-wise reduction of the Dipp-BIAN ligand from radical anion salt $[(Dipp\text{-}BIAN)Na]_2$ to tetra-anion salt $[(Dipp\text{-}BIAN)\{Na_4(THF)_4\}]$, with the first two electrons being located at the aryl(diimine) moiety and the last two electrons delocalized into the acenaphthene backbone.[15] Other than the complexes formed with groups 1 and 2 metals, a limited number of main group Ar-BIAN complexes were synthesized and crystallographically characterized, most of which were already discussed in section 1.5.

In chapter 2, we have discussed a mechanochemical approach to the synthesis of new indium(III) Ar-BIAN complexes. To obtain a comprehensive study on the spectroscopic and electrochemical properties of a wider range of main group Ar-BIAN complexes, in this chapter, the synthesis of four new indium(III) Ar-BIAN complexes bearing different substituents at the aryl-diimine moiety will be reported (**3.1b** – **3.4b**). This is followed by the study of their optical and electrochemical properties by UV-vis spectroscopy and cyclic voltammetry respectively. Our previously discussed two structures $[(p\text{-}MeOAr\text{-}BIAN)_2InCl_2]^+[InCl_4]^-$ (**2.3**) and $[(p\text{-}BrAr\text{-}BIAN)InCl_3]$ (**2.4**) will also be compared with the other compounds in this chapter for a more comprehensive and complete analysis.

3.2 Results and discussion

3.2.1 Synthesis of Ar-BIAN ligands and indium(III) complexes

Four Ar-BIAN ligands with *2,6*-diisopropyl (Dipp-BIAN, **3.1a**), *2,6*-dimethyl (Me_2Ar-BIAN, **3.2a**), *para*-nitro (*p*-NO_2Ar-BIAN, **3.3a**) and *para*-dimethylamino (*p*-NMe_2Ar-BIAN, **3.4a**) substituents on the diimine fragment were synthesized using different methodologies. The synthesis of **3.1a** involved refluxing acenaphthoquinone with 2,6-diisopropylaniline in a mixture of acetonitrile (ACN) and acetic acid (AcOH) for 4 h.[110] (Scheme 3.1) In the case of **3.2a** and **3.3a**, condensation of acenaphthoquinone with the corresponding aniline were carried out in the presence of Lewis acidic $ZnCl_2$, followed by demetallation with K_2CO_3 or $Na_2C_2O_4$ in aqueous solution.[11, 111] (Scheme 3.2)

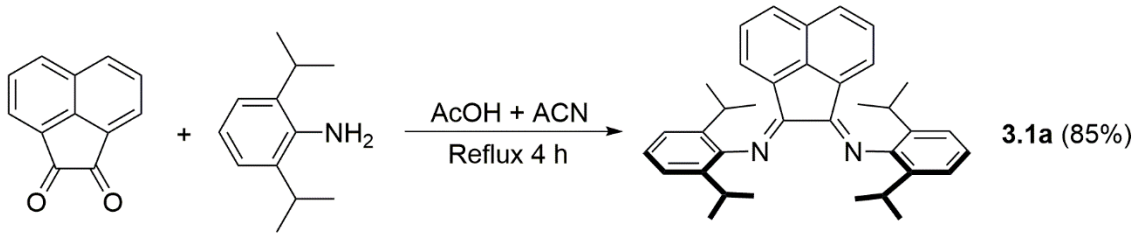

Scheme 3.1 *Synthesis of Dipp-BIAN (**3.1a**).*

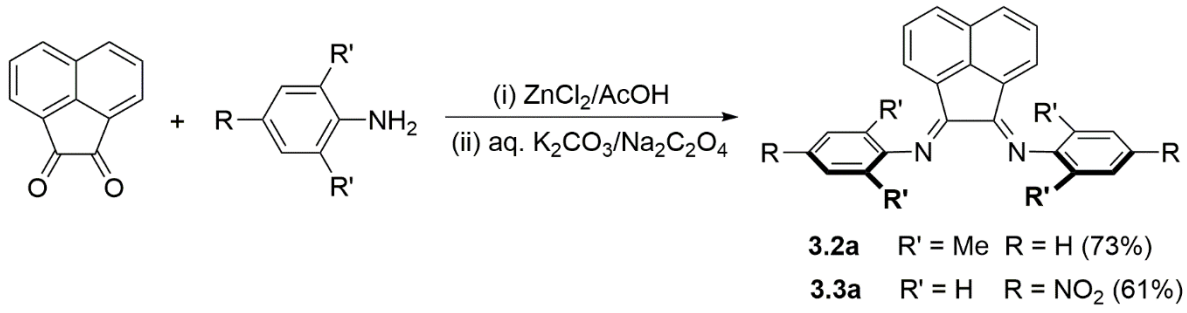

Scheme 3.2 *Synthesis of Me_2Ar-BIAN (**3.2a**) and p-NO_2Ar-BIAN (**3.3a**).*

However, when the $ZnCl_2$ templated method was attempted on the synthesis of *para*-amino substituted analog **3.4a**, ligand hydrolysis accompanied by mono-imine formation was always observed after demetallation with an aqueous solution of $Na_2C_2O_4$, which led to very little isolated

yield of the final product. (Figure 3.1) Therefore, we turned to the mechanochemical methodology which, as demonstrated in chapter 2, was successfully employed on the synthesis of substituted Ar-BIAN ligands. Accordingly, **3.4a** was prepared *via* ball milling in the presence of a small amount of AcOH and sodium sulfate (Na_2SO_4). (Scheme 3.3) A typical procedure involved putting all reactants and additives into a stainless steel grinder jar equipped with a 1 mm stainless steel ball (4 g by weight). This grinder jar was then put in a mixer mill machine and grinded at 30 Hz for 5 h.[64, 66] The ^{1}H NMR spectrum obtained after 5 h milling revealed quantitative formation of **3.4a** with only a trace amount of unreacted precursors, which can be removed after a simple workup procedure. (Figure 3.2)

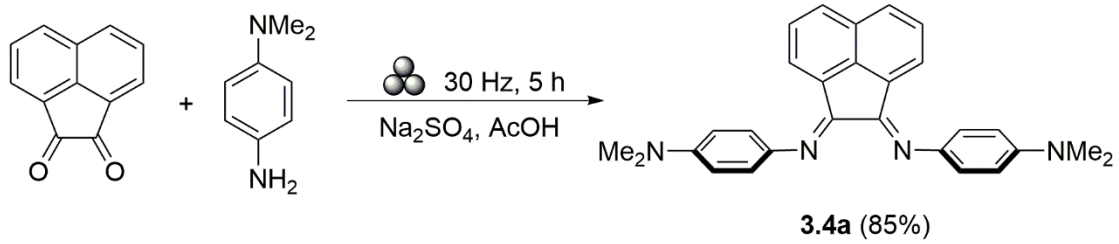

Scheme 3.3 *Synthesis of p-NMe_2Ar-BIAN (**3.4a**). The symbol for ball billing above the arrow of the equation was proposed by Hanusa et al.*[66]

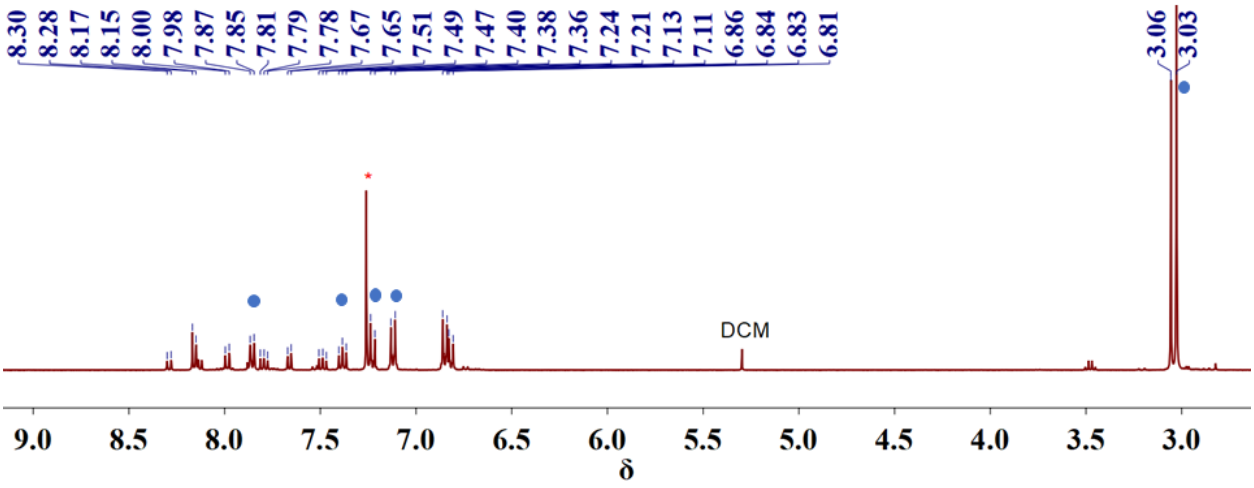

Figure 3.1 *The ^{1}H NMR spectrum of **3.4a** recorded in $CDCl_3$, synthesized by $ZnCl_2$ templated solution based method. (blue circles: desired product **3.4a**)*

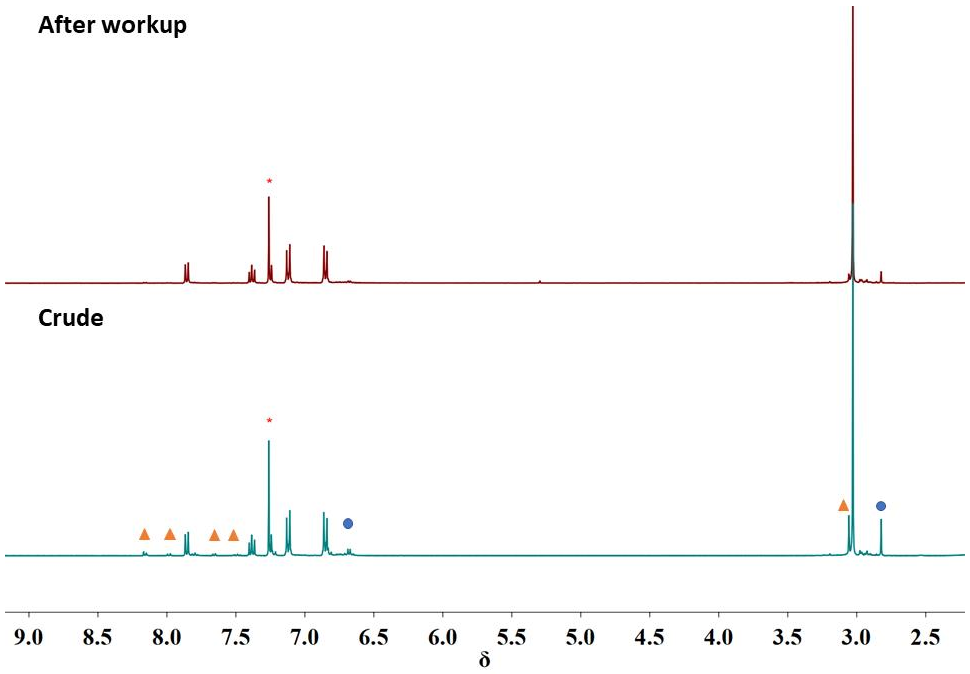

Figure 3.2 *The ^{1}H NMR spectrum of **3.4a** before and after purification recorded in $CDCl_3$, synthesized by ball milling. (Blue circles: N,N-Dimethyl-p-phenylenediamine, orange triangles: monoimine side product)*

The indium(III) Ar-BIAN complexes (**3.1b**-**3.4b**) were synthesized by reacting one equivalent of each Ar-BIAN ligands (**3.1a**-**3.4a**) with $InCl_3$ in tetrahydrofuran (THF). The syntheses of **3.1b**, **3.2b**, and **3.4b** were conducted at room temperature, whereas **3.3b** was prepared under reflux condition in THF. (Scheme 3.4) As previously discussed in chapter 2, compound **2.3** supported by the methoxy substituted Ar-BIAN ligand **2.1** (*vide supra*) formed a bis(BIAN) complex when ACN was used as the solvent for recrystallization. However, when **2.3** was recrystallized from a strongly coordinating solvent like DMF, a mono-BIAN complex was obtained, namely compound **3.5b** which will be discussed in this chapter together with **3.1b** – **3.4b**. In general, the ^{1}H and $^{13}C\{^{1}H\}$ NMR spectra obtained for **3.1b** to **3.4b** exhibit a downfield shift compared to the

corresponding spectra of the ligands **3.1a** to **3.4a**, concurring with the de-shielded ^{1}H environments on the ligand after coordination. Complexes **3.1b** and **3.2b** were purified by recrystallization from a combination of 1,2-dimethoxyethane (DME) and pentane, and tetrahydrofuran (THF) and pentane, respectively. In the case of **3.3b**, an analytically pure sample was obtained from diethyl ether (Et_2O) and *N*,*N*-dimethylformamide (DMF). However, single crystals suitable for single crystal X-ray diffraction analysis cannot be grown from this solvent combination and therefore, acetonitrile (ACN) was used for recrystallization instead. For **3.4b** and **3.5b**, recrystallization was carried out by vapor diffusion of Et_2O into a DMF solution of each complexes and therefore, one DMF molecule is coordinated to each indium(III) metal centers. (*vide infra*) The formation of **3.5b** was attributed to the stronger coordination provided by DMF as compared to ACN.

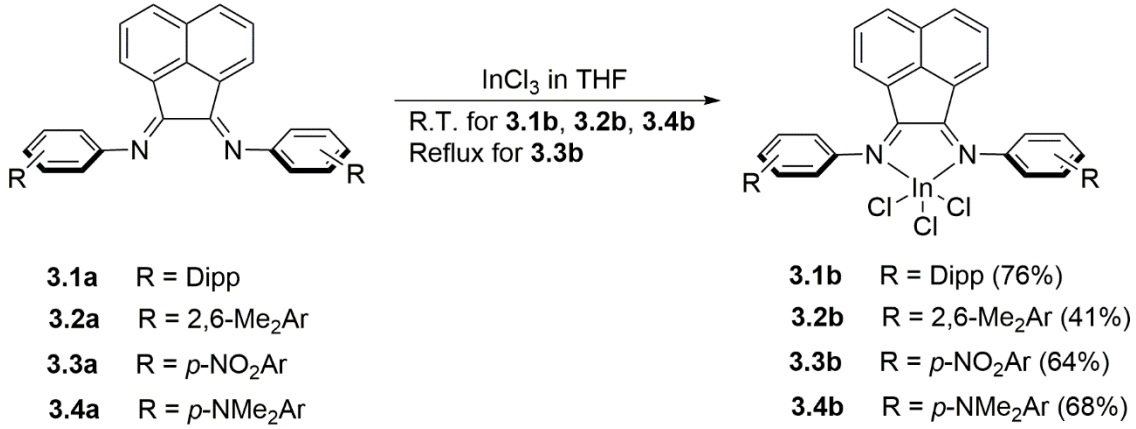

Scheme 3.4 *Synthesis of* ***3.1b*** *–* ***3.4b****.*

3.2.2 Spectroscopic and Crystallographic Studies

All indium(III) Ar-BIAN complexes **3.1b** to **3.5b** were successfully crystallized to give samples suitable for single crystal X-ray analysis. (Figure 3.3) In the following discussion, the two compounds reported in chapter 2, [(*p*-MeOAr-BIAN)$_2$InCl$_2$]$^+$[InCl$_4$]$^-$ (**2.3**) and [(*p*-BrAr-BIAN)InCl$_3$] (**2.4**), will be referred to for comparison. Complexes formed with *para*-substituents on the ligands (*i.e.* **3.3b**, **3.4b** and **3.5b**) generally adopt distorted octahedral geometry with

coordinating solvents (H_2O in **3.3b**, DMF in **3.4b** and **3.5b**) bound to each indium centers. The equatorial bond angles range from 72.6° to 101.1° in **3.3b**, 72.9° to 97.9° in **3.4b**, and 72.7° to 96.8° in **3.5b**, all of which deviate significantly from the ideal value of 90° for octahedral geometry. Similarly, the average of the three possible axial bond angles (164.7°, 164.6°, and 164.3° in **3.3b**, **3.4b**, and **3.5b**, respectively) also deviate from the expected 180°. This deviation of axial and equatorial bond angles in a distorted octahedral geometry was also reported in a complex of formula [(Mes-BIAN)In(THF)Cl_3].[47] In contrast, complexes **3.1b** and **3.2b** exhibit distorted square pyramidal geometries around the indium(III) center with Cl3 (for **3.1b**) and Cl2 (for **3.2b**) atoms being the apex of the square pyramid. The formation of this geometry is probably due to the increased steric hindrance around the metal center induced by the isopropyl (in **3.1b**) and methyl (in **3.2b**) substituents at the *ortho* positions of the aniline moiety.[47] The axial bond angles range from 95.9° to 110.1° in **3.1b** and from 100.9° to 107.4° in **3.2b**, comparable to the corresponding bond angles reported in the related indium(III) tetrakis(imino)pyracene (TIP) complexes which also adopt a distorted square pyramidal geometry around the indium center (94.2° – 117.4°).[112] Complex **3.2b** contains a plane of symmetry bisecting the acenaphthene moiety, passing through the indium metal center and Cl. This was further confirmed by the visulization of the asymmetric unit of the unit cell being exactly half of the whole complex. The presence of this mirror plane makes the two diimine N and Cl atoms at the equatorial positions equivalent.

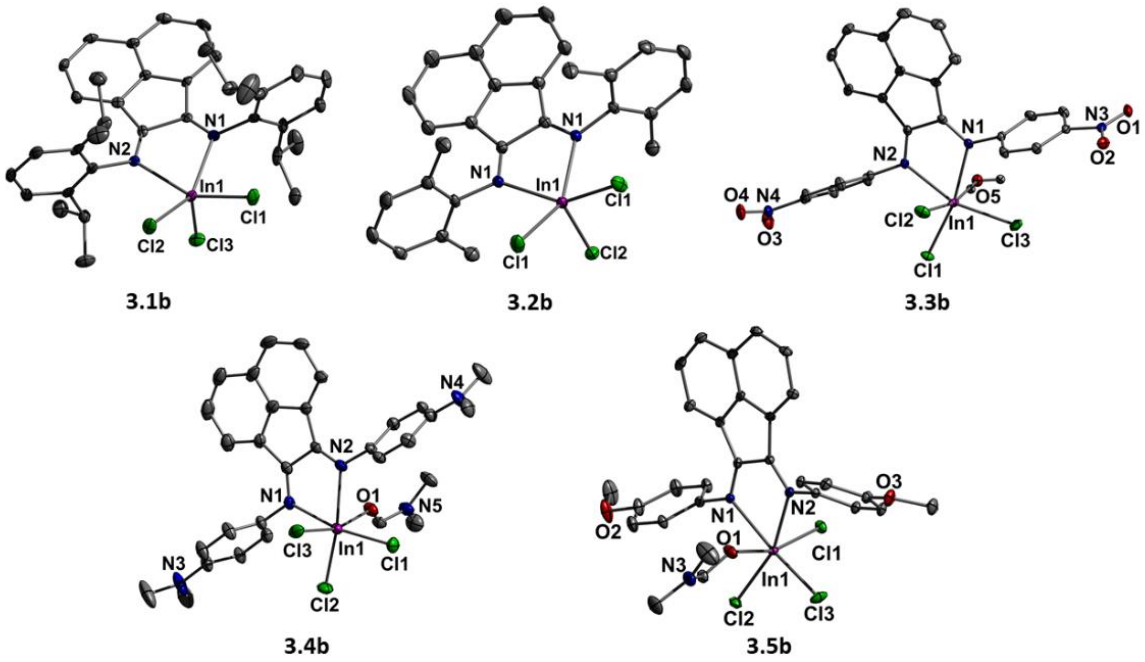

Figure 3.3 *Thermal ellipsoid plots (50%) of* ***3.1b*** *-* ***3.5b****. Hydrogen atoms have been omitted for clarity. Selected bond lengths (Å) and angles (°) of complexes (****3.1b****) In1-N1 2.342(5), In1-N2 2.339(5), In1-Cl1 2.3835(16), In1-Cl2 2.3800(17), In1-Cl3 2.3643(17); (3.****2b****) In1-N1 2.3196(15), In1-Cl1 2.3897(5), In1-Cl2 2.3769(7); (****3.3b****) In1-N1 2.3230(14), In1-N2 2.3114(14), In1-Cl1 2.4013(4), In1-Cl2 2.4722(5), In1-Cl3 2.4032(5), In1-O5 2.2733(13); (****3.4b****) In1-N1 2.317(3), In1-N2 2.331(3), In1-Cl1 2.4029(10), In1-Cl2 2.4241(9), In1-Cl3 2.4408(10), In1-O1 2.259(3); (****3.5b****) In1-N1 2.3182(14), In1-N2 2.3444(13), In1-Cl1 2.4417(4), In1-Cl2 2.4301(4), In1-Cl3 2.4058(5), In1-O1 2.2306(13).*

The C-C and average C=N bond distances within the diimine framework in **3.1b** – **3.5b** range from 1.52 Å to 1.54 Å and 1.27 Å to 1.29 Å respectively, and are consistent with the typical C-C single bond and C=N double bond lengths observed in many other similar diimine frameworks.[47, 112] Hence, all indium(III) complexes synthesized herein consist of neutral Ar-BIAN ligands coordinated to the indium metal center *via* dative bonds. The average In-N bond distances in **3.1b** and **3.2b** are 2.34 Å and 2.32 Å respectively, and are comparable to that reported in [(Mes-BIAN)In(THF)Cl_3] (2.35 Å).[47] This suggests that a variation of alkyl substituents on the aryl-

amine moiety did not induce significant changes on the binding strength of the ligands. For hexacoordinated mono BIAN complexes bearing electron donating NMe_2 and -OMe groups, the average In-N bond distances are 2.32 Å, 2.33 Å, and 2.33 Å in **3.4b**, **3.5b**, and **2.3** respectively. In the case of **3.3b** which is supported by electron withdrawing $-NO_2$ groups, the In-N bond distances range from 2.31 Å – 2.32 Å. Therefore, there does not exists a clear relationship between the substituents on the aryl diimine moiety of the Ar-BIAN ligand and the In-N bond distances of the resulting complex.

3.2.3 UV-vis and Electrochemical Studies

The absorption profile of the indium(III) complexes **3.1b** – **3.5b** were examined by UV-vis absorption spectroscopy. (Figure 3.4) The absorption maximum bands were collected in Table 3.1. In general, complexes **3.1b** to **3.5b** exhibit two major sets of absorption bands, consistent with that observed for **2.3** and **2.4** as discussed in Chapter 2. The relatively lower energy absorption bands were assigned to the intraligand n-π* transitions between the arylimine and the acenaphthene moiety, whereas those occurring at the higher energy region were attributed a mixture of the π-π* transitions, based on the TD-DFT calculations. (*vide infra)* A significant bathochromic shift was observed on the lower energy absorption band in **3.4b** as compared to those of the others. This is due to the presence of the electron donating $-NMe_2$ group on the *para*-position of the di(arylimino) moiety, which destabilized the HOMO and therefore induces a smaller HOMO-LUMO gap of the molecule.[113] Although the inductively electron donating alkyl groups, 2,6-diisopropyl and 2,6-dimethyl groups were present in **3.1b** and **3.2b** respectively, the effect is not as significant as the mesomerically electron donating $-NMe_2$ substituent present in **3.4b**. This hypothesis is also consistent with the DFT calculations carried out by Zysman-Colman's group.[17] They have reported that the HOMO of the ligand is destabilized by 1.1 eV when a mesomerically electron donating

group (*e.g.* NMe_2) is present on the diimine moiety, whereas a destabilization of only 0.29 eV is achieved when an inductively electron rich alkyl group (*e.g.* 2,4,6-trimethyl) is introduced. In contrast to the others, only a single intense absorption band at *ca.* 320 nm was observed for **3.3b**. This may result from a coincidental convergence of intraligand charge transfer transitions since the n-π* transition may have been hypsochromically shifted due to the presence of electron withdrawing $-NO_2$ group.

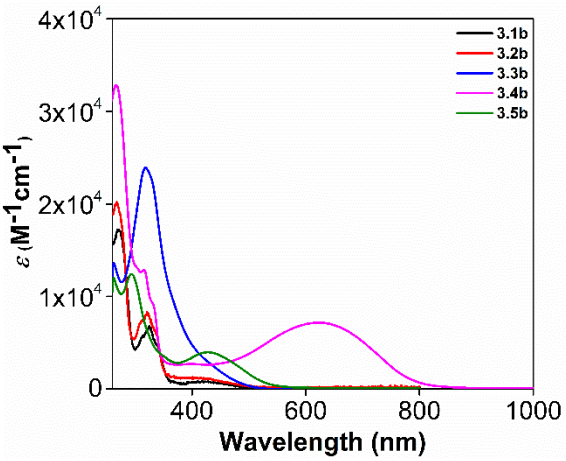

Figure 3.4 *UV-vis spectra for* ***3.1b*** *and* ***3.2b*** *in THF,* ***3.3b*** *and* ***3.5b*** *in DMF, and* ***3.4b*** *in DCM solution recorded at 298 K.*

Table 3.1 *Spectroscopic data for* ***3.1b*** *-* ***3.5b****.*

	Absorption maxima λ_{max} (nm)
3.1b	271, 325, 428
3.2b	268, 322, 428
3.3b	317
3.4b	267, 315, 625
3.5b	294, 429

The electrochemical behavior of **3.1b** to **3.4b** was studied by cyclic voltammetry with an initial objective to identify a suitable reducing agent with an adequate reduction potential to obtain the indium(I) derivatives of complexes **3.1b** to **3.4b**. (Figure 3.5) The electrochemical data is

summarized in Table 3.2. All potentials were reported relative to the ferrocenium/ferrocene (Fc^+/Fc) redox couple. The voltammogram for **3.5b** is not included in this chapter since its redox potential is expected to be identical to the previously reported complex **2.3** in chapter 2, which has been recorded in ACN.

During the cathodic scan, the electrochemical behavior of **3.1b**, **3.2b** and **3.3b** consists of four irreversible reductions followed by a series of oxidation processes. (Figure 3.5a, b, c and Figure 3.6a, b, c) These irreversible reductions may be due to the following. Firstly, dissociation of a Cl^- anion or coordination of a solvent molecule to the metal center may occur upon reduction of the indium(III) center, leading to structural changes during the voltammetric sweep. Secondly, the ligand itself may be reduced due to its non-innocent nature. Thirdly, the putative indium(I) species formed at the electrode surface may undergo disproportionation, which is also supported by our experimental findings (*vide infra*). In contrast, a chemically reversible reduction wave at -1.2 V was observed during the cathodic scan of **3.4b**. (Figure 3.5d and Figure 3.6d) This suggested an increased stability of the putative $[(NMe_2Ar\text{-}BIAN)InCl_3]^-$. Similar finding was also reported in chapter 2, whereby complex **2.3** bearing an electron donating methoxy group exhibited an electrochemically reversible reduction wave at -1.46 V. This was also attributed to the stronger electron donation from the corresponding ligand **2.1**. Although the assignment of each reduction and oxidation waves in **3.1b** to **3.4b** was hampered because of the complex processes at the electrode surface, their voltammograms still indicate that the as synthesized indium(III) complexes can be reduced electrochemically using mild reduction agents with potentials between -1.0 V to -2.0 V.[114]

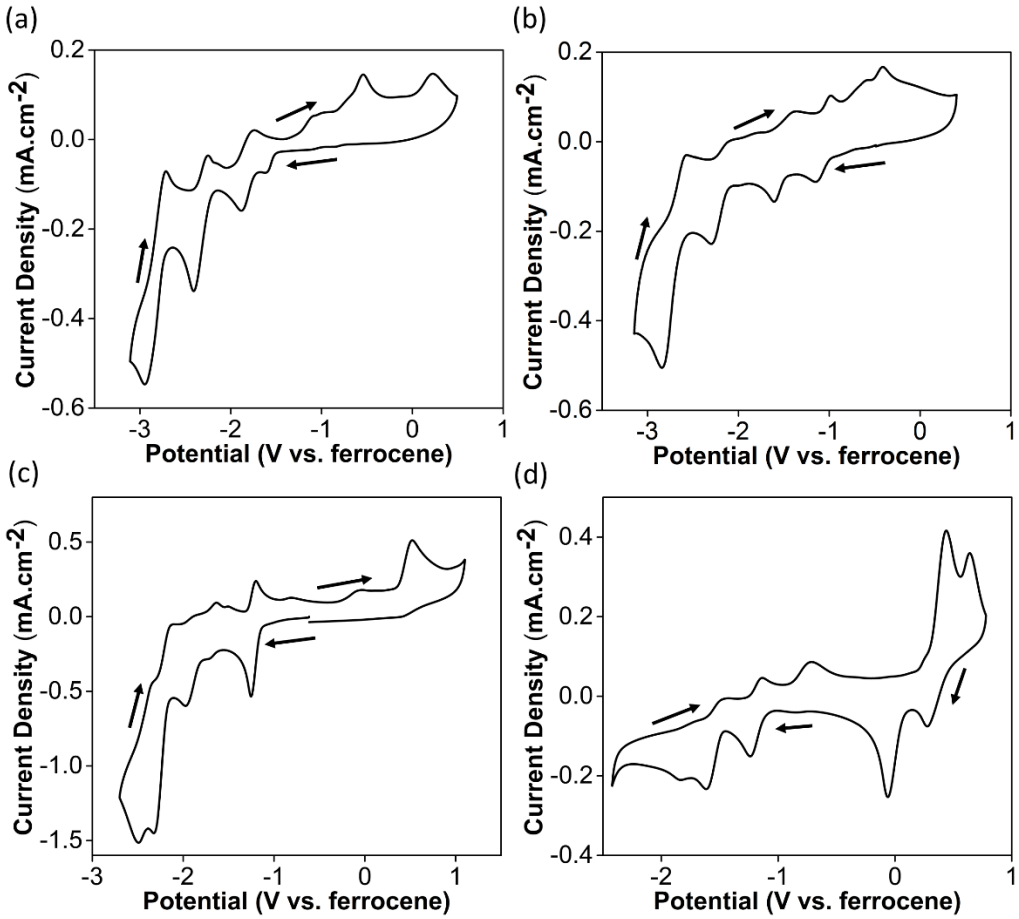

Figure 3.5 *Cyclic voltammograms for (a)* ***3.1b*** *in THF, (b)* ***3.2b*** *in THF, (c)* ***3.3b*** *in DMF, and (d)* ***3.4b*** *in DCM solution at 298 K, with 0.10 M* $(nBu_4N)PF_6$ *as the supporting electrolyte and glassy carbon (3 mm in diameter) as the working electrode. Scan rate: 100 mV* s^{-1}.

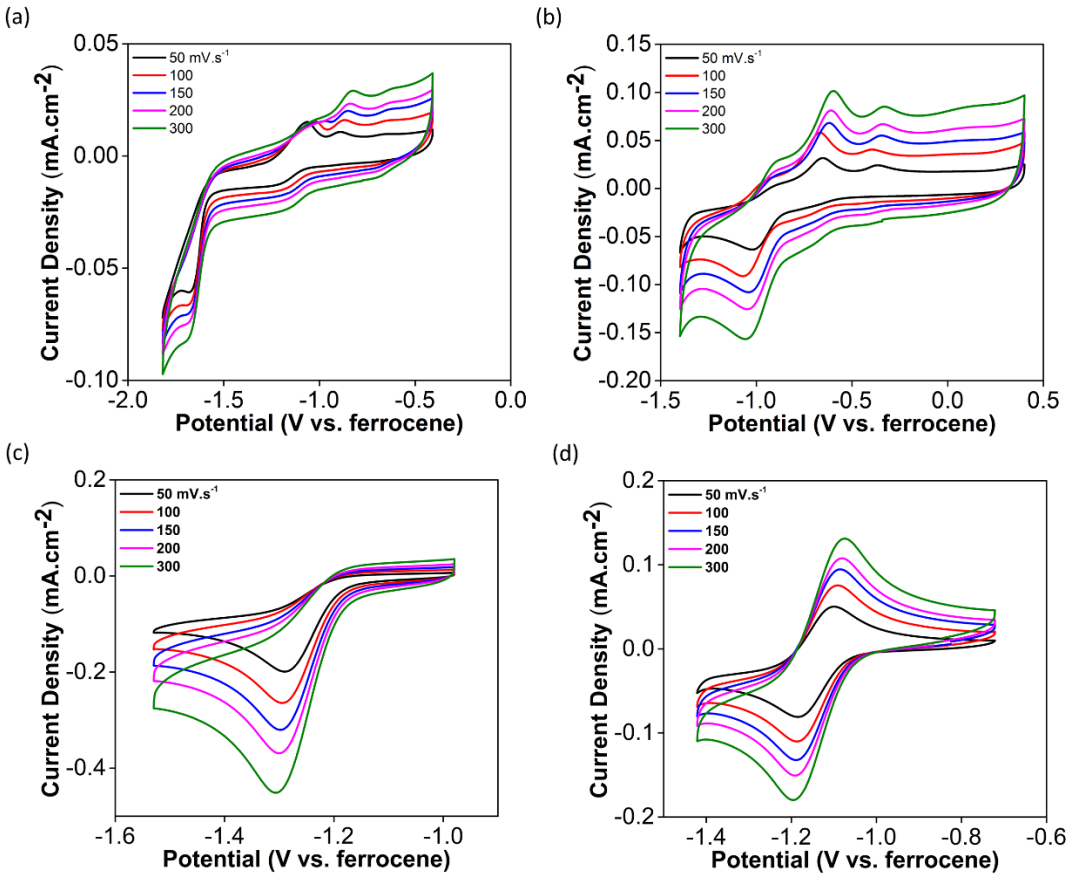

Figure 3.6 *Cyclic voltammograms of the first reduction wave for* ***3.1b*** *(a) in THF,* ***3.2b*** *(b) in THF,* ***3.3b*** *(c) in DMF, and* ***3.4b*** *(d) in DCM solution at 298 K with different scan rates.*

Table 3.2 *Electrochemical data **3.1b** to **3.4b**.*

	Potential (V vs. Fc^+/Fc)	
	Cathodic peaks	Anodic peaks
3.1b	-1.61	-2.72
	-1.87	-2.26
	-2.41	-1.75
	-2.95	-0.54
		+0.22
3.2b	-1.14	-2.57
	-1.61	-2.11
	-2.30	-1.38
	-2.84	-0.98
		-0.42
3.3b	-1.25	-2.14
	-1.97	-1.64
	-2.32	-1.21
	-2.49	-0.08
		+0.51
3.4b	+0.28	-1.47
	-0.06	-1.15
	-1.24	-0.72
	-1.62	+0.44
	-1.85	+0.64

In view of the possible electrochemical reduction of the indium(III) BIAN complexes as indicated by the cyclic voltammetry studies, the reduction of **3.1b** was attempted using magnesium anthracene in THF. Unfortunately, indium metal deposition was observed from the reaction mixture and the protonated form of the reduced **3.1a** was formed from this reaction, as indicated by a singlet at 5.06 ppm in the ^{1}H NMR spectrum which corresponds to the N-H hydrogen atoms. Similar reduction reaction was also carried out for complex **2.3** using $CoCp_2$. Again, only ligand reduction was observed instead of reduction of the complex. The structure of the reduced and protonated ligand **2.1**, namely **3.6**, was confirmed by single crystal X-ray analysis. (Figure 3.7) The observed formation of reduced ligands in the attempted reduction reactions of **3.1b** and **2.3** may be attributed to two possible reasons. The first one is the redox non-innocent nature of the Ar-BIAN ligand. As discussed in Chapter 1, in coordination complexes bearing redox active ligands, reduction reactions sometimes occur on the ligand rather than on the metal centre for both main group[43, 104] and transition metals.[115] We propose that when complexes **3.1b** and **2.3** are dissolved in solution, the Ar-BIAN ligands may dissociate and quickly exchange with the solvent molecules by coordinating to $InCl_3$. Therefore, upon introduction of the reducing agents, the reduction of the Ar-BIAN ligands occur

concurrently with the indium(III) metal centre, and in the presence of trace amount of water, reduced ligands with a structure similar to **3.6** would form. The second possible reason may be the instability of the putative In(I) species. This may cause ligand dissociation from the metal after reduction, which leads to disproportionation of In(I) to indium metal and In(III) on one hand and reduction a the free Ar-BIAN ligand on the other hand.

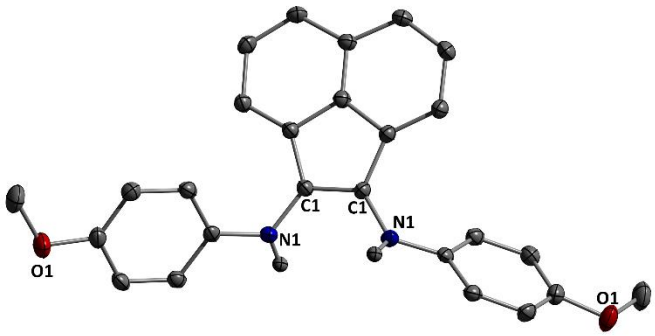

Figure 3.7 *Crystal structure of **3.6**. Thermal ellipsoids are drawn at the 50% probability level. Hydrogen atoms have been omitted for clarity.*

3.2.4 Computational studies

DFT and TD-DFT calculations were carried out to predict the electronic absorption spectra of the indium(III) complexes **3.1b** – **3.4b** described herein. Since the calculation from a larger basis set 6-31++G* produced almost identical outcomes as the smaller 6-31+G* basis set for complexes **2.3** and **2.4** discussed in chapter 2, all geometry optimizations were carried out with the smaller 6-31+G* basis set in this chapter since it is computationally more cost effective. Other parameters remained identical as those reported in Chapter 2. The optimized structures of complexes **3.1b** and **3.2b** both contained a plane of symmetry bisecting the acenaphthene moiety and the indium metal center. For complexes **3.3b** and **3.4b**, one H_2O and one DMF molecule were included for the geometry optimization respectively, resulting in an octahedral geometry around the metal center. In general,

the optimized ground state structures for **3.1b** – **3.4b** agreed well with our X-ray crystallographic studies. (Figure 3.8)

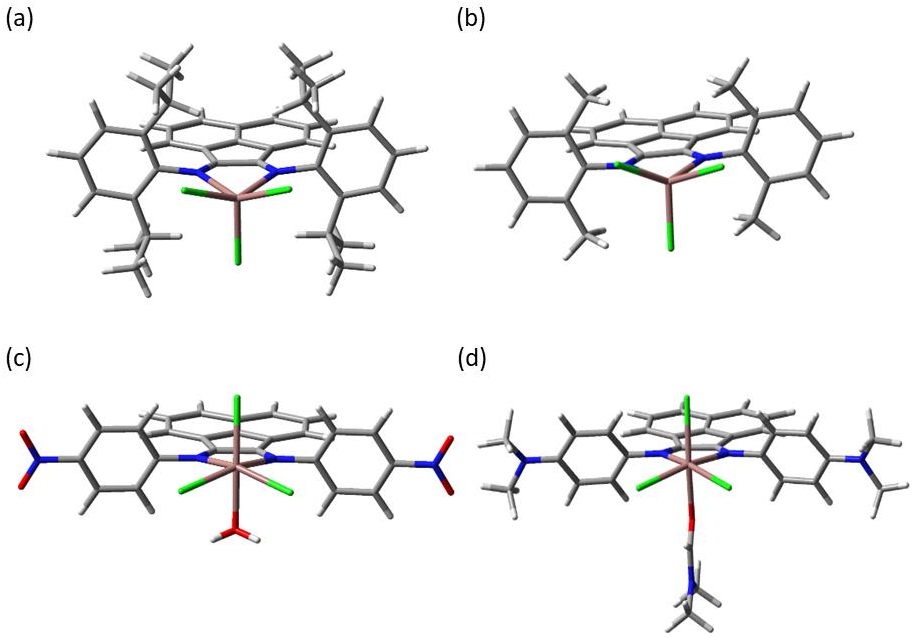

Figure 3.8 *Geometry optimization at the B3LYP/6-31+G*/LANL2DZ level of theory for (a)* ***3.1b****, (b)* ***3.2b****, (c)* ***3.3b****, and (d)* ***3.4b****.*

The theoretical electronic absorption spectra of **3.1b** – **3.4b** were predicted by TD-DFT calculations. (Figure 3.9) In general, the experimentally determined absorption profiles match well with the calculated ones, especially when solvent effects are taken into account. The calculated predominant contributions to the absorption maxima for **3.1b** and **3.2b** (λ_{max} = 320 nm) correspond mainly to electronic transitions from HOMO-3 → LUMO+1 in both cases, while for **3.3b** (λ_{max} = 318 nm), it corresponds largely to a combination of HOMO → LUMO+3, HOMO-1 → LUMO+2, and HOMO-8 → LUMO transitions. (Tables 3.3 to 3.5) In the case of **3.4b**, the lower energy absorption maximum (λ_{max} = 630 nm) is attributed exclusively to the HOMO → LUMO transition, while the higher energy absorption band (λ_{max} = 267 nm) consists of a mixture of HOMO-14 → LUMO and HOMO-15 → LUMO transitions. (Table 3.6)

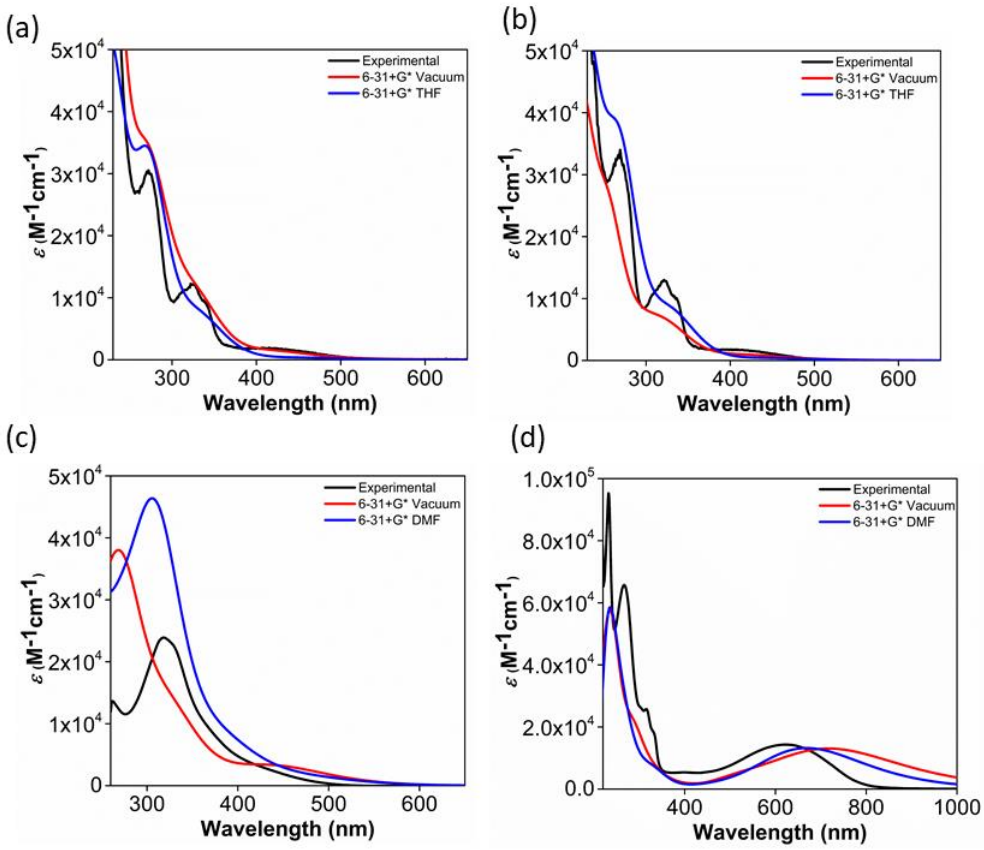

Figure 3.9 *Calculated and experimental absorption spectra for (a)* ***3.1b*** *and (b)* ***3.2b*** *in THF****,*** *(c)* ***3.3b*** *in DMF and (d)* ***3.4b*** *in DCM.*

Table 3.3 *Orbital contributions to the electronic absorption transitions of* ***3.1b*** *using a B3LYP/6-31+G* level of theory; only transitions with oscillator strengths >0.03 have been taken into account*.

Transition	λ_{max} (nm)	*f*	Orbital contributions (%)
HOMO-13 →LUMO HOMO-3 →LUMO+1	332	0.1340	4.64 90.93

Table 3.4 *Orbital contributions to the electronic absorption transitions of* ***3.2b*** *using a B3LYP/6-31+G* level of theory; only transitions with oscillator strengths >0.03 have been taken into account*.

Transition	λ_{max} (nm)	*f*	Orbital contributions (%)
HOMO-12 → LUMO	330	0.1492	4.49
HOMO-4 → LUMO+1			18.33
HOMO-3 → LUMO+1			69.74
HOMO-1 → LUMO+1			2.34

Table 3.5 *Orbital contributions to the electronic absorption transitions of* ***3.3b*** *using a B3LYP/6-31+G* level of theory; only transitions with oscillator strengths >0.03 have been taken into account*.

Transition	λ_{max} (nm)	*f*	Orbital contributions (%)
HOMO-1 → LUMO	391	0.1017	94.6
HOMO-1 → LUMO+2			2.40
HOMO-6 → LUMO	334	0.1113	2.79
HOMO → LUMO+3			87.7
HOMO-5 → LUMO+1	313	0.4282	6.58
HOMO-4 → LUMO+2			8.46
HOMO-3 → LUMO+1			6.04
HOMO-2 → LUMO+1			14.5
HOMO-1 → LUMO+2			56.5
HOMO-8 → LUMO	308	0.1450	53.37
HOMO-5 → LUMO+1			2.80
HOMO-4 → LUMO+2			5.37
HOMO-3 → LUMO+1			3.42
HOMO-2 → LUMO+1			13.97
HOMO-1 → LUMO+2			18.4

Table 3.6 *Orbital contributions to the electronic absorption transitions of* ***3.4b*** *using a B3LYP/6-31+G* level of theory; only transitions with oscillator strengths >0.03 have been taken into account*.

Transition	λ_{max} (nm)	*f*	Orbital contributions (%)
HOMO → LUMO	709	0.3773	99
HOMO-15 → LUMO	288	0.1201	3.1
HOMO-14 → LUMO			79.7
HOMO-1 → LUMO+3			5.8
HOMO → LUMO+4			4.1
HOMO-15 → LUMO	281	0.1223	76.7
HOMO-14 → LUMO			5.96
HOMO-1 → LUMO+3			9.48

The frontier orbitals illustrating the electron density distribution for **3.1b** to **3.4b** are shown in Figure 3.10. For **3.1b**, **3.2b**, and **3.4b**, the HOMO is largely distributed on the aryl(diimine) part of the Ar-BIAN ligand, while the LUMO is mainly localized on the acenaphthene moiety. In contrast, for **3.3b**, a reverse in electron density distribution is observed with the HOMO being localized on the acenaphthene bay region, whereas the LUMO has distributed contributions throughout the entire ligand. This intriguing reversal in orbital density when strongly electron-withdrawing groups are introduced on the aryl(diimine) motif is consistent with the previously reported DFT calculations performed on a series of Ar-BIAN ligand by Zysman-Colman's group.[17]

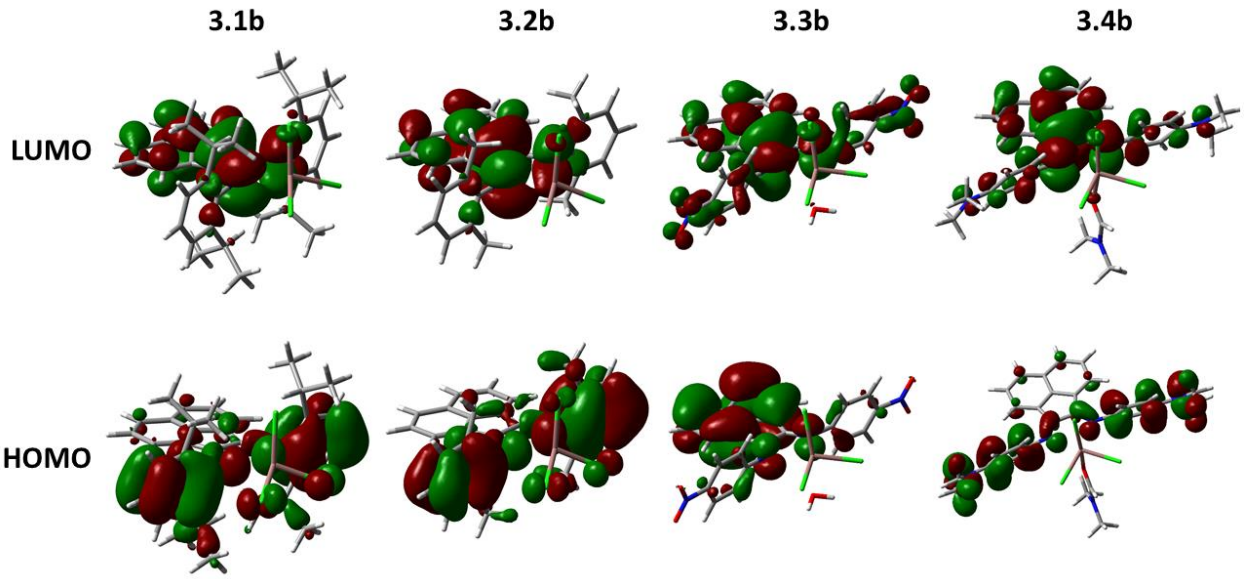

Figure 3.10 *Electron density distributions of the frontier orbitals for* ***3.1b*** *to* ***3.4b****.*

3.3 Conclusions

In this chapter, a comprehensive study on the synthesis, absorption, and electrochemical properties of five indium(III) complexes bearing redox non-innocent Ar-BIAN ligands (**3.1b** – **3.5b**) was reported. All complexes discussed herein absorb light in the UV and visible region of the electromagnetic spectrum, with complex **3.4b** absorbing the lower energy end due to the presence of strongly electron donating -NMe_2 substituents, which reduced the HOMO-LUMO gap of the complex. On the contrary, the absorption profile of **3.3b** revealed a single intense band at 320 nm resulting from enlarged frontier orbital energy gaps arising from the electron withdrawing -NO_2 substituents. Although cyclic voltammetry studies for **3.1b** – **3.4b** suggested the feasibility of electrochemical reduction of the indium(III) complexes to their indium(I) counterpart, attempted reduction of **3.1b** using magnesium anthracene resulted in reduction of the ligand and disproportionation with concomitant indium metal deposition. This was attributed to the non-innocent redox behavior of the Ar-BIAN ligand, which can accommodate extra electrons more

readily than the indium metal center. In future syntheses, even bulkier substituents at the 2,6-position of aryl-imine moiety will be explored to kinetically stabilize the indium(I) products, which has been successfully adopted by Jurca *et. al.* for the formation bis(imino)pyridine indium(I) complexes.[116]

3.4 Experimental and analytical techniques

General considerations and instrument specifications stay the same as those described in chapter 2.

3.4.1 Synthesis of Ar-BIAN ligands (3.1a - 3.4a)

*Dipp-BIAN (**3.1a**)*

The procedure was adopted from the literature.[110] Acenaphthenequinone (0.21 g, 1.1 mmol) was suspended in acetonitrile (10 mL) and heated under reflux for 1 h. Acetic acid (1.90 mL) was then added and continue to reflux for 1 h until an orange solution was formed. To this hot solution, 2,6-diisopropylaniline (0.51 mL, 2.7 mmol) was added and the resulted mixture was heated under reflux for 3 h and then cooled to room temperature. The resultant orange suspension was filtered, washed twice with hexane (10 × 2 mL) and air dried. The isolated yield of the product was 0.48 g (85%). ^{1}H NMR (400 MHz, CD_2Cl_2): δ = 0.97 (d, J = 6.8 Hz, 12 H), 1.23 (d, J = 6.8 Hz, 12 H), 3.03 (sept, J = 6.8 Hz, 4 H), 6.63 (d, J = 7.2 Hz, 2 H), 7.26 (m, overlapping with $CDCl_3$ signal), 7.36 (t, J = 7.8 Hz, 2 H), 7.87 (d, J = 8.4 Hz, 2 H). HRMS (ESI+, *m/z*) calculated for $C_{36}H_{41}N_2$ $[M+H]^+$ *m/z* = 501.3270, found 501.3269.

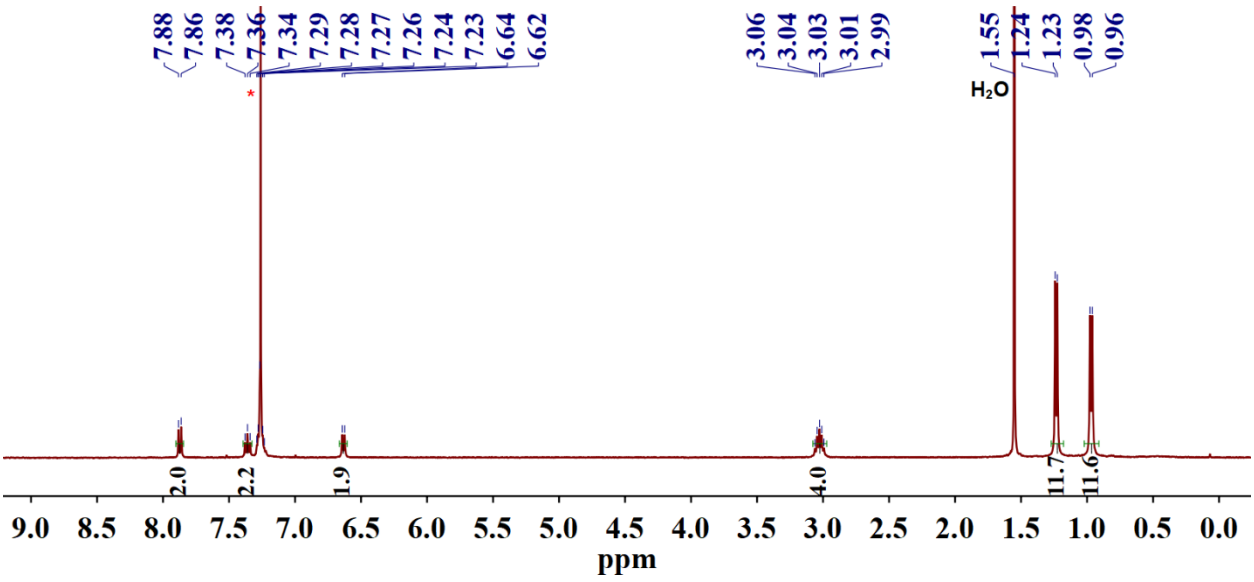

Figure 3.11 *The ^{1}H NMR spectrum of* ***3.1a*** *recorded in $CDCl_3$.*

*2,6-Me_2Ar-BIAN (**3.2a**)*

The procedure was adopted from a literature procedure.[111] An oven dried two neck round bottom flask was charged with $ZnCl_2$ (0.97 g, 7.1 mmol) and it was vacuumed for 1 h. A suspension of acenaphthoquinone (0.48 g, 2.6 mmol) in acetic acid (20 mL) was added and the mixture was warmed to 60 °C. 2,6-dimethylaniline (0.74 mL, 6.0 mmol) was then added and heated to reflux for 1 h. The suspension was filtered through Buchner funnel while hot and the residue was washed with ether (4 × 20 ml). The resultant zinc chloride complex was suspended in CH_2Cl_2 (40 mL) in a separatory funnel. A solution of sodium oxalate (0.46 g, 3.4 mmol) in water (20 mL) was added. The layers were separated, and the organic layer was washed with water (2 x 10 mL), dried over $MgSO_4$ and concentrated under vacuum. The isolated yield of the product was 0.74 g (73%). ^{1}H NMR (400 MHz, $CDCl_3$): δ = 2.14 (s, 12 H), 6.71 (d, J = 7.2 Hz, 2 H), 7.06-7.10 (m, 2 H), 7.16-7.17 (m, 4 H), 7.39 (t, J = 7.8 Hz, 2 H), 7.90 (d, J = 8.0 Hz, 2 H). HRMS (ESI+, *m/z*) calculated for $C_{28}H_{25}N_2$ $[M+H]^+$ *m/z* = 389.2018, found 389.2028.

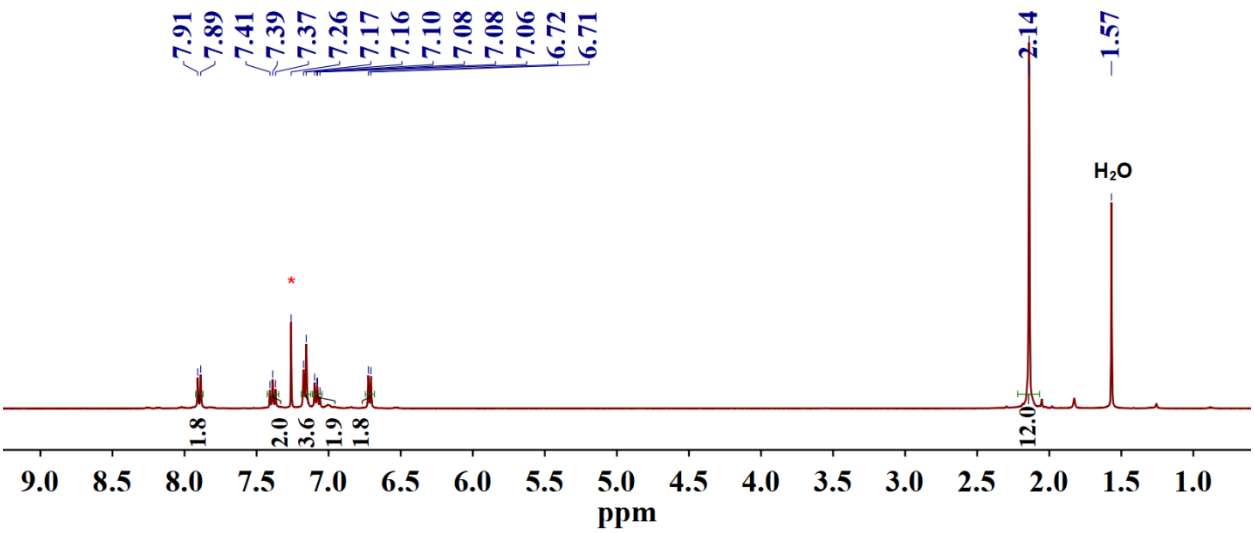

Figure 3.12 *The ^{1}H NMR spectrum of* ***3.2a*** *recorded in $CDCl_3$.*

*p-NO_2Ar-BIAN (**3.3a**)*

This procedure was adopted from the literature.[11] An oven dried two neck round bottom flask was charged with $ZnCl_2$ (1.00 g, 7.3 mmol) and it was vacuumed for 1 h. A suspension of acenaphthoquinone (0.50 g, 2.7 mmol) in acetic acid (10 mL) was added and the mixture was warmed to 60 °C. 4-nitroaniline (0.74 mL, 6.0 mmol) was then added and heated to reflux for 1 h. The reaction mixture was filtered through Buchner funnel while hot and the residue was washed with ether (4 × 10 ml). The resultant khaki zinc chloride complex was suspended in CH_2Cl_2 (60 mL) in a separatory funnel. A solution of sodium oxalate (1.29 g, 9.7 mmol) in water (20 mL) was added. The layers were separated, and the organic layer was washed with water (2 x 10 mL), dried over $NaSO_4$ and concentrated under reduce pressure. The isolated yield of the product was 0.69 g (61%). ^{1}H NMR (400 MHz, $CDCl_3$): δ = 6.91 (d, J = 7.2 Hz, 2 H), 7.25-7.27 (m, overlapping with $CDCl_3$ signal, 4 H), 7.48 (t, J = 7.6 Hz, 2 H), 8.02 (d, J = 8.4 Hz, 2 H), 8.41 (d, J = 8.4 Hz, 4 H). HRMS (ESI+, m/z) calculated for $C_{24}H_{15}N_4O_4$ $[M + H]^+$ m/z = 423.1093, found 423.1086.

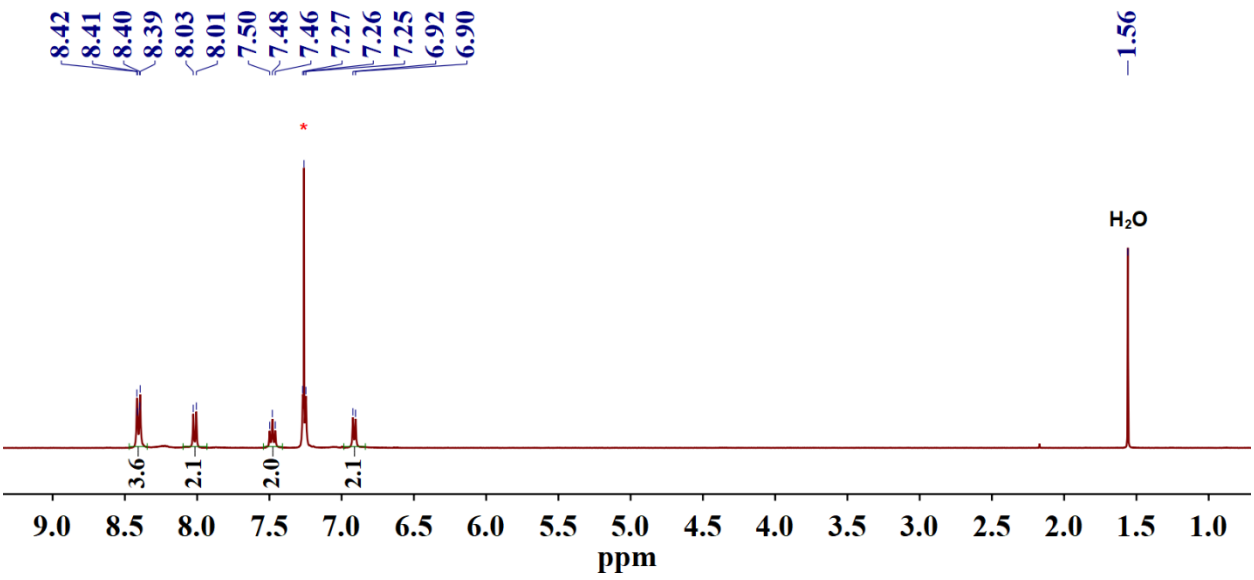

Figure 3.13 *The ^{1}H NMR spectrum of* ***3.3a*** *recorded in $CDCl_3$.*

*p-NMe_2Ar-BIAN (**3.4a**)*

The synthesis was carried out by a mechanochemical approach. A stainless steel grinder jar was charged with acenaphthoquinone (0.055 g, 0.30 mmol), *N*,*N*-dimethyl-1,4-phenylenediamine (0.094 g, 0.69 mmol), catalytic amounts of acetic acid (4.3 µL, 0.075 mmol, 25 mol%), and Na_2SO_4 (0.043 g, 0.30 mmol), and a 10 mm stainless steel ball. The jar was then grinded for 5 h at 30 Hz. The resultant dark purple solid was washed with Et_2O and the isolated yield was 0.11 g (85%). ^{1}H NMR (400 MHz, $CDCl_3$): δ = 3.03 (s, 12 H), 6.84-6.86 (m, 4 H), 7.11-7.13 (m, 4 H), 7.24-7.26 (d, overlapping with $CDCl_3$ signal, 2 H), 7.39 (t, J = 7.8 Hz, 2 H), 7.86 (d, J = 8.4 Hz, 2 H). HRMS (ESI+, m/z) calculated for $C_{28}H_{27}N_4$ $[M + H]^+$ m/z = 419.2236, found 419.2229.

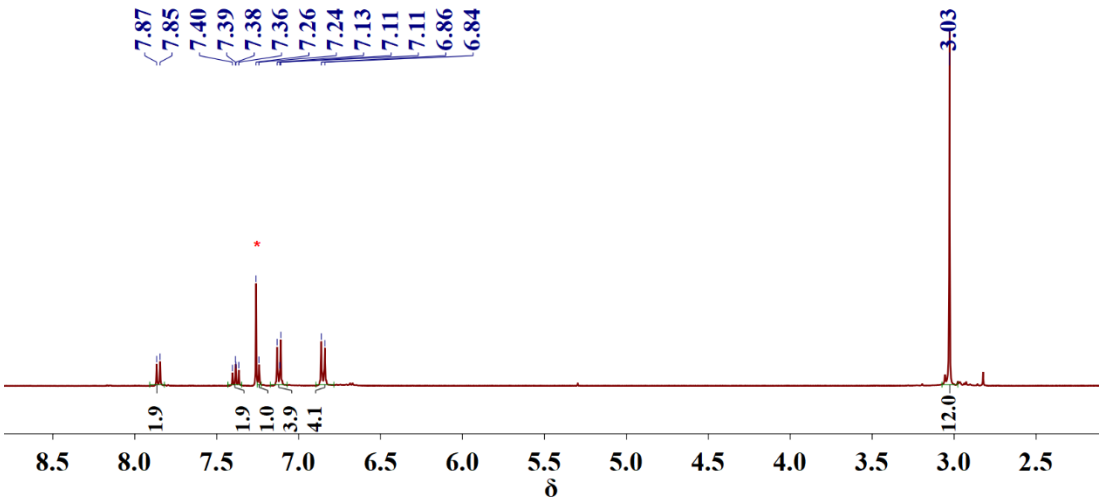

Figure 3.14 *The ^{1}H NMR spectrum of* ***3.4a*** *recorded in $CDCl_3$.*

3.4.2 Synthesis of indium(III) complexes (3.1b – 3.5b)

*[(Dipp-BIAN)$InCl_3$] (**3.1b**)*

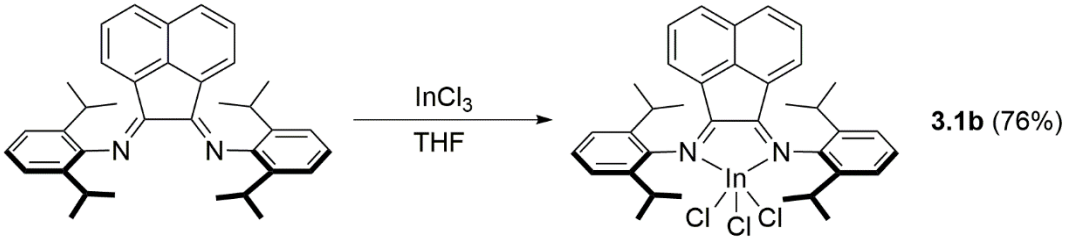

Scheme 3.5 *Synthesis of [(Dipp-BIAN)$InCl_3$] (**3.1b**).*

A solution of $InCl_3$ (0.025 g, 0.11 mmol) in THF (5 mL) was added to a solution of Dipp-BIAN (0.056 g, 0.11 mmol) in THF (5 mL) at room temperature. The resulting orange solution was stirred overnight, after which all volatiles were removed under vacuum. The resultant orange powder was recrystallized by vapor diffusion of pentane into a DME solution of the crude product and the isolated yield was 0.061 g (76%). ^{1}H NMR (400 MHz, $CDCl_3$): δ = 0.87 (d, J = 7.2 Hz, 12 H), 1.38 (d, J = 6.8 Hz, 12 H), 3.07 (sept, J = 6.8 Hz, 4 H), 6.75 (d, J = 7.2 Hz, 2 H), 7.40 (d, J = 7.6 Hz, 4 H), 7.50-7.54 (m, 2 H), 7.60 (t, J = 8.0 Hz, 2 H), 8.17 (d, J = 8.0 Hz, 2 H). $^{13}C\{^{1}H\}$ NMR (100 MHz, $CDCl_3$): δ = 24.4, 24.8, 29.9, 125.1, 126.2, 127.8, 129.1, 129.3, 131.1, 133.2, 140.0,

140.3, 144.3, 162.7. m.p.: decomposed at 280 °C. HRMS (ESI+, *m/z*) calculated for $C_{36}H_{40}N_2InCl_3Na$ $[M+Na]^+$ *m/z* = 743.1194, found 743.1179. Anal. Calcd. for $C_{36}H_{40}N_2InCl_3$: C, 59.90; H, 5.59; N, 3.88. Found: C, 59.56; H, 5.43; N, 3.82.

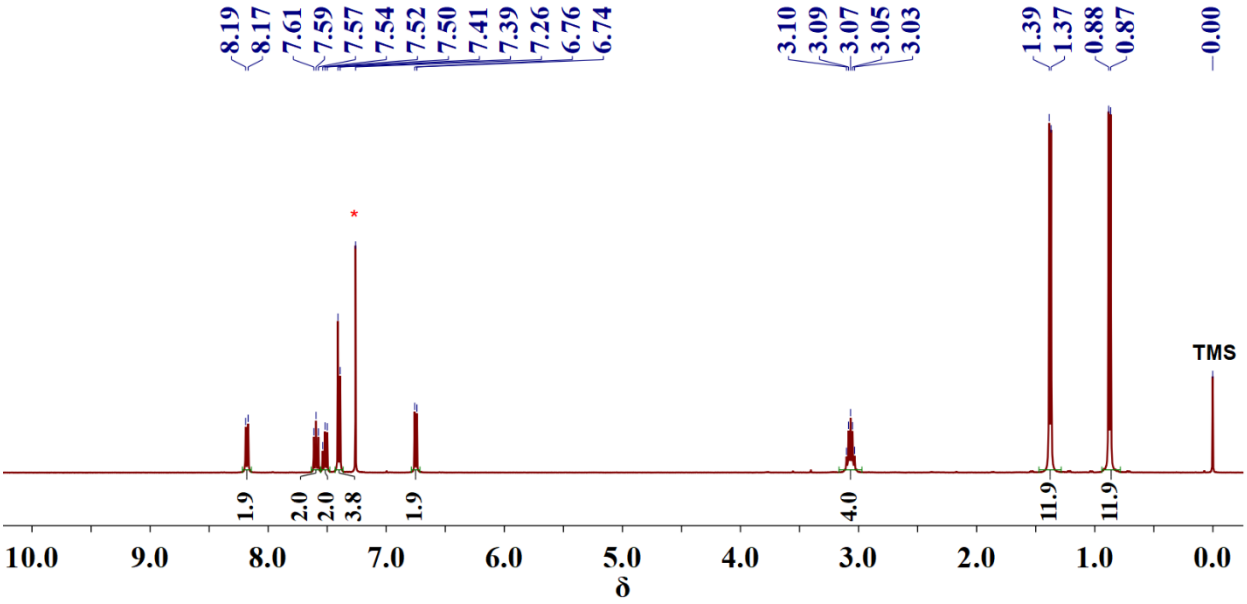

Figure 3.15 *The ^1H NMR spectrum of* ***3.1b*** *recorded in $CDCl_3$.*

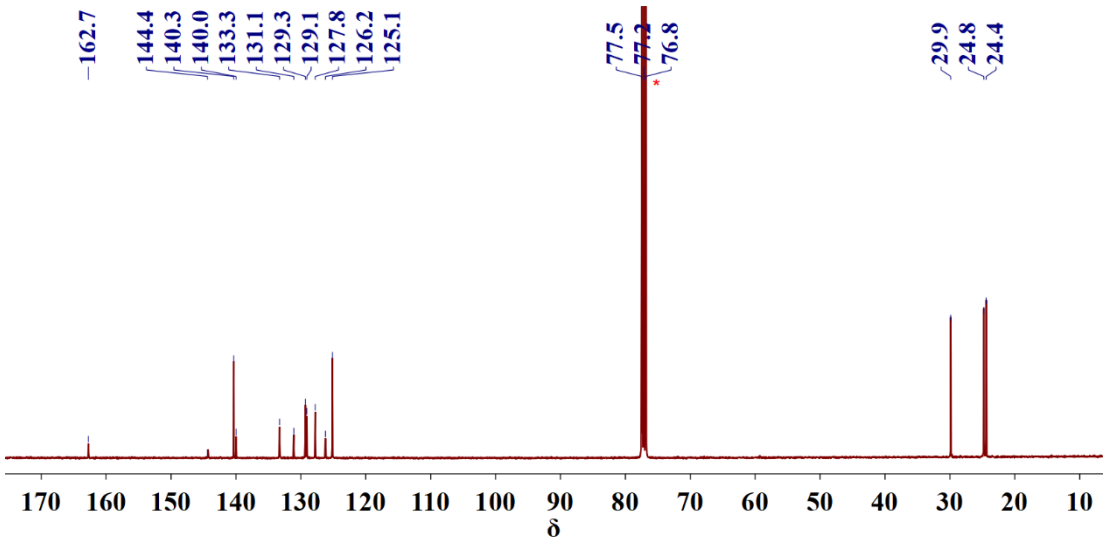

Figure 3.16 *The ^{13}C NMR spectrum of* ***3.1b*** *recorded in $CDCl_3$.*

*[(2,6-Me$_2$Ar-BIAN)InCl$_3$] (**3.2b**)*

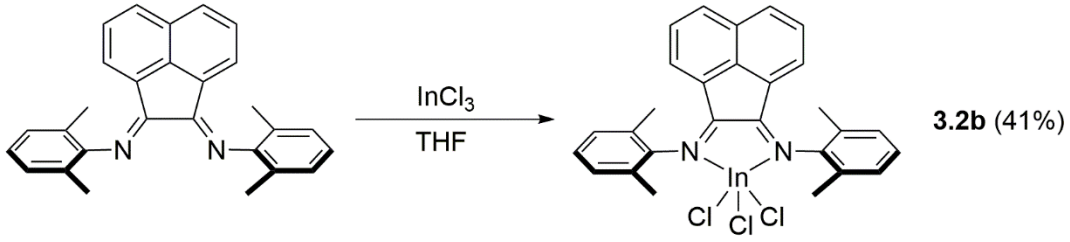

***Scheme 3.6** Synthesis of [(2,6-Me$_2$Ar-BIAN)InCl$_3$] (**3.2b**).*

The procedure was identical to the one reported above for **3.1b**. The following quantities of reagents were used: $InCl_3$ (0.023 g, 0.10 mmol) in THF (5 mL), 2,6-Me$_2$Ar-BIAN (0.040 g, 0.10 mmol) in THF (5 mL). Orange block-like crystals suitable for single crystal X-ray analysis were obtained by recrystallization via vapor diffusion of pentane into a THF solution of the crude product and the isolated yield was 0.026 g (41%). ^{1}H NMR (400 MHz, $CDCl_3$): δ = 2.30 (s, 12 H), 6.79 (d, J = 7.2 Hz, 2 H), 7.28-7.30 (m, overlapping with $CDCl_3$ signal, 4 H), 7.33-7.37 (m, 2 H), 7.62 (t, J = 7.8 Hz, 2 H), 8.21 (d, J = 8.4 Hz, 2 H). ^{13}C{^{1}H} NMR (100 MHz, $CDCl_3$): δ = 19.0, 125.8, 126.7, 128.4, 129.6 (two overlapping signals), 129.9, 131.1, 133.5, 142.1, 144.6, 162.3. m.p.: decomposed at 273 °C. HRMS (ESI+, *m/z*) calculated for $C_{28}H_{24}N_2InCl_3Na$ $[M+Na]^+$ *m/z* = 630.9942, found 630.9954. Anal. Calcd. for $C_{28}H_{24}N_2InCl_3 \cdot THF \cdot H_2O$: C, 54.92; H, 4.90; N, 4.00. Found: C, 55.16; H, 4.93; N, 4.26.

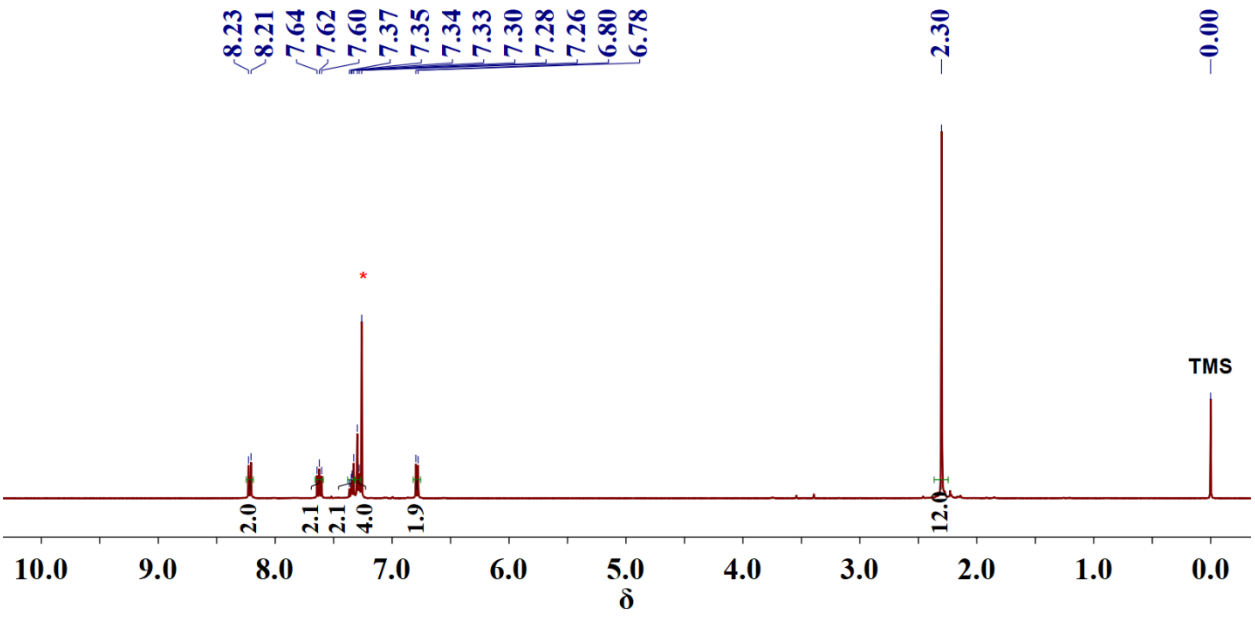

Figure 3.17 *The ^{1}H NMR spectrum of* ***3.2b*** *recorded in $CDCl_3$.*

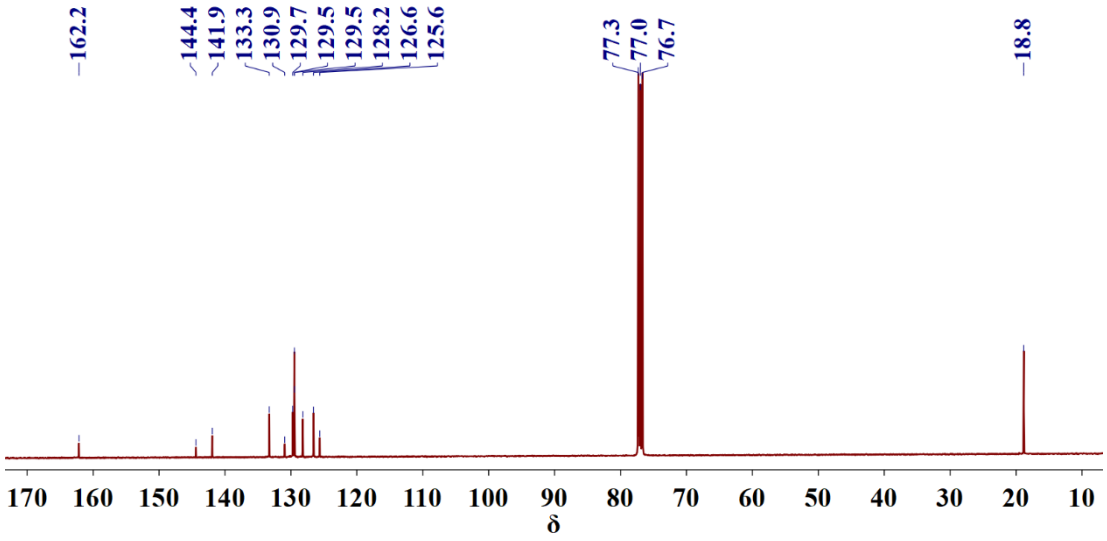

Figure 3.18 *The ^{13}C NMR spectrum of* ***3.2b*** *recorded in $CDCl_3$.*

*[(p-NO_2Ar-BIAN)$InCl_3$] (**3.3b**)*

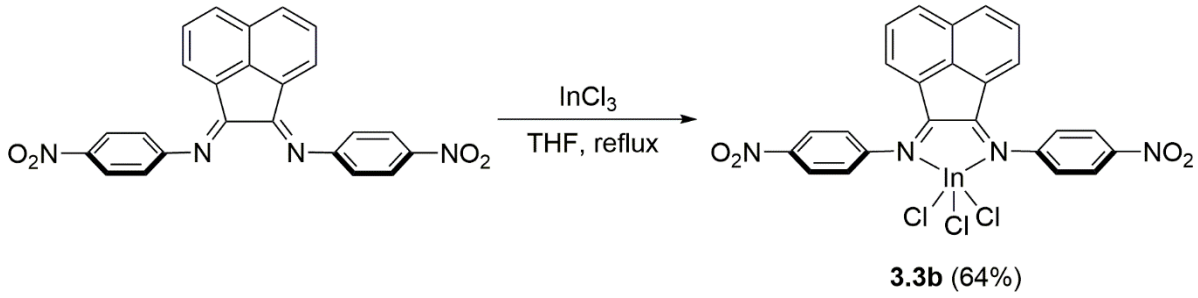

Scheme 3.7 *Synthesis of [(p-NO_2Ar-BIAN)$InCl_3$] (**3.3b**).*

The procedure was similar to the one reported above for complex **3.1b** except that this reaction was carried out under reflux conditions overnight. The following quantities of compounds were used: $InCl_3$ (0.044 g, 0.20 mmol) and *p*-NO_2Ar-BIAN (0.084 g, 0.20 mmol) in THF (7 mL). The resultant yellow solid was washed with THF and then purified from vapor diffusion using Et_2O/DMF mixture. The isolated yield was 0.083 g (64%). The purity of the product was confirmed by elemental analysis. Yellow block-like crystals suitable for single crystal X-ray analysis were obtained by recrystallization from an ACN solution of the crude product. ^{1}H NMR (400 MHz, acetone-d_6): δ = 7.27 (d, *J* = 6.8 Hz, 2 H), 7.75-7.79 (m, 6 H), 8.44 (d, *J* = 8.4 Hz, 2 H), 8.55-8.58 (m, 4 H). The ^{13}C{^{1}H} NMR could not be obtained due to the poor solubility of **3.3b** in most of the available deuterated solvents. m.p.: decomposed after 320 °C. HRMS (ESI+, *m/z*) calculated for $C_{24}H_{14}Cl_3InN_4O_4Na$ $[M+Na]^+$ *m/z* = 664.9017, found 664.9005. Anal. Calcd. for $C_{24}H_{14}Cl_3InN_4O_4$·THF: C, 46.99; H, 3.10; N, 7.83. Found: C, 46.63; H, 3.45; N, 8.15.

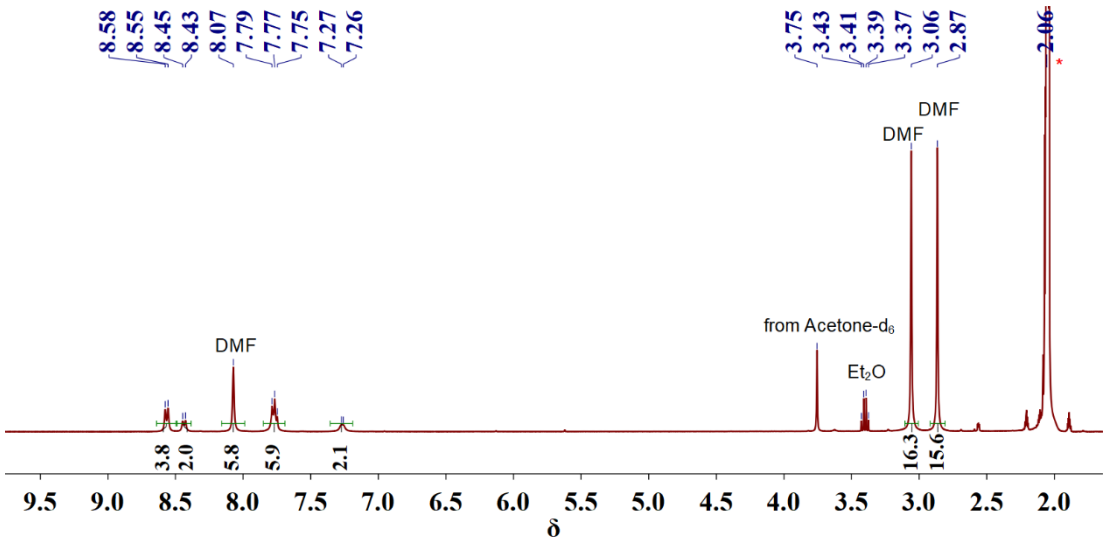

Figure 3.19 *The ^{1}H NMR spectrum of* ***3.3b*** *recorded in acetone-d_6.*

[(p-NMe$_2$Ar-BIAN)InCl$_3$] ***(3.4b)***

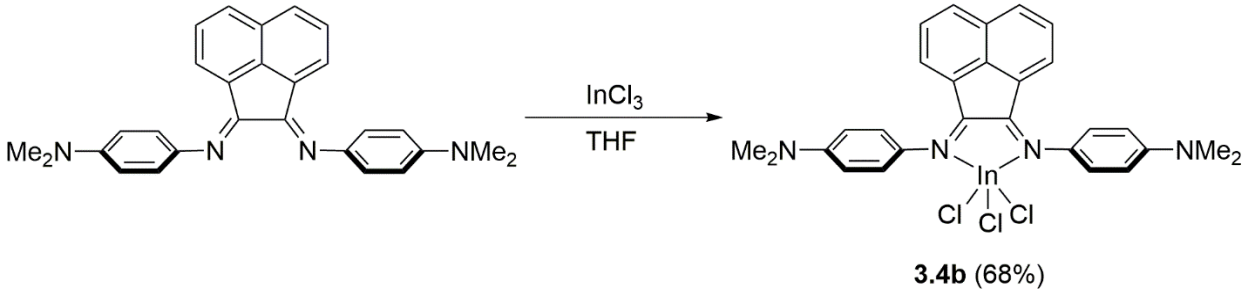

Scheme 3.8 *Synthesis of [(p-NMe$_2$Ar-BIAN)InCl$_3$] (**3.4b**).*

The procedure was identical to the one reported above for **3.1b.** The following quantities of reagents were used: $InCl_3$ (0.066 g, 0.30 mmol) in THF (5 mL), *p*-NMe_2Ar-BIAN (0.130 g, 0.30 mmol) in THF (5 mL). The purple solution was stirred overnight, after which all volatiles were removed under vacuum. The resultant deep blue solid was washed with Et_2O. Purple needle-like crystals suitable for single crystal X-ray analysis were obtained from recrystallization by vapor diffusion of Et_2O into a DMF solution of the crude product and the isolated yield was 0.13 g (68%). ^{1}H NMR (400 MHz, CD_2Cl_2, 25 °C, *fac*-isomer): δ = 3.09 (s, broad, 12 H), 6.88 (d, J = 9.2, 2 H), 7.04-7.06 (m, 4 H), 7.40 (d, J = 6.8, 2 H), 7.54-7.60 (m, 4 H), 8.17 (d, J = 8.0 Hz, 2 H). ^{13}C{^{1}H}

NMR (100 MHz, CD_2Cl_2): δ = 40.6, 40.7, 112.5, 123.0 (broad, may have peaks overlapping), 124.3, 126.1 (broad, may have peaks overlapping), 127.2, 128.8, 129.1, 131.3 (two peaks), 131.7, 132.8 (broad, may have peaks overlapping), 133.5, 143.8, 144.1, 150.9, 151.3 (broad, may have peaks overlapping), 157.7. m.p. 198-202 °C. HRMS (ESI+, *m/z*) calculated for $C_{31}H_{33}N_5InCl_3Na$ $[M+Na]^+$ *m/z* = 734.0687, found 734.0652. Anal. Calcd. for $C_{31}H_{33}N_5OInCl_3 \cdot H_2O$: C, 50.95; H, 4.83; N, 9.58. Found: C, 50.90; H, 4.90; N, 9.32.

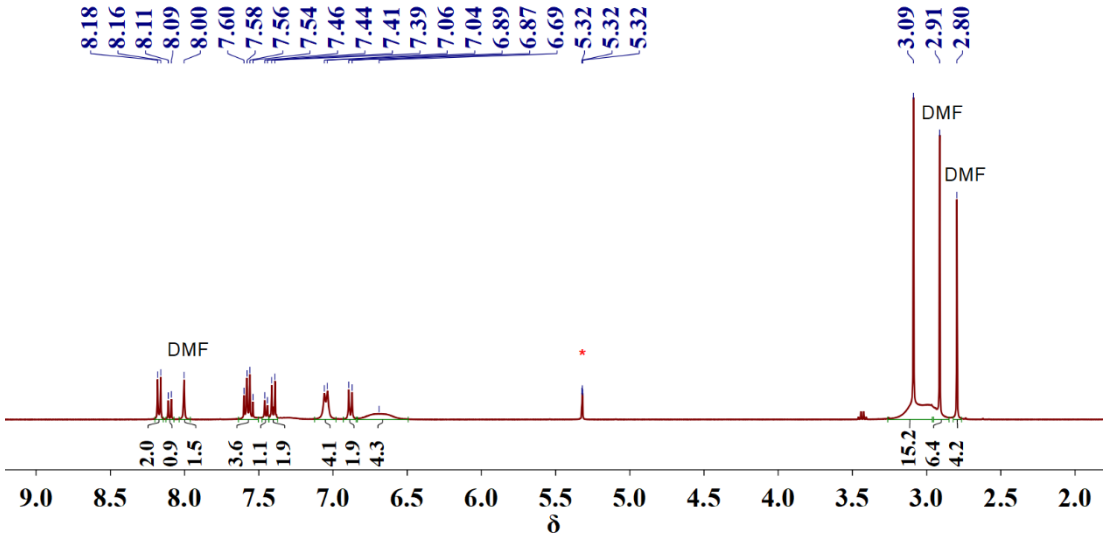

Figure 3.20 *The ^1H NMR spectrum of **3.4b** recorded in CD_2Cl_2.*

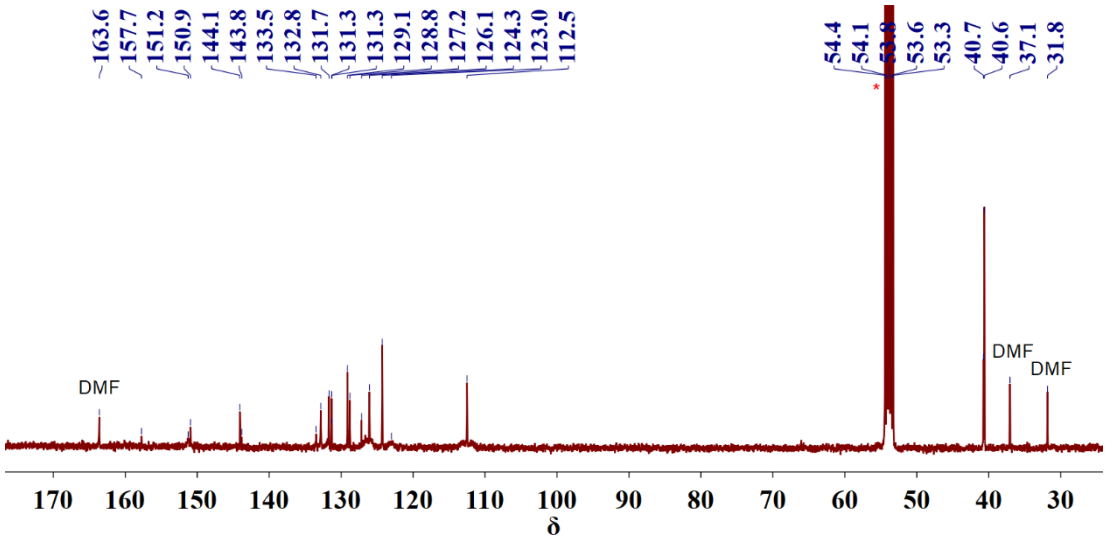

Figure 3.21 The ^{13}C NMR spectrum of **3.4b** recorded in CD_2Cl_2.

*[(p-MeOAr-BIAN)(DMF)InCl$_3$] (**3.5b**)*

The synthetic procedure was reported in chapter 2. Recrystallization by vapor diffusion of Et_2O into a DMF solution of the red solid resulted in samples suitable for single crystal X-ray analysis. ^{1}H NMR (400 MHz, CD_3CN, *fac*-isomer): δ = 3.92 (s, 6 H), 7.16-7.18 (m, 4 H), 7.33-7.36 (m, 4 H), 7.56-7.65 (m, 4 H), 8.31 (d, J = 6.8 Hz, 2 H). The ^{13}C{^{1}H} NMR recorded in DMF-d_7 show multiple broad overlapping peaks which may be a result of the *fac-mer* isomerization process. The intensity of peaks were low due to the poor solubility of **3.5b** in DMF-d_7. HRMS (ESI+, *m/z*) calculated for $C_{26}H_{20}Cl_3InN_2O_2Na$ $[M+Na]^+$ *m/z* = 634.9520, found 634.9514. Anal. Calcd. for $C_{29}H_{27}N_3O_3InCl_3 \cdot H_2O$: C, 49.43; H, 4.15; N, 5.96. Found: C, 49.84; H, 4.55; N, 6.12.

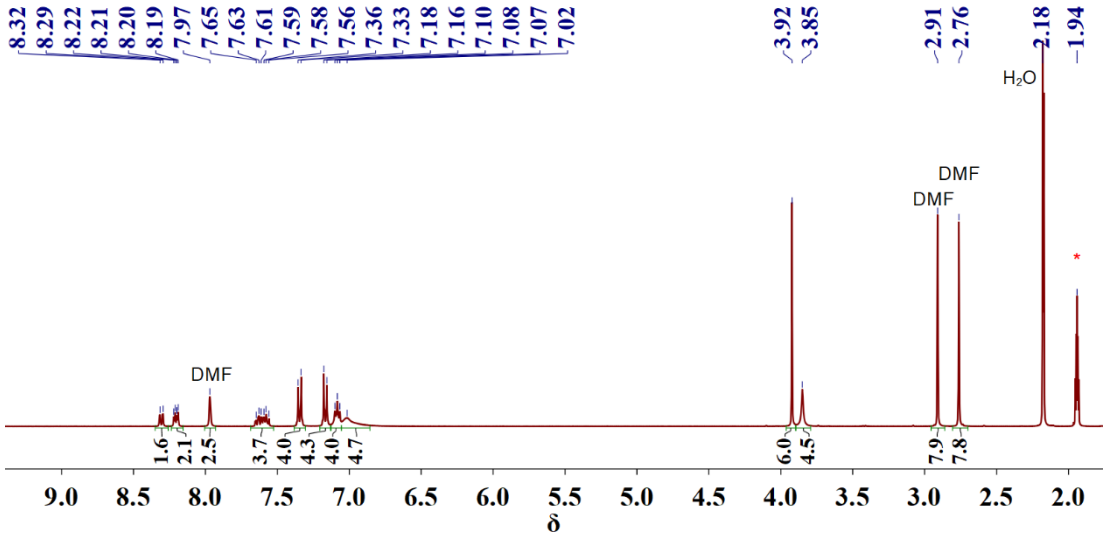

***Figure 3.22** The ^{1}H NMR spectrum of **3.5b** recorded in CD_3CN.*

3.4.3 Reduction of [(*p*-MeOAr-BIAN)$_2$InCl$_2$]$^+$[InCl$_4$]$^-$

*MeOAr-BIAN-H$_2$ (**3.6**)*

A THF solution (5 mL) of $CoCp_2$ was added dropwise to a THF suspension (5 mL) of **2.3** at room temperature. The resulting brown suspension was stirred for 2 h, after which all volatiles were removed under vacuum. The crude purple solid was washed with Et_2O and the purple filtrate was

filtered and concentrated. The ^{1}H NMR experiments were conducted on the resultant purple solid (**3.6**). ^{1}H NMR (400 MHz, C_6D_6): 3.33 (s, 6 H), 4.93 (s, 2 H), 6.72-6.77 (m, 8 H), 7.12-7.42 (m, overlapping with signal from C_6D_6), 7.43 (d, J = 8.0 Hz, 2 H).

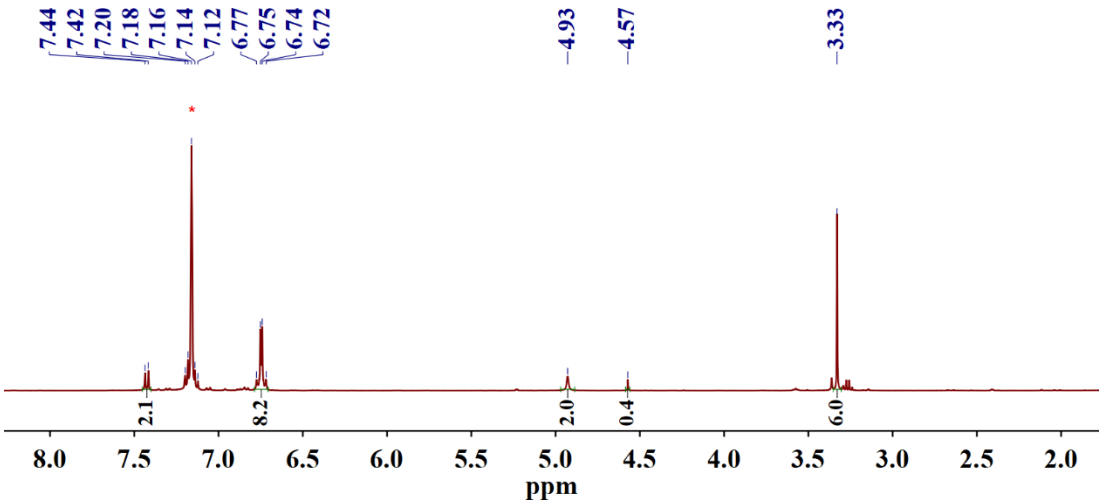

Figure 3.23 *The purified ^{1}H NMR spectrum of the reduction reaction of* ***3.2*** *using $CoCp_2$ recorded in C_6D_6. (crude mixture dissolved in Et_2O and then filtered, filtrate collected)*

3.4.4 X-ray data of indium(III) complexes 3.1b – 3.5b

Table 3.7 *X-ray data for* ***3.1b*** *–* ***3.5b****.*

	3.1b	**3.2b**	**3.3b**	**3.4b**	**3.5b**	**3.6**
Chemical formula	$C_{36}H_{40}Cl_3InN_2$	$C_{28}H_{24}Cl_3InN_2$	$C_{28}H_{22}Cl_3InN_6O_5$ (with 2 ACN)	$C_{34}H_{40}Cl_3InN_6O_2$ (with 1 DMF)	$C_{30.5}H_{30.5}Cl_3InN_{3.5}O_{3.5}$ (with half DMF)	$C_{26}H_{22}N_2O_2$
Formula weight/ $gmol^{-1}$	721.87	609.66	743.68	785.89	723.25	394.45
Temperature/ K	103(2)	103(2)	103(2)	103(2)	103(2)	103(2)
Wavelength/ Å	0.71073	0.71073	0.71073	0.71073	0.71073	1.54178
Crystal size/ mm^3	0.040 x 0.060 x 0.420	0.280 x 0.320 x 0.420	0.120 x 0.240 x 0.300	0.140 x 0.160 x 0.420	0.200 x 0.210 x 0.400	0.020 x 0.060 x 0.380
Crystal habit	Orange needle	Orange block	Yellow block	purple needle	red block	red plate
Crystal system	monoclinic	monoclinic	monoclinic	triclinic	triclinic	monoclinic
Space group	C 1 c 1	P 1 21/m 1	P 1 21/n 1	P -1	P -1	C 1 2/c 1
a/ Å	9.6585(3)	8.5861(9)	9.2235(8)	8.9217(3)	8.9265(5)	27.3734(9)
b/ Å	21.4348(8)	17.7036(19)	13.9416(11)	14.6932(6)	12.3564(7)	9.3669(3)
c/ Å	16.7319(7)	11.4783(13)	24.3021(19)	16.1692(7)	14.3910(8)	7.7757(3)
α/°	90	90	90	112.451(2)	99.6119(15)	90
β/°	101.7562(15)	105.462(2)	96.327(4)	92.719(2)	90.3519(14)	100.331(2)
γ/°	90	90	90	95.175(2)	106.1023(14)	90
Volume/ $Å^3$	3391.3(2)	1681.6(3)	3106.0(4)	1943.22(14)	1501.33(15)	1961.40(12)
Z	4	2	4	2	2	4
ρ (Calc)/$mg.m^{-3}$	1.414	1.251	1.590	1.343	1.600	1.336
Absorp. Coeff./ mm^{-1}	0.960	0.956	1.066	0.850	1.095	0.674
F(000)	1480	636	1488	804	732	832
Θ range/ °	1.90 to 28.34	2.17 to 24.67	2.66 to 31.14	1.37 to 31.26	1.44 to 35.11	3.28 to 66.79
Index range	-12<=h<=12,	-12<=h<=12,	-11<=h<=13,	-13<=h<=12,	-14<=h<=14,	-31<=h<=32,

	-28<=k<=28, -11<=l<=22	-25<=k<=25, 0<=l<=16	-20<=k<=20, -35<=l<=31	-21<=k<=21, -23<=l<=23	-20<=k<=19, -23<=l<=23	-10<=k<=11, -8<=l<=9
Refl. collected	11216	10810	47312	43022	50446	5667
Indep. Refns. (R_{int})	5953 (0.0373)	5569 (0.0437)	10012 (0.0525)	12623 (0.1008)	13260 (0.0521)	1714 (0.0622)
Coverage of independent reflections	99.6%	99.7%	99.7%	99.6%	99.4%	98.3%
Max., min., transmission	0.9630, 0.6880	0.7740, 0.6880	0.8830, 0.7400	0.8900, 0.7170	0.8110, 0.6690	0.9870, 0.7840
Data/ restraint/parameters	5953 / 2 / 387	5569 / 0 / 165	10012 / 107 / 425	12623 / 56 / 471	13260 / 0 / 403	1714 / 0 / 142
Goodness-of-fit on F^2	1.056	0.866	1.043	1.080	1.050	1.045
Final R indices [I>2σ(I)]	R1 = 0.0399, wR2 = 0.0957	R1 = 0.0309, wR2 = 0.0562	R1 = 0.0301, wR2 = 0.0638	R1 = 0.0576, wR2 = 0.1546	R1 = 0.0346, wR2 = 0.0684	R1 = 0.0479, wR2 = 0.1295
R indices (all data)	R1 = 0.0473, wR2 = 0.1093	R1 = 0.0453, wR2 = 0.0591	R1 = 0.0377, wR2 = 0.0669	R1 = 0.0814, wR2 = 0.1728	R1 = 0.0487, wR2 = 0.0737	R1 = 0.0553, wR2 = 0.1366
Largest diff. peak and hole/ e. $Å^{-3}$	1.430 and -1.834	0.923 and -0.609	0.564 and -0.671	1.595 and -0.884	0.918 and -0.910	0.253 and -0.214
Refinement method: Full-matrix least-squares on F^2						

3

Chapter 4

Synthesis of modified Ar-BIAN ligand and the transient absorption studies of its Ir(III) complexes

4.1 Introduction

In the previous two chapters, we have not only introduced an alternative solid state mechanochemical grinding approach to the synthesis of Ar-BIAN ligands, but also discussed the absorption and electrochemical properties of the indium(III) complexes supported by a series of Ar-BIAN ligands. Although different substituents were introduced onto the aryl-diimine moiety to investigate the effect of electron donating and withdrawing groups on the optical properties of the resulting complex, such effect was not explored with functionalization on the acenaphthene backbone of these Ar-BIAN ligands. Therefore, in this chapter, firstly, the synthesis of an Ar-BIAN ligand with functionalization on the acenaphthene moiety will be introduced; and secondly, the excited state characteristics of a heterolytic iridium(III) complex bearing the functionalized Ar-BIAN ligand will be studied using transient absorption spectroscopy.

Late transition metals have been widely investigated as potential light harvesters for various photovoltaics and artificial photosynthetic systems. In particular, heterolytic ruthenium complexes[117] (*e.g.* **N3** and **N719**) and complicated transition metal based porphyrin systems[118] have been predominantly employed as the photosensitizer in the study of dye-sensitized solar cells (DSSC). On the other hand, iridium based photosensitizers are more extensively explored in the field of photocatalysis for organic syntheses rather than in DSSCs or other photovoltaic systems. Iridium complexes have potential benefits of high chemical and thermal stability, long excited state lifetimes and high emission quantum yields that are comparable to the ruthenium complexes.[119] Moreover, iridium complexes have been successfully employed in many electroluminescent devices, for instance, organic light emitting diodes (OLEDs).[120] It has been demonstrated that iridium cyclometalated (C^N) complexes exhibit excellent photoluminescence quantum yield and their emission color is easily tunable *via* functional modifications on the C^N

ligand.[121] Therefore an iridium complex bearing two cyclometalating (C^N) ligands and one Ar-BIAN (N^N) ligand was chosen here to study the effect of functionalization at the acenaphthene backbone of the Ar-BIAN ligand on the excited state characteristics of the resulting complex.

4.1.1 Design of the functionalized Ar-BIAN ligand

Ar-BIAN ligands are known for their extensive π system of the naphthalene unit and therefore serve as a good π-acceptor ligand. However, both the HOMO and LUMO of these ligands are mainly localized at the aryl-diimine region as discussed in chapters 2 and 3. This may result in fast electron transfer from the aryl-diimine moiety to the LUMO of the ligand which further lead to a shortening of the excited state lifetime. Tkachenko's group has investigated the excited state dynamics of a series of Cu(I) Ar-BIAN complexes using time resolved electronic absorption spectroscopy. They have reported that the fast deactivation of ^{3}MLCT state to a non-emissive ^{3}IL (IL = intraligand) state is the cause of the short lifetime observed in related Cu(I) Ar-BIAN complexes.[122] (Figure 4.1) For the free Ar-BIAN ligands, when the sample was excited at 390 nm, the ^{1}IL state was populated and then transforms through inter-system crossing (ISC) to the ^{3}IL state on the time scale of 0.2 ps. This ^{3}IL state is non-emissive and quickly decays back to the ground state with a time frame of 30-40 ps. In the case of the Cu(I) complexes, after population of the ^{1}IL state *via* the same excitation, the excited state molecules either decay *via* ISC to the ^{3}IL state (pathway 1 in Figure 4.1) or populate the lower laying ^{1}MLCT state (pathway 2 in Figure 4.1). This indirectly populated charge transfer (CT) state rapidly transforms into the ^{3}MLCT state *via* ISC and then decays back to the lower-laying ^{3}IL state. Similar decay pathway was followed when the samples were excited with a lower energy at 780 nm, which resulted in direct population of the ^{1}MLCT state. The aforementioned two pathways proceed simultaneously, and both resulted

in population of the non-emissive ^{3}IL state, which hence explains the lack of luminescence from the resulting complexes.

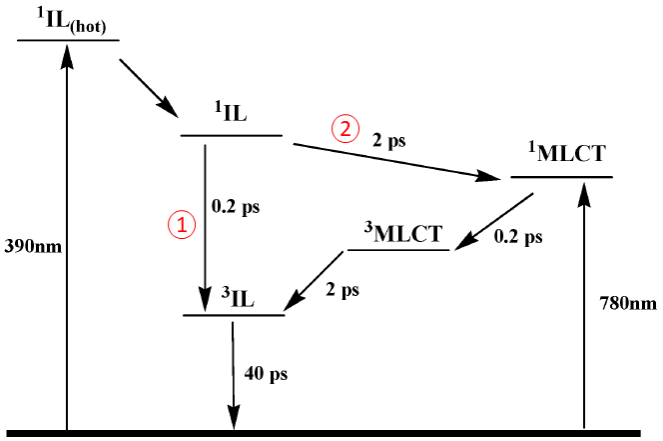

Figure 4.1 *Proposed energy level diagram and deactivation pathways of the Ar-BIAN ligands and their corresponding complexes after excitation.*

We hypothesized that one possible method to resolve the lack of luminescence from Ar-BIAN complexes could be to introduce electron withdrawing groups on the acenaphthene moiety. (Figure 4.2)

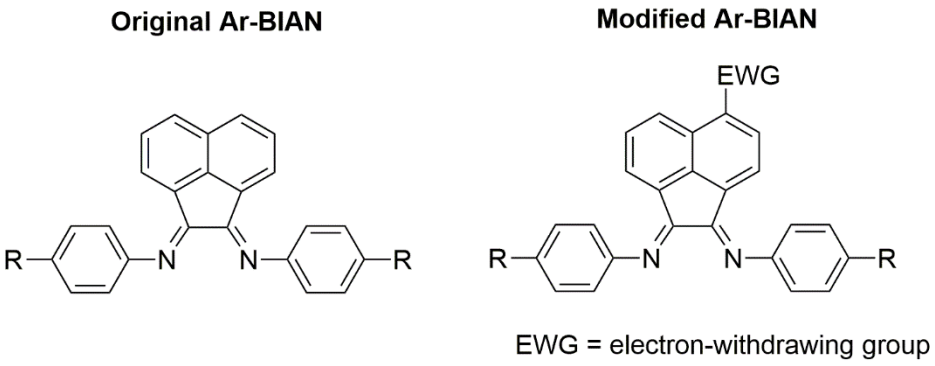

Figure 4.2 *Molecular structure of the modified Ar-BIAN.*

Extensive orbital mixing of the frontier molecular orbitals (FMOs) occurs in Ar-BIAN ligands due to the fact that both HOMO and LUMO of these systems are comprised of contributions from the aryl-diimine fragment, which increases the rate of ISC that transforms the ^{1}MLCT to the ^{3}MLCT

state.[123] By introducing an electron withdrawing group on the acenaphthene backbone of the Ar-BIAN ligand, we hope to localize the electron accepting π* orbitals on the acenaphthene moiety and therefore, provide spatial separation of the electrons from the metal after excitation. Also, de-population of the ^{3}IL state may be achieved by stabilizing and therefore, lowering the energy of the emissive MLCT state. (Figure 4.3)

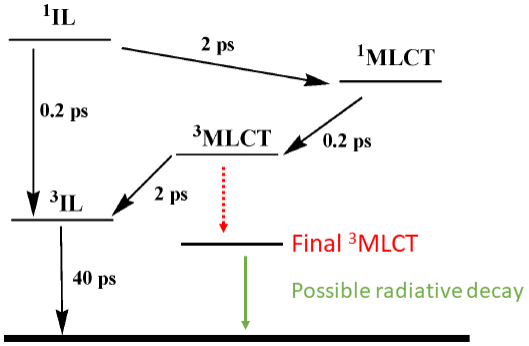

Figure 4.3 *Proposed deactivation pathways of the metal complexes supported by modified Ar-BIAN ligands.*

4.1.2 General introduction to transient absorption spectroscopy

Transient absorption spectroscopy belongs to a method of flash photolysis and it is used in the study of dynamic processes of chemical compounds (*e.g.* unstable radicals and short lived intermediates when compounds are excited).[124] In each time resolved optical spectroscopic experiment, a small fraction of the molecules (~ 0.1%) in the sample is promoted to an electronically excited state by a pump pulse. The sample was then probed by a broadband xenon lamp beam (probe pulse) at a delayed time (*t*) with respect to the pump pulse. (Figure 4.4) The excited state dynamics of the sample can be studied by calculating a difference in the absorption spectrum of the excited sample and the sample in its ground state. In the transient absorption spectra, the detected intensity of the transmitted signal is presented as a change in optical density (ΔOD). By changing the time delay *t* between the pump and the probe pulse, ΔOD can be obtained

as a function of wavelength (λ) and time (t). The construction of ΔOD (λ, t) is described by Equation 1, where $I(\lambda)_{\text{pumped}}$ and $I(\lambda)_{\text{unpumped}}$ stands for the intensity of the probe beam of a ‘‘pumped’’ and “unpumped” sample respectively.

$$\Delta OD\ (\lambda, t) = -\log\left(\frac{I(\lambda,t)\text{pumped}}{I(\lambda)\text{unpumped}}\right) \qquad \text{Equation 1}$$

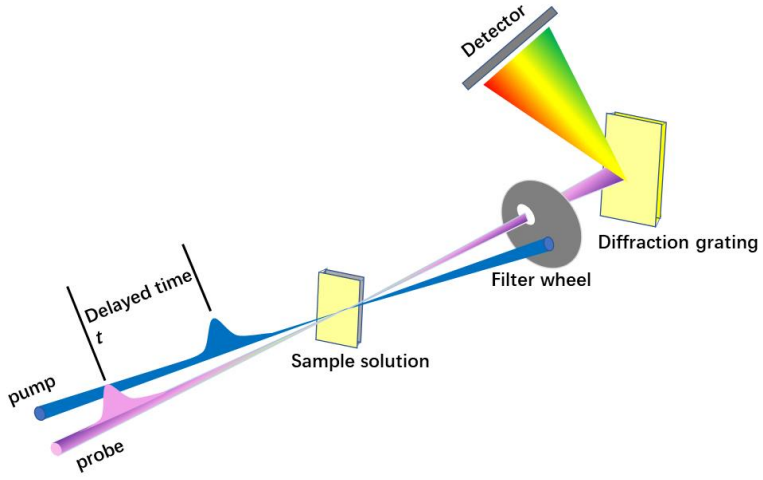

Figure 4.4 *Schematic diagram describing the working principle of transient absorption spectroscopy.*[125]

Since ΔOD is described by the logarithmic ratio between the light intensity from the probe beam before and after laser excitation, a positive ΔOD refers to an increase in absorption while a negative ΔOD refers to a decrease in absorption or emission of the excited state relative to the ground state. In general, a ΔOD spectrum contains contributions from the following processes.[125] The first process is ground state bleaching. Due to a decreased number of ground state molecules after the pump pulse, the ground state absorption in the excited sample is less than that of the ground state sample. This results in a negative signal in the ΔOD spectrum. The second process is excited state emission (stimulated emission). After population of the excited state, stimulated emission back to the ground state would occur for optically allowed transitions when the probe pulse passes through the excited volume. Therefore, the light intensity detected would increase and based on Equation

1, would results in a negative signal in the *ΔOD* spectrum. The third process is excited state absorption. This process occurs when excited state molecules absorb the energy from the probe pulse at wavelength regions that promote them to even higher excited states. Consequently, a decrease in light intensity on the detector is expected and therefore, leads to a positive signal in the *ΔOD* spectrum. The fourth contribution is provided by product absorption. For certain biological or photochemical systems, reactions may occur after excitation that produces a transient species, and the absorption of such products will result in a positive signal in the *ΔOD* spectrum.

4.2 Results and discussion

4.2.1 Synthesis of modified Ar-BIAN ligand (CO_2Me-NMe_2Ar-BIAN) (4.1)

In this study, a carboxylate functionality was incorporated into the acenaphthene moiety of the Ar-BIAN ligand since it not only acts as an electron withdrawing group which is expected to enhance the emission profile of the resulting ligand, but also serves as an anchoring functionality that potentially facilitates grafting on metal oxide surfaces.[126] On the other hand, dimethylamino (-NMe_2) groups were substituted at the *para*-positions of the aryl-diimine part of the Ar-BIAN ligand. As demonstrated in chapter 3, the strongly electron donating -NMe_2 substituents is expected to destabilize the non-bonding orbital and therefore shifts the n-π* absorption band to the lower energy visible region of the electromagnetic spectrum, which constitutes about 42% of the solar spectrum.[127]

The preparation of CO_2Me-NMe_2Ar-BIAN (**4.1**) involved the synthesis of 5-carboxymethyl substituted acenaphthoquinone (**4.1c**) (Scheme 4.1), followed by condensation with 4-(dimethylamino)aniline using the mechanochemical grinding approach. (Scheme 4.2) Firstly, 5-bromoacenaphthene was lithiated and quenched with dry ice to give the carboxylated product (**4.1a**)

in high yield. Esterification was then carried out using thionyl chloride and methanol to afford the carboxymethyl substituted acenaphthene (**4.1b**). The carboxymethyl substituted acenaphthoquinone (**4.1c**) was synthesized by oxidation of **4.1b** with chromium trioxide (CrO_3) in acetic anhydride (Ac_2O). Initially, condensation of **4.1c** with 4-(dimethylamino)aniline was carried out using the solution based $ZnCl_2$ templated method, followed by demetallation. However, hydrolysis was observed which often hindered purification of the ligand. Similar problems were also encountered in the synthesis of **3.4a** as discussed in chapter 3. Hence, a mechanochemical grinding approach was employed for the synthesis of ligand **4.1,** using Na_2SO_4 as the dehydrating agent and AcOH as the acid catalyst. Analytically pure samples of **4.1** was obtained after recrystallization.

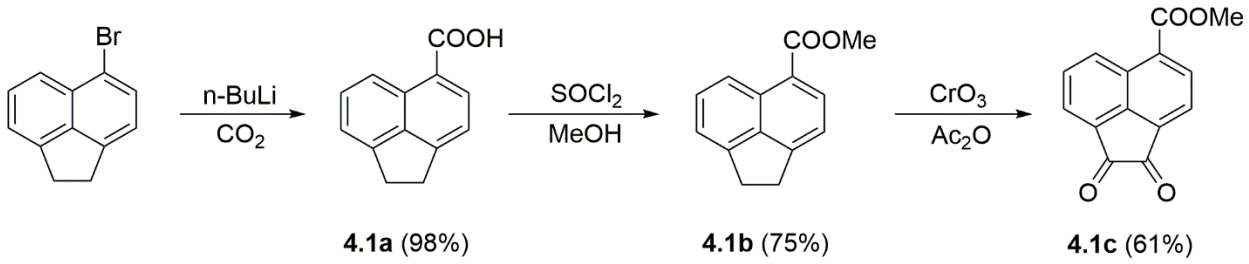

Scheme 4.1 *Synthesis of 5-carboxymethylacenaphthoquinone (**4.1c**).*

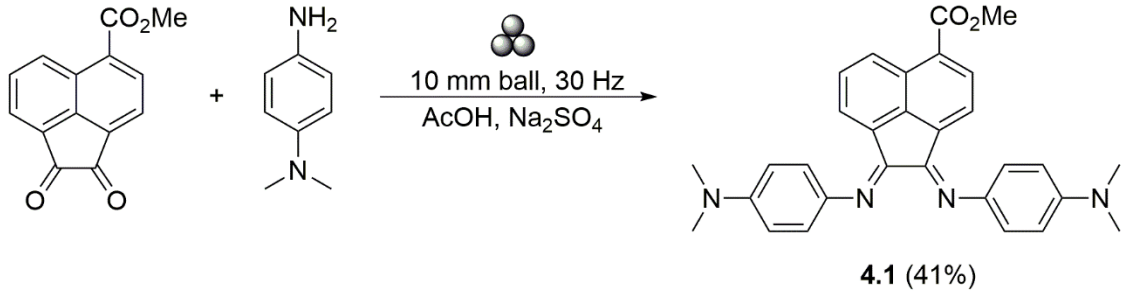

Scheme 4.2 *Mechanochemical synthesis of 5-carboxymethyl substituted Ar-BIAN ligand **4.1**.*

Two equivalents of the carboxymethyl substituted Ar-BIAN ligand (N^N) (**4.1**) were then reacted with the chloro-bridged iridium(III) complex bearing two 2-(3'-anisyl)-5-methylpyridines (C^N)

on each iridium center (**4.2**), affording the corresponding iridium(III) complex (**4.3** and **4.4**) in high yields. The synthesis of compounds **4.2** - **4.4** were carried out by our collaborator Prof. Eli Zysman Colman's group and therefore the synthetic procedure will not be discussed in detail. However, a reaction scheme for the synthesis of **4.3** and **4.4** is included here for better completeness of the thesis. (Scheme 4.3) Both **4.3** and **4.4** are octahedral cationic coordination complexes of iridium(III) supported by two C^N ligands and one N^N ligand (**4.1**) each. The N^N ligand in **4.3** possesses an ester group at the acenaphthene backbone, whereas that in **4.4** possesses a carboxylic acid group which can potentially facilitate anchoring onto semiconductor surfaces.

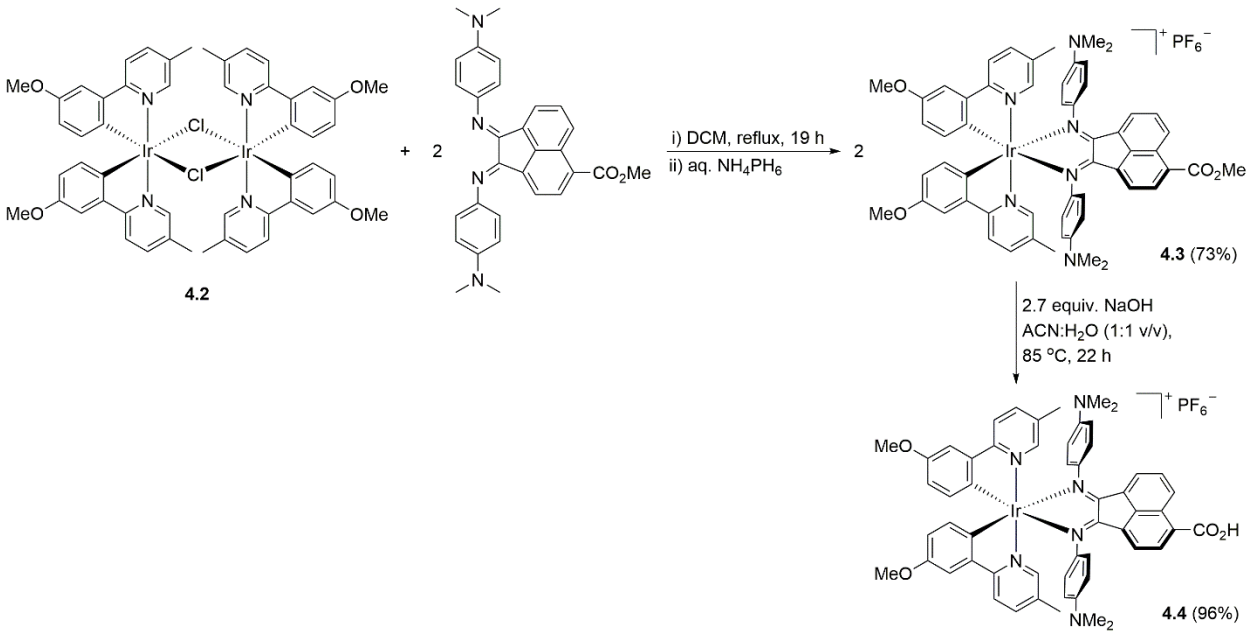

Scheme 4.3 *Synthesis of iridium(III) complexes* ***4.3*** *and* ***4.4*** *with the general formula* $[Ir(C^N)_2(N^N)][PF_6]$.

4.2.2 Transient absorption spectroscopic study on iridium(III) complexes

The ground state photophysical properties of the iridium(III) complexes **4.3** and **4.4** were studied by steady state photoluminescence spectroscopy (PL). The PL spectrum for **4.3** was recorded at 298 K in dichloromethane (DCM) while that for **4.4** was recorded in acetonitrile (ACN) due to its poor solubility in DCM. For complex **4.3**, weak emissions signals were observed at 540 and 410

nm when the sample was excited at 420 and 340 nm respectively. (Figure 4.5a) In the case of **4.4** in which the carboxymethyl substituent in the Ar-BAIN ligand was replaced by a carboxylic acid group, a similar emission profile was obtained upon excitation at the same wavelength region. (Figure 4.5b) The two emission bands may be attributed to a mixture of metal to ligand charge transfer (MLCT) and intra-ligand charge transfer (ILCT) processes due to the presence of two ligand motifs which are both π-acceptors. The π* orbitals of the Ar-BIAN ligand are expected to be lower in energy than those of 2-(3'-anisyl)-5-methylpyridines due to more extensive conjugation provided by the naphthene unit. Therefore, there could be a mixture of MLCT, ILCT, and ligand to ligand charge transfer (LLCT) excited states arising from promotion of the Ir *d* electrons to the two-distinct ligand π* orbitals. This may result in radiative deactivation of the excited electrons from the ligands back to Ir, within the Ar-BIAN ligand, and between the 2-(3'-anisyl)-5-methylpyridines and Ar-BIAN ligands. The overall photoluminescence quantum yield (Φ_{PL}) for **4.3** was estimated to be 0.03% in DCM, calculated using the comparative method described by Williams *et al*.[128]

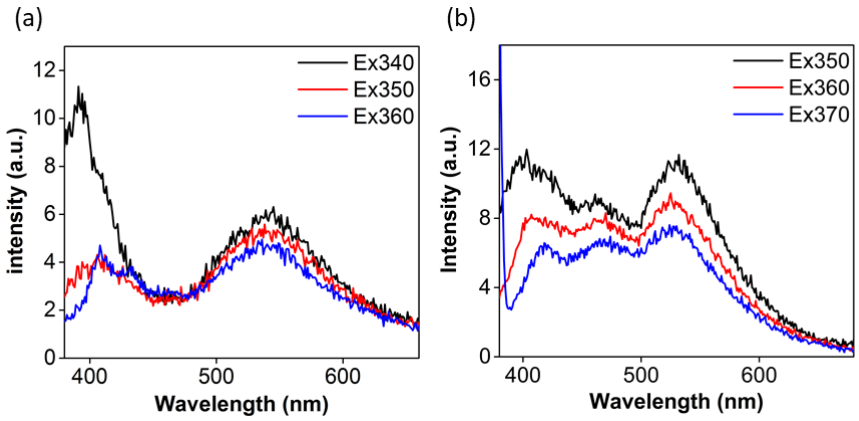

Figure 4.5 *Steady-state photoluminescence spectra of (a)* ***4.3*** *recorded in DCM and (b)* ***4.4*** *recorded in ACN at 298 K.*

The triplet spin density distributions of the complexes **4.3** and **4.4** were obtained from DFT calculations with UB3LYP/SBKJC-VDZ basis set for Ir(III) metal center and 6-31G** for C, H, N, and O atoms using a CPCM (ACN) solvent model. (Figure 4.6) It was observed that the triplet spin state is predominantly distributed within the Ar-BIAN ligand for both **4.3** and **4.4,** with minor contributions from the 2-(3'-anisyl)-5-methylpyridine ligands. This suggests that the emission signals observed in the PL spectra may arise mainly from a mixed MLCT/ILCT transition between the Ir metal center and the Ar-BIAN ligand. Further, the expected stabilization of π-accepting orbitals provided by introduction of electron withdrawing groups on the acenaphthene backbone of Ar-BIAN ligands was confirmed by DFT calculations, as shown from the calculated Kohn-Sham molecular orbitals for **4.3** and **4.4**. (Figure 4.7) A reference iridium(III) complex (**4.5**) bearing the unmodified Ar-BIAN ligand (*i.e.* ligand **3.4a** from chapter 2) was included here to illustrate the effect of electron withdrawing carboxyl substituents. The HOMO-LUMO gap for compound **4.5** was calculated to be 2.26 eV, and the LUMO for compounds **4.3** and **4.4** were stabilized by about 0.1 eV, resulting in an energy gap of around 2.1 V between the HOMO and the LUMO. In addition, the electron density distribution of iridium(III) complexes **4.3** and **4.4** revealed that HOMO and LUMO are largely located around the Ar-BIAN ligands, with minor contribution from the 2-(3'-anisyl)-5-methylpyridine ligands.

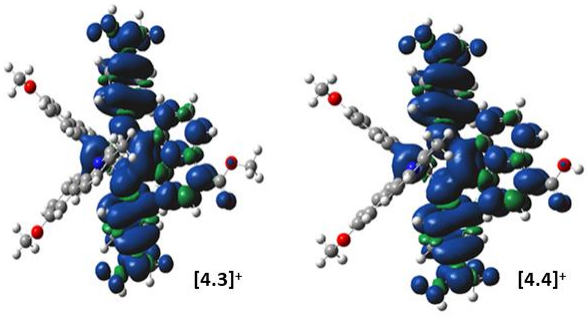

Figure 4.6 *Triplet spin density distributions of* ***4.3*** *and* ***4.4****.*

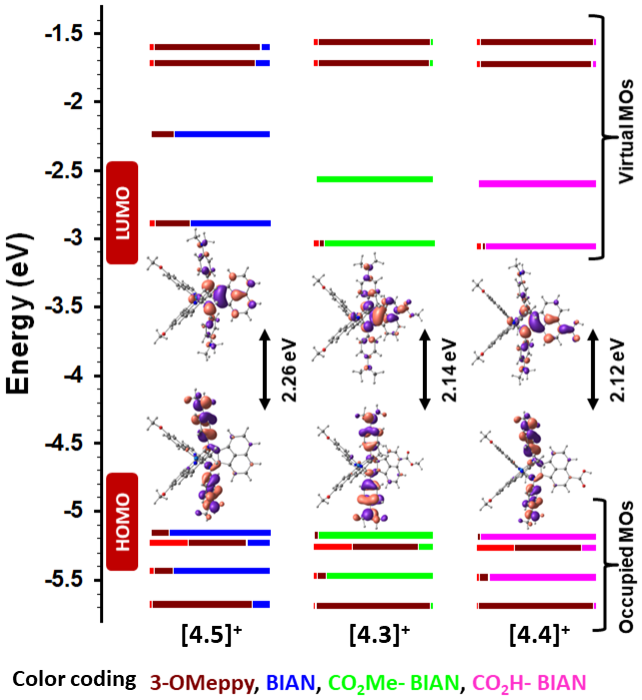

Figure 4.7 *Calculated frontier Kohn-Sham MOs of* ***4.3, 4.4,*** *and the reference compound* ***4.5****.*

To obtain greater insight into the excited state characteristics of complexes **4.3** and **4.4**, nanosecond transient absorption and emission spectroscopic measurements were conducted. The transient emission spectrum for complex **4.3** was recorded in DCM and it revealed two broad emission bands at 410 nm and 530 nm, upon irradiation by a 355 nm laser pulse. (Figure 4.8a) This matches with the spectral profile obtained from the steady-state PL measurement (*vide supra*). Meanwhile, the transient absorption spectrum for **4.3** showed two bands with negative *ΔOD* at 410 nm and 630 nm, which may arise from a superposition of both the ground state bleach and the excited state emission. (Figure 4.8b) The excited state lifetime of the $[Ir]^{+*}$ species was estimated to be 9.7 ns and 7.0 ns when probed at 520 nm and 630 nm using the transient emission spectrum and transient absorption spectrum respectively. However, this range of lifetimes is shorter than the time-resolution of our instrument and therefore did not allow for any accurate results to be determined. (Figure 4.9)

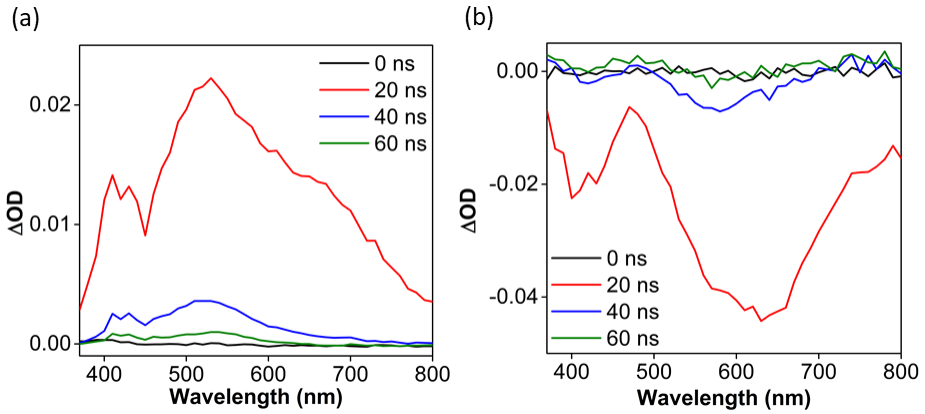

Figure 4.8 *Transient (a) emission and (b) absorption spectra of 0.05 mM solutions of* ***4.3*** *recorded in DCM at 298 K.*

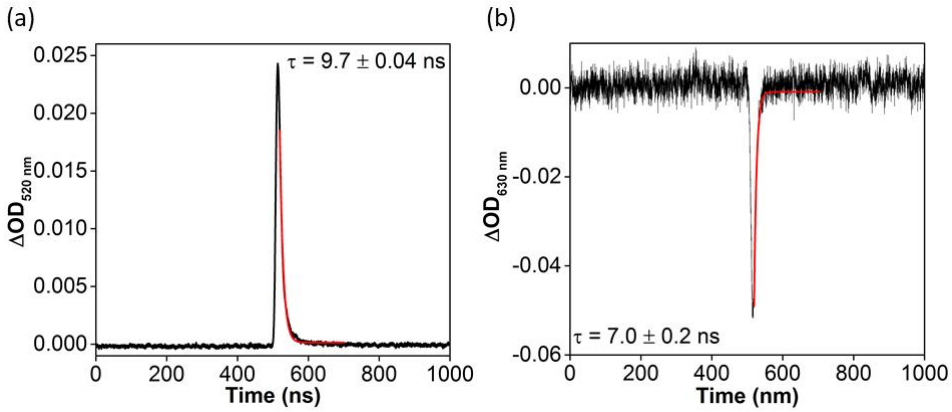

Figure 4.9 *Transient (a) emission spectrum at 520 nm and (b) absorption spectrum at 630 nm for* ***4.3*** *in DCM solution.*

Similarly, the transient emission spectrum for complex **4.4** recorded in ACN showed two emission signals at 420 nm and 470 nm when irradiated by the same laser pulse. (Figure 4.10) On the other hand, one band with negative *ΔOD* was observed at 420 nm in the transient absorption spectrum of **4.4**, which was contributed by ground state bleach and excited state emission. Excited state lifetime measurements at 480 nm and 420 nm were also attempted using the transient emission and absorption spectrum respectively. However, both excitations had very short-lived lifetimes *ca.* 10 ns, which was shorter than the time-resolution of our instrument. (Figure 4.11) Nevertheless,

both the steady-state and time-resolved spectroscopic measurements indicated that the iridium(III) complexes **4.3** and **4.4** exhibited weak photoluminescence. However, this represents an improvement on the photophysical properties of iridium(III) complexes bearing the modified Ar-BIAN ligands, since no photoluminescence was observed for complex **4.5** in which the unmodified Ar-BIAN **3.4a** was incorporated.

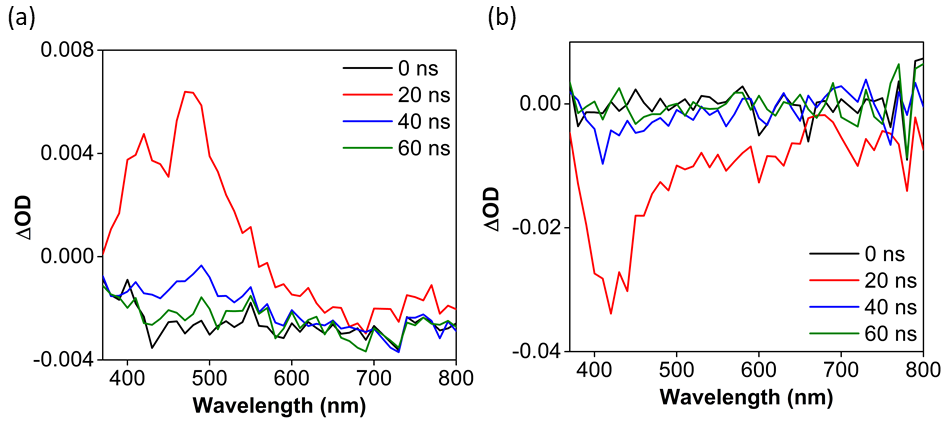

Figure 4.10 *Transient (a) emission and (b) absorption spectra of 0.05 mM solutions of* ***4.4*** *recorded in ACN at 298 K.*

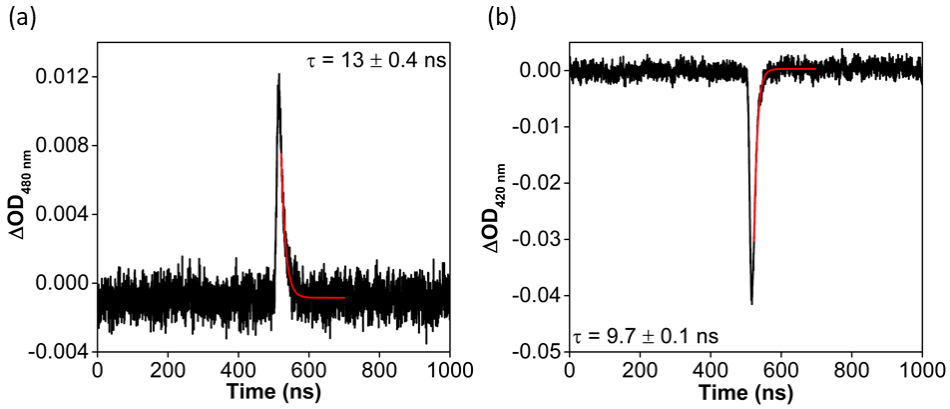

Figure 4.11 *Transient (a) emission spectrum at 480 nm and (b) absorption spectrum at 420 nm for* ***4.4*** *in ACN solution.*

4.3 Conclusions

As previously discussed, the MLCT excited state for complexes with Ar-BIAN ligands typically decays to non-emissive intra-molecular triplet state (^{3}IL) on the order of picoseconds. This may be due to the extensive spatial overlap of the HOMO and LUMO at the aryl-diimine part of the Ar-BIAN ligand that facilitates recombination. By incorporating electron withdrawing groups, we had hoped to localize π-accepting orbitals on the acenaphthene backbone, which can potentially provide better spatial separation of electrons from the Ir metal center after excitation, and thus lead to sufficiently long-lived singlet photoexcited states. Experimental observations from both steady state and time resolved spectroscopic measurements validated this proof of concept study on enhancing the photophysical lifetimes of the iridium(III) Ar-BIAN complexes, through a simple modification and incorporating electron withdrawing groups at the bay region of the ligand. Such strategy demonstrated the possibility of other functional group incorporation on the acenaphthene backbone, which can lead to a broader range of investigation on how the photophysical properties of Ar-BIAN complexes can be further fine-tuned.

4.4 Experimental and analytical techniques

4.4.1 General considerations

Synthesis

Synthesis of the CO_2Me-NMe_2Ar-BIAN ligand (**4.1**) was carried out in a stainless steel grinder jar using a Retsch Mixer Mill MM400. The iridium dimer $[(ppy)_2Ir\text{-}(\mu\text{-}Cl)]_2$[129] (**4.2**) and the two iridium(III) complexes bearing 2-(3'-anisyl)-5-methylpyridines and Ar-BIAN ligand (**4.2** and **4.3**) were prepared by Prof. Eli Zysman Colman's group. Anhydrous dichloromethane (DCM) and acetonitrile (ACN) used for transient absorption and photoluminescence measurements were

distilled over calcium hydride (CaH_2) and collected from a PURE SOLV MD-5 solvent purification system respectively. Both solvents were then stored in a Vacuum Atmospheres N_2 glovebox. All other considerations and instrument specification stay the same that described in chapter 2.

Steady-state photoluminescence measurements

The steady-state photoluminescence (PL) measurements for **4.3** and **4.4** were conducted using a Cary Eclipse Fluorescence Spectrophotometer from Varian Technologies. The samples were prepared, each with a concentration of 0.050 mM, in a glovebox under a N_2 atmosphere. The excitation and emission slit widths were opened to the maximum of 10 nm for all PL measurements of **4.3** and **4.4** due to their weak signals.

Fluorescence quantum yield measurements

The fluorescence quantum yield Φ for **4.4** was obtained by comparing its PL intensity with that from $[Ru(bpy)_3](PF_6)_2$ in a 0.050 mM DCM solution. The calculation was conducted using the following expression:

$$\Phi = \Phi_{ref} \frac{I}{A} \frac{Aref}{Iref}$$

where Φ_{ref} is the quantum yield of the reference compound (Φ_{ref} = 0.029 for $[Ru(bpy)_3](PF_6)_2$ in DCM);[130] I and I_{ref} refer to the integrated fluorescence intensities of the sample and the reference compound respectively; A and A_{ref} are the absorbances at the wavelength of excitation for the sample and for the reference compound respectively.

Transient absorption and emission spectroscopic measurements

The transient absorption and emission spectra were obtained using a LP920 transient absorption spectrometer from Edinburgh instrument, with a power of 1.39 kV and a Q-switch delay of 106

μs. Each sample was prepared with a concentration of 0.050 mM in a glovebox under a N_2 atmosphere. UV-vis spectra were collected before and after the transient absorption/emission spectroscopic measurements to ensure that minimal compound decomposition occurred during these studies.

DFT calculations

All calculations were performed with the Gaussian09, revision D.01 suite of programs employing the B3LYP DFT method. Singlet and triplet ground state geometry optimizations and single point energy calculations for [**4.3**]$^+$-[**4.5**]$^+$ were carried out at the (R)B3LYP and (U)B3LYP levels, using their respective crystallographic structures as starting points. All elements except Ir were assigned the 6-31G(d,p) basis set.[130] The double-ζ quality SBKJC VDZ ECP basis set[131] with an effective core potential was employed for the Ir(III) center. Vertical electronic excitations based on (R)B3LYP-optimized geometries were computed for [**4.3**]$^+$-[**4.5**]$^+$ using the TD-DFT formalism[132] in acetonitrile using conductor-like polarizable continuum model (CPCM).[133] Vibrational frequency calculations were performed to ensure that the optimized geometries represent the local minima and only positive eigenvalues were obtained. The electronic distribution and localization of the singlet excited states were visualized using the electron density difference maps (ED-DMs).[134] All calculated structures and Kohn-Sham orbitals were visualized with ChemCraft.[135]

4.4.2 Synthesis of compound 4.1

*Synthesis of CO_2H-acenaphthene (**4.1a**)*

This procedure was adopted from the literature.[136] 5-bromoacenaphthene (0.47 g, 2.0 mmol) was dissolved in Et_2O (10 ml) and cooled to -78 °C using a dry ice/acetone bath. To this solution, *n*-BuLi (2.5 M in hexane) was added slowly and stirred at -78 °C for 30 min before warming up to room temperature and continue to stir for 1 h. Chunks of dry ice was added to the reaction mixture

and allowed to stir overnight. The white precipitate obtained was washed with Et_2O, filtered and air dried. The isolated yield of the product was 0.35 g (98%). ^{1}H NMR (400 MHz, D_2O): δ = 8.14 (d, J = 8.0 Hz, 1 H), 7.81 (d, J = 7.2 Hz, 1 H), 7.57 (t, J = 7.6 Hz, 1 H), 7.37 (dd, J = 13, 6.8 Hz, 2 H), 3.37 (s, 4 H). ^{13}C{^{1}H} NMR (100 MHz, D_2O): 177.3, 149.3, 146.8, 138.9, 131.1, 128.8, 128.7, 121.2, 119.5, 118.6, 29.7.

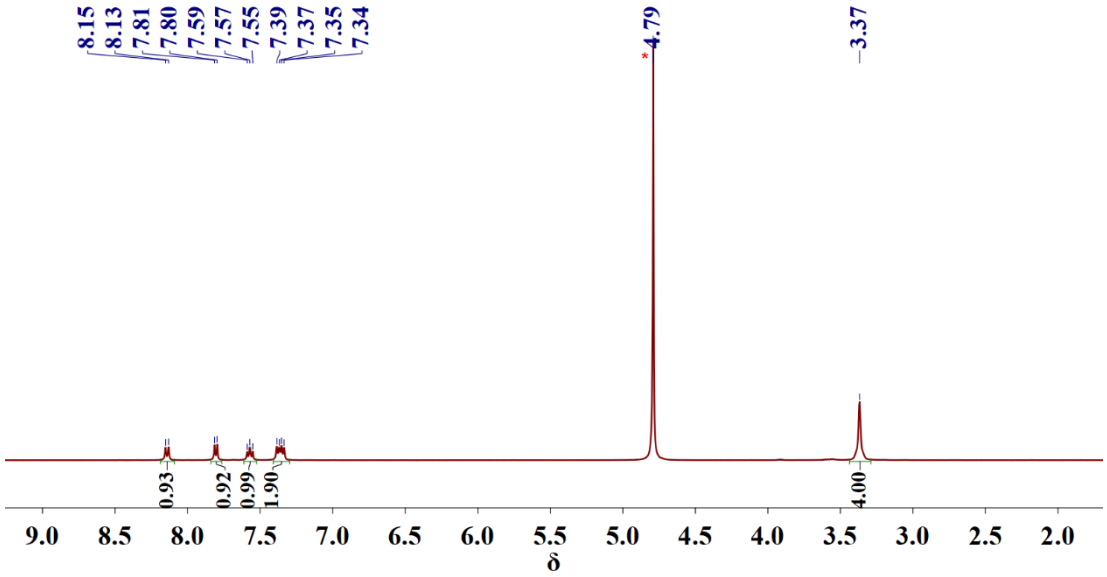

Figure 4.12 *The ^{1}H NMR spectrum of* ***4.1a*** *recorded in D_2O.*

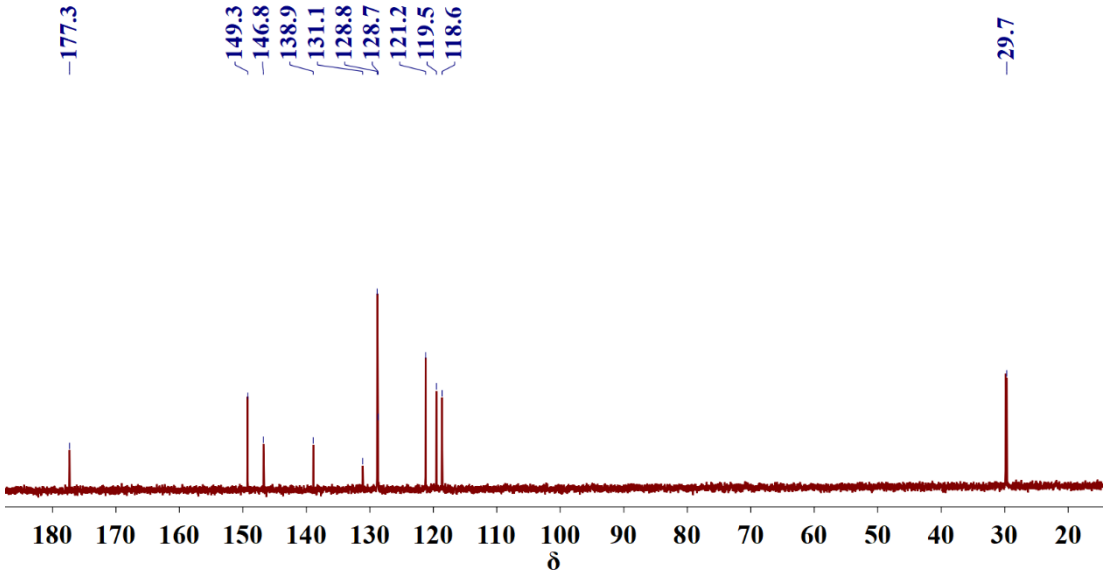

Figure 4.13 *The ^{13}C NMR spectrum of* ***4.1a*** *recorded in D_2O.*

*Synthesis of CO_2Me-acenaphthene (**4.1b**)*

This procedure was also adopted from the literature.[137] Compound **4.1a** (0.50 g, 2.5 mmol) was dissolved in methanol (MeOH) (8 mL) and cooled in an ice/water bath. Thionyl chloride solution (1 M in DCM, 6.3 mL, 6.3 mmol) was added dropwise over 5 min. An off white precipitate was formed. The reaction mixture was stirred at 0 °C for 10 min and then bring to reflux for 12 h. After cooling down to room temperature, MeOH was removed by rotary evaporation and the yellow precipitate formed was dissolved in DCM and extracted with H_2O. The organic layer was separated, dried with $MgSO_4$ and concentrated *in vacuo*. The yellow precipitate was isolated obtaining 0.37 g (75%). ^{1}H NMR (400 MHz, $CDCl_3$): δ = 8.64 (d, J = 8.4 Hz, 1 H), 8.25 (d, 7.2 Hz, 1 H), 7.57 (dd, J = 8.4, 7.2 Hz, 1 H), 7.30 (d, J = 6.8 Hz, 1 H), 7.22 (d, J = 7.6 Hz, 1 H). 3.40 (s, 3 H), 3.29-3.34 (m, 4 H). ^{13}C{^{1}H} NMR (100 MHz, $CDCl_3$): 168.0, 153.0, 146.3, 139.7, 133.2, 130.3, 129.9, 122.2, 122.1, 120.0, 118.5, 51.8, 30.5, 30.4.

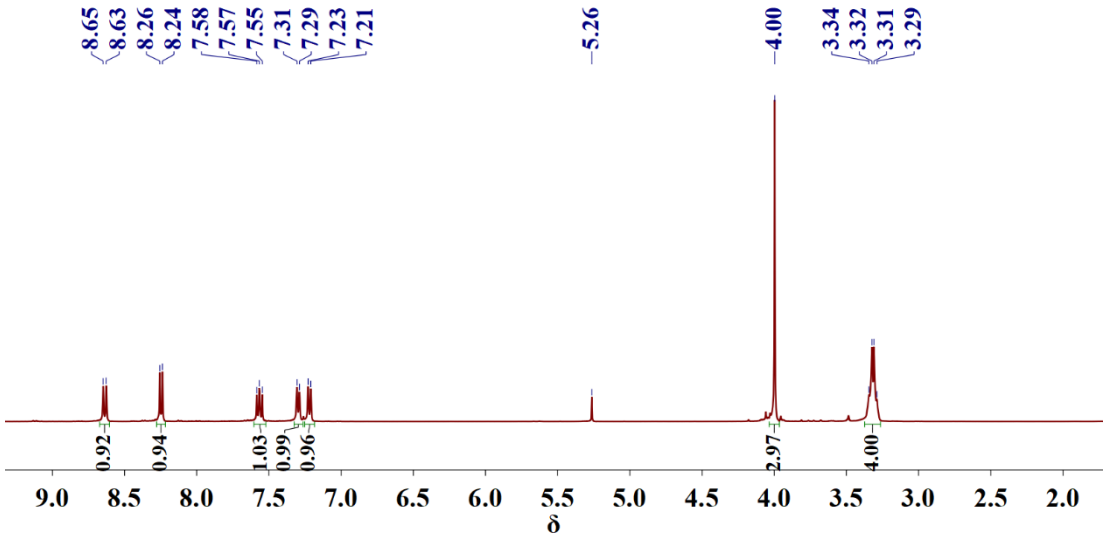

Figure 4.14 *The ^{1}H NMR spectrum of **4.1b** recorded in $CDCl_3$.*

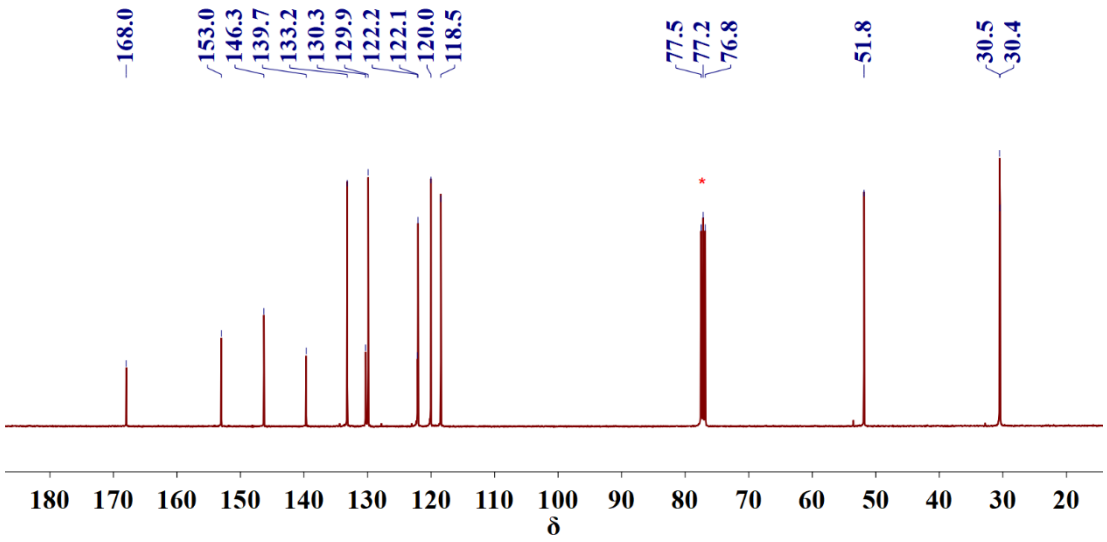

Figure 4.15 *The ^{13}C NMR spectrum of* ***4.1b*** *recorded in $CDCl_3$.*

*Synthesis of CO_2Me-acenaphthoquinone (**4.1c**)*

This procedure was adopted from the literature with slight modification.[138] Compound **4.1b** (0.31 g, 1.4 mmol) was dissolved in acetic anhydride (Ac_2O) (14 mL) and heated to 75 °C. Chromium trioxide (0.46 g, 4.6 mmol) was added slowly and stirred at 75 °C for 1.5 h. The reaction mixture was then poured into ice and quenched by conc. HCL (1 mL). An orange precipitate resulted. After warming up to room temperature, the orange precipitate was dissolved in DCM and the organic layer was extracted three times with H_2O. The organic layer was collected, dried with $MgSO_4$ and concentrated *in vacuo*. The orange precipitate was isolated obtaining 0.19 g (61%). ^1H NMR (400 MHz, $CDCl_3$): δ = 9.31 (d, J = 8.8 Hz, 1 H), 8.60 (d, J = 7.6 Hz, 1 H), 8.21 (d, J = 6.8 Hz, 1 H), 8.14 (d, J = 7.2 Hz, 1 H), 8.00 (dd, J = 8.6, 6.8 Hz, 1 H), 4.10 (s, 3 H). $^{13}C\{^1H\}$ NMR (100 MHz, $CDCl_3$): 188.2, 187.4, 166.1, 145.9, 132.9, 132.5, 132.0, 131.2, 130.3, 129.7, 129.3, 122.8, 120.9, 53.0.

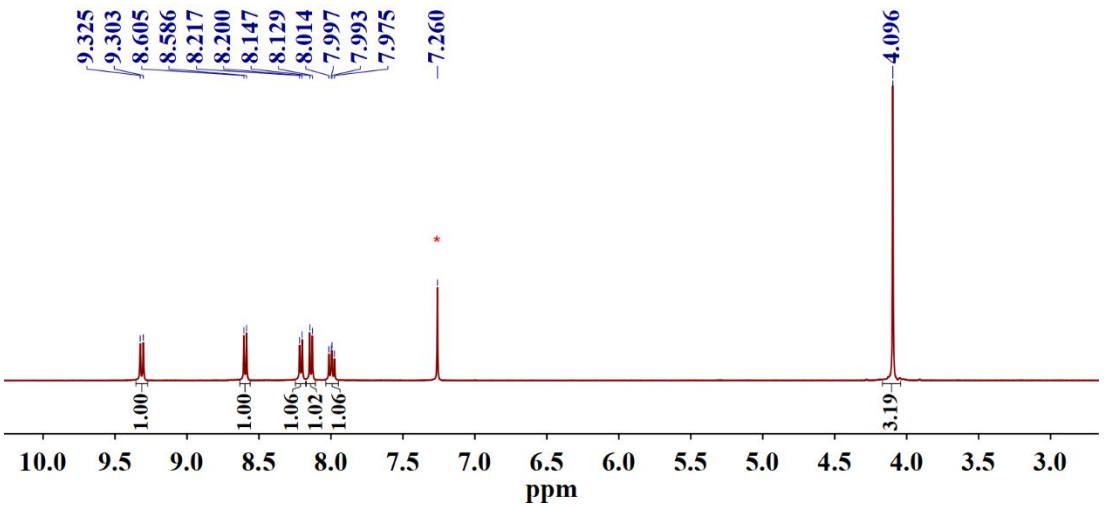

Figure 4.16 *The ^{1}H NMR spectrum of* ***4.1c*** *recorded in $CDCl_3$.*

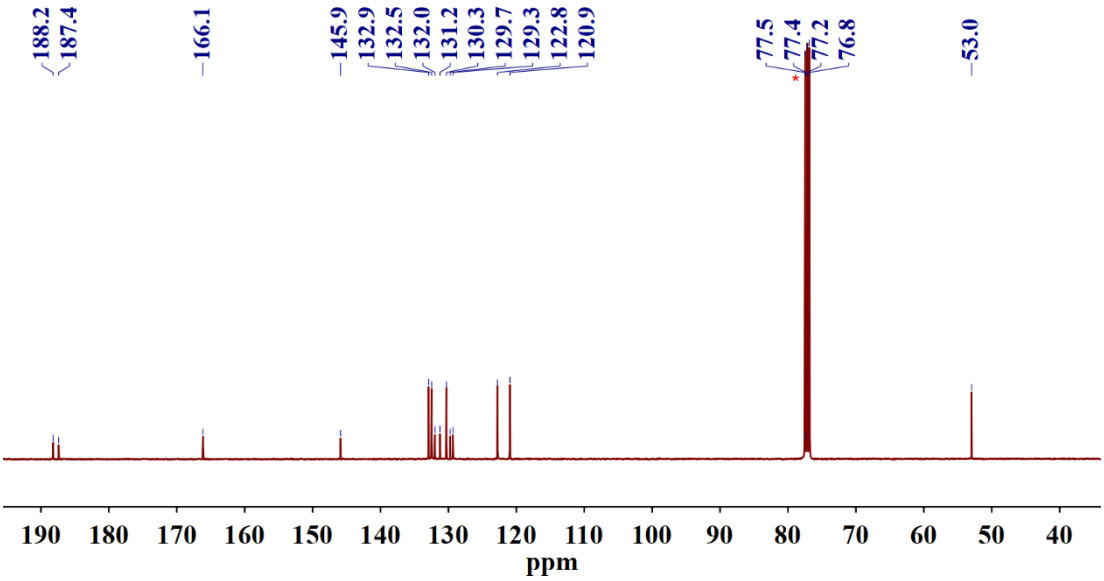

Figure 4.17 *The ^{13}C NMR spectrum of* ***4.1c*** *recorded in $CDCl_3$.*

*Synthesis of CO_2Me-NMe_2Ar-BIAN (**4.1**)*

A stainless steel grinder jar was dried in an oven at 120 ºC overnight prior to use. The grinder jar was charged with **4.1c** (0.072 g, 0.30 mmol), *N*,*N*-dimethyl-4-phenylenediamine (0.094 g, 0.67 mmol), acetic acid (AcOH) (4.3 µL, 0.075 mmol, 25 mol%), and Na_2SO_4 (0.043 g, 0.30 mmol), and equipped with a 10 mm stainless steel ball. The contents in the jar were then ground for 4 h at 30 Hz. The resultant purple gel was suspended in DCM, filtered, and the filtrate was concentrated

to dryness and rinsed with cyclohexane. The purple reside was recrystallized from Et_2O and the isolated yield was 0.054 g (41%). ^{1}H NMR (400 MHz, $CDCl_3$): δ = 8.90 (d, J = 8.4 Hz, 1 H), 8.16 (d, J = 7.6 Hz, 1 H), 7.51 (t, J = 8.0 Hz, 1 H), 7.32-7.35 (m, 2 H), 7.10-7.14 (m, 4 H), 6.82-6.86 (m, 4 H), 3.99 (s, 3 H), 3.04 (s, 6 H), 3.03 (s, 6 H). ^{13}C{^{1}H} NMR (100 MHz, $CDCl_3$): δ = 166.9, 160.3, 159.7, 148.8, 148.5, 141.6, 141.5, 141.2, 133.3, 132.0, 130.0, 129.7, 129.3, 128.2, 127.2, 123.7, 121.9, 120.8, 120.5, 113.4, 113.1, 52.4, 41.1, 41.0. HRMS (ESI+, m/z) calculated for $C_{30}H_{29}N_4O_2$ $[M + H]^+$ m/z = 477.2291, found 477.2268. Anal. Calcd. for $C_{30}H_{28}N_4O_2$: C, 75.61; H, 5.92; N, 11.76. Found: C, 75.89; H, 5.57; N, 11.29.

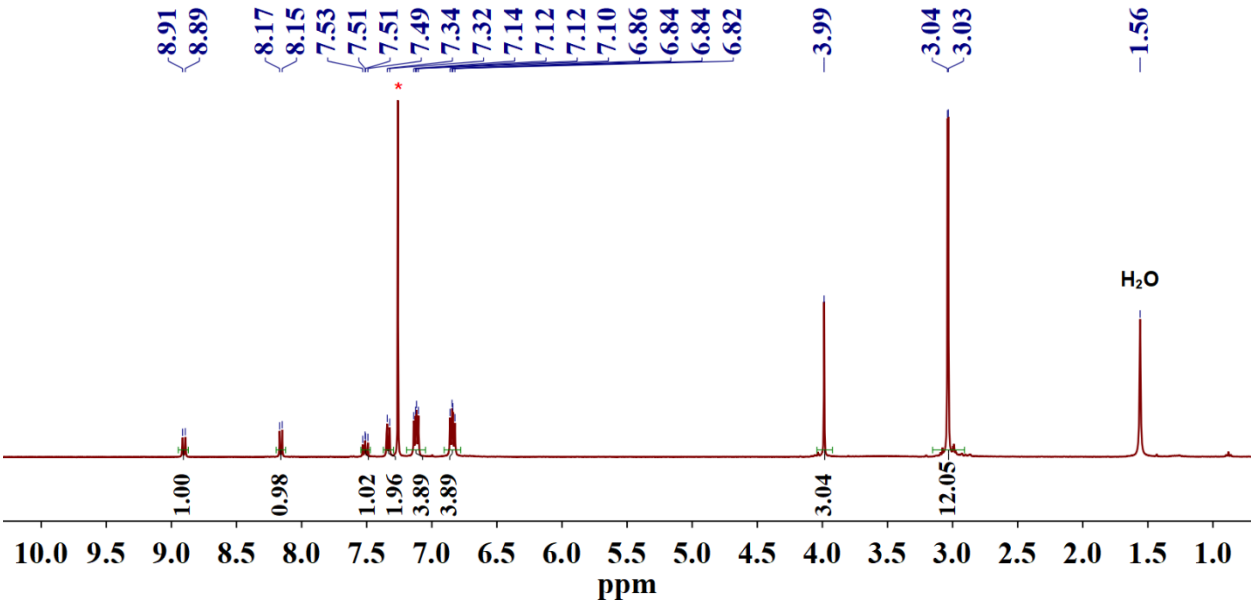

Figure 4.18 *The ^{1}H NMR spectrum of* ***4.1*** *recorded in $CDCl_3$.*

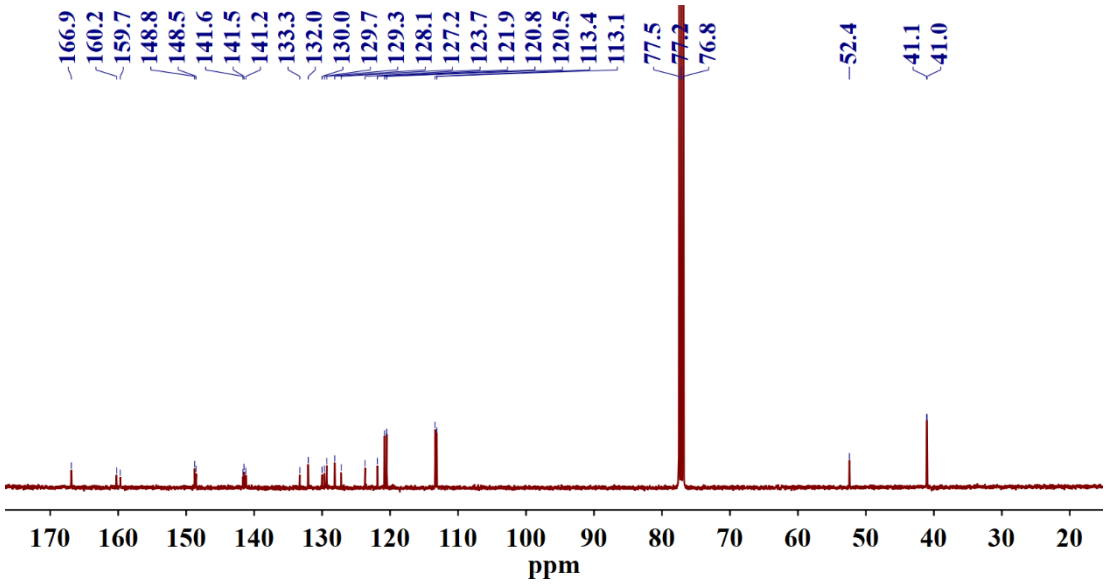

Figure 4.19 *The ^{13}C NMR spectrum of* ***4.1*** *recorded in $CDCl_3$.*

Chapter 5

Summary and outlook

In summary, this thesis has addressed the synthesis and characterization of main group metal complexes supported by Ar-BIAN ligands, including a comprehensive study on their absorption and electrochemical properties. Firstly, an atom efficient and essentially solvent free mechanochemical ball milling method to the synthesis of Ar-BIAN ligands and their corresponding indium(III) complexes was introduced. The time efficient, and simple reaction procedures for the synthesis of Ar-BIAN ligands, together with the accessibility of indium(III) complexes directly from the ligand precursors *via* a "one-pot two-step" or "one-pot one-step" manner was highlighted in this chapter. Following on, more indium(III) Ar-BIAN complexes were synthesized and characterized to attain a comprehensive study on the spectroscopic and electrochemical properties of a wider range of Ar-BIAN complexes. All attempts on the reduction of the indium(III) complexes to their indium(I) counterpart resulted in disproportionation of the indium(III) center and reduction of the ligand alone. In addition, it was proposed that electron-withdrawing groups on the acenaphthene backbone of the Ar-BIAN may help to enhance the photoexcited lifetime of its complexes by providing better spatial separation of electrons from the metal center after excitation. This concept was then validated through steady state and time-resolved spectroscopic measurements on an iridium(III) Ar-BIAN complex bearing the modified Ar-BIAN ligand.

The influence of ligand motifs on the structural and reactivity properties of the resulting metal complex has enabled the exploration of a wide range of metal catalysts with important applications in organic transformations.[139] Despite the extensive study on catalytic transformations mediated by "redox active" transition metal complexes,[140] little was explored on the reactivity of their main group counterparts. Therefore, catalytic activities exhibited by main group Ar-BIAN complexes may be a future area to be explored as a continuation of this project. Currently, on-going efforts

have been devoted to the synthesis of other main group Ar-BIAN Lewis acidic complexes, such as Sn(II)/Sn(IV) complexes, to be potentially used as catalysts.

The use of Lewis acids in catalyzing organic transformation has become an important field in organic synthetic chemistry. Classically, many carbon-carbon and carbon-heteroatom bond formation reactions such as the Friedel-Crafts reaction, Diels-Alder reactions, and Aldol reactions are catalyzed by simple Lewis acids like $AlCl_3$, $TiCl_4$, $BF_3.OEt_2$, and $SnCl_4$.[141] However, most of these Lewis acid catalysts are unstable, and form toxic and corrosive HCl in the presence of air and moisture, which makes them difficult to handle and hampered large scale application.[142]

Comparatively, tin(II) catalysts exhibit many advantageous properties such as being stable solids, water tolerant, and less corrosive, which allow them to be widely employed in industrial scale polyester synthesis. One example of such Sn(II) complex is tin(II) 2-ethylhexanoate ($Sn(Oct)_2$), a commonly used catalyst for ring opening polymerization of cyclic L-lactide to form poly(L-lactide) (PLLA), which is an important biodegradable polymer with applications ranging from industrial plastics to medical devices.[143] (Scheme 5.1) Although the toxicity associated with most of these organotin compounds has limited the exploitation of such reagents in pharmaceutical and biomedical applications,[144] considerable strategies have been developed to overcome this problem. For instance, grafting the organotin catalysts onto insoluble macromolecular or mesoporous silica support allows them to be easily removed and recycled from the reaction mixture by simple filtration.[145]

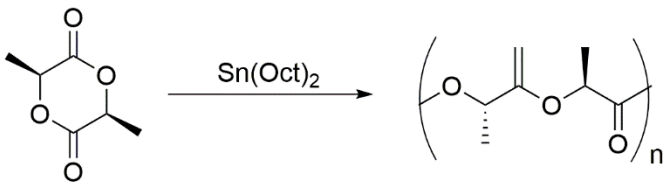

Scheme 5.1 *Ring opening polymerization of L-Lactide catalyzed by $Sn(Oct)_2$.*[146]

Other than the important application of Sn(II) based catalysts for polymer synthesis, organotin(IV) compounds also exhibit interesting catalytic reactivity, especially towards dehydrocoupling reactions, which is an important host of element-element bond forming reactions.[147] In 2010, Naseri *et al.* reported a stoichiometric and catalytic dehydrocoupling reaction of primary phosphines mediated by Cp^*_2Sn and $Cp^*_2SnCl_2$ respectively (Cp* = pentamethylcyclopentadienyl).[148] It was observed that treatment of RPH_2 with Sn(IV) complexes in THF under reflux conditions for 4 days resulted in formation of diphosphanes RP(H)P(H)R as the major product as well as other cyclo-phosphanes $[RP]_4$, $[RP]_5$, *etc.* as the minor products. Although the precise mechanism for main group catalyzed P-P bond formation remains unknown, it was proposed by the authors that the initial step of this reaction involves an activation of RPH_2 *via* loss of Cp*H with concurrent formation of Sn-PHR based intermediates. Inspired by the developing area of main group compound mediated dehydrocoupling reactions, it may be potentially interesting to explore the reactivity of Ar-BIAN Sn based complexes towards primary phosphines, especially given the absorption properties of Ar-BIAN ligands, which may allow for these reactions to be conducted *via* photocatalysis.

In conjunction with the aforementioned interest in the development of main group photosensitizers, syntheses of Sn(II) complexes supported by the modified Ar-BIAN ligands are currently ongoing. As demonstrated in chapter 4, the carboxymethyl modified Ar-BIAN ligand system is expected to improve the excited state lifetimes of the resulting complex and therefore, this ligand system is employed here instead of the original Ar-BIAN ligands. Upon successful syntheses of these Sn(II) Ar-BIAN complexes, their photophysical properties and excited state dynamics will be studied in the future, to examine their potential as photosensitizers.

References

[1] (a) L. A. Berben, B. de Bruin, A. F. Heyduk, *Chem. Commun.* **2015**, *51*, 1553-1554; (b) M. D. Ward, J. A. McCleverty, *J. Chem. Soc., Dalton Trans.* **2002**, 275-288.

[2] C. K. Jørgensen, *Coord. Chem. Rev.* **1966**, *1*, 164-178.

[3] F. R. Morral, in *Werner Centennial, Vol. 62*, American Chemical Society, **1967**, pp. 70-77.

[4] P. J. Chirik, *Inorg. Chem.* **2011**, *50*, 9737-9740.

[5] B. de Bruin, P. Gualco, N. D. Paul, in *Ligand Design in Metal Chemistry*, John Wiley & Sons, Ltd, **2016**, pp. 176-204.

[6] G. N. Schrauzer, V. Mayweg, *J. Am. Chem. Soc.* **1962**, *84*, 3221-3221.

[7] (a) A. Davison, N. Edelstein, R. H. Holm, A. H. Maki, *Inorg. Chem.* **1963**, *2*, 1227-1232; (b) M. J. Baker-Hawkes, E. Billig, H. B. Gray, *J. Am. Chem. Soc.* **1966**, *88*, 4870-4875; (c) E. Billig, R. Williams, I. Bernal, J. H. Waters, H. B. Gray, *Inorg. Chem.* **1964**, *3*, 663-666; (d) A. Davison, N. Edelstein, R. H. Holm, A. H. Maki, *J. Am. Chem. Soc.* **1963**, *85*, 2029-2030.

[8] E. K. Beloglazkina, A. A. Moiseeva, A. A. Chizhevskii, B. N. Tarasevich, N. V. Zyk, K. P. Butin, *Russ. Chem. Bull.* **2003**, *52*, 1990-2004.

[9] N. J. Hill, I. Vargas-Baca, A. H. Cowley, *Dalton Trans.* **2009**, 240-253.

[10] R. van Asselt, C. J. Elsevier, W. J. J. Smeets, A. L. Spek, R. Benedix, *Recl. Trav. Chim. Pays-Bas* **1994**, *113*, 88-98.

[11] M. Gasperini, F. Ragaini, S. Cenini, *Organometallics* **2002**, *21*, 2950-2957.

[12] (a) B. D. Rossenaar, M. W. George, F. P. A. Johnson, D. J. Stufkens, J. J. Turner, A. Vlcek, *J. Am. Chem. Soc.* **1995**, *117*, 11582-11583; (b) H. A. Nieuwenhuis, M. C. E. van de Ven, D. J. Stufkens, A. Oskam, K. Goubitz, *Organometallics* **1995**, *14*, 780-788; (c) H. A. Nieuwenhuis, A. van Loon, M. A. Moraal, D. J. Stufkens, A. Oskam, K. Goubitz, *J. Organomet. Chem.* **1995**, *492*, 165-177; (d) M. P. Aarnts, D. J. Stufkens, A. Vlček, *Inorg. Chim. Acta* **1997**, *266*, 37-46; (e) B. D. Rossenaar, C. J. Kleverlaan, M. C. E. Van De Ven, D. J. Stufkens, A. VlčEk, *Chem. Eur. J.* **1996**, *2*, 228-237.

[13] (a) M. P. Aarnts, F. Hartl, K. Peelen, D. J. Stufkens, C. Amatore, J.-N. Verpeaux, *Organometallics* **1997**, *16*, 4686-4695; (b) B. D. Rossenaar, F. Hartl, D. J. Stufkens, C. Amatore, E. Maisonhaute, J.-N. Verpeaux, *Organometallics* **1997**, *16*, 4675-4685; (c) M. P. Aarnts, M. P. Wilms, K. Peelen, J. Fraanje, K. Goubitz, F. Hartl, D. J. Stufkens, E. J. Baerends, A. Vlček, *Inorg. Chem.* **1996**, *35*, 5468-5477; (d) A. Klein, S. Hasenzahl, W. Kaim, *J. Chem. Soc., Perkin Trans. 2* **1997**, 2573-2578; (e) S. P. M. Disley, R. W. Grime, E. J. L. McInnes, D. M. Spencer, N. Swainston, M. W. Whiteley, *J. Organomet. Chem.* **1998**, *566*, 151-158; (f) M. Sieger, M. Wanner, W. Kaim, D. J. Stufkens, T. L. Snoeck, S. Záliš, *Inorg. Chem.* **2003**, *42*, 3340-3346.

[14] C. B. Wooster, F. B. Smith, *J. Am. Chem. Soc.* **1931**, *53*, 179-187.

[15] I. L. Fedushkin, A. A. Skatova, V. A. Chudakova, G. K. Fukin, *Angew. Chem. Int. Ed.* **2003**, *42*, 3294-3298.

[16] D. P. Gates, S. A. Svejda, E. Oñate, C. M. Killian, L. K. Johnson, P. S. White, M. Brookhart, *Macromolecules* **2000**, *33*, 2320-2334.

[17] K. Hasan, E. Zysman-Colman, *J. Phys. Org. Chem.* **2013**, *26*, 274-279.

[18] M. Gasperini, F. Ragaini, *Organometallics* **2004**, *23*, 995-1001.

[19] G. L. M. D. A. Tarr, *Inorganic Chemistry*, Prentice-Hall, New Jersey, **1990**.

[20] F. Garcia, University of Cambridge **2005**.

[21] H. J. H. Anthony J. Downs, *The group 13 metals aluminium, gallium, indium and thallium*, John Wiley & Sons. Ltd, **2011**.

[22] P. Atkins, T. Overton, J. Rourke, M. Weller, F. Armstrong, *Inorganic chemistry*, W.H. Freeman and Company, United States and Canada, **2006**.

[23] M. Kaupp, in *The Chemical Bond*, Wiley-VCH Verlag GmbH & Co. KGaA, **2014**, pp. 1-24.
[24] D. N. Coventry, A. S. Batsanov, A. E. Goeta, J. A. K. Howard, T. B. Marder, *Polyhedron* **2004**, *23*, 2789-2795.
[25] (a) A. Paulovicova, U. El-Ayaan, K. Umezawa, C. Vithana, Y. Ohashi, Y. Fukuda, *Inorg. Chim. Acta* **2002**, *339*, 209-214; (b) A. Paulovicova, U. El-Ayaan, K. Shibayama, T. Morita, Y. Fuk, *Eur. J. Inorg. Chem.* **2001**, *2001*, 2641-2646; (c) M. Villa, D. Miesel, A. Hildebrandt, F. Ragaini, D. Schaarschmidt, A. Jacobi von Wangelin, *ChemCatChem* **2017**, *9*, 3203-3209.
[26] U. El-Ayaan, A. A. M. Abdel-Aziz, *Eur. J. Med. Chem.* **2005**, *40*, 1214-1221.
[27] R. Van Asselt, C. J. Elsevier, *Organometallics* **1992**, *11*, 1999-2001.
[28] R. van Asselt, C. J. Elsevier, *J. Mol. Catal.* **1991**, *65*, L13-L19.
[29] (a) M. Shiotsuki, P. S. White, M. Brookhart, J. L. Templeton, *J. Am. Chem. Soc.* **2007**, *129*, 4058-4067; (b) S. A. Svejda, M. Brookhart, *Organometallics* **1999**, *18*, 65-74.
[30] S. Cenini, F. Ragaini, S. Tollari, D. Paone, *J. Am. Chem. Soc.* **1996**, *118*, 11964-11965.
[31] (a) F. Ragaini, S. Cenini, S. Tollari, *J. Mol. Catal.* **1993**, *85*, L1-L5; (b) F. Ragaini, S. Cenini, M. Gasperini, *J. Mol. Catal. A: Chem.* **2001**, *174*, 51-57; (c) F. Ragaini, S. Cenini, E. Borsani, M. Dompé, E. Gallo, M. Moret, *Organometallics* **2001**, *20*, 3390-3398.
[32] G. A. Grasa, A. C. Hillier, S. P. Nolan, *Org. Lett.* **2001**, *3*, 1077-1080.
[33] H. A. Jenkins, C. L. Dumaresque, D. Vidovic, J. A. C. Clyburne, *Can. J. Chem.* **2002**, *80*, 1398-1403.
[34] F. S. Mair, R. Manning, R. G. Pritchard, J. E. Warren, *Chem. Commun.* **2001**, 1136-1137.
[35] H. Schumann, M. Hummert, A. N. Lukoyanov, I. L. Fedushkin, *Organometallics* **2005**, *24*, 3891-3896.
[36] A. N. Lukoyanov, I. L. Fedushkin, M. Hummert, *Russ. Chem. Bull.* **2006**, *55*, 422–428.
[37] A. N. Lukoyanov, I. L. Fedushkin, H. Schumann, M. Hummert, *Z. Anorg. Allg. Chem.* **2006**, *632*, 1471-1476.
[38] R. J. Baker, C. Jones, M. Kloth, D. P. Mills, *New J. Chem.* **2004**, *28*, 207-213.
[39] (a) R. J. Baker, R. D. Farley, C. Jones, M. Kloth, D. M. Murphy, *J. Chem. Soc., Dalton Trans.* **2002**, 3844-3850; (b) T. Pott, P. Jutzi, W. Kaim, W. W. Schoeller, B. Neumann, A. Stammler, H.-G. Stammler, M. Wanner, *Organometallics* **2002**, *21*, 3169-3172.
[40] I. L. Fedushkin, A. N. Lukoyanov, S. Y. Ketkov, M. Hummert, H. Schumann, *Chem. Eur. J.* **2007**, *13*, 7050-7056.
[41] I. L. Fedushkin, A. A. Skatova, S. Y. Ketkov, O. V. Eremenko, A. V. Piskunov, G. K. Fukin, *Angew. Chem. Int. Ed.* **2007**, *46*, 4302-4305.
[42] I. L. Fedushkin, A. A. Skatova, S. Y. Ketkov, O. V. Eremenko, A. V. Piskunov, G. K. Fukin, *Angew. Chem.* **2007**, *119*, 4380-4383.
[43] I. L. Fedushkin, V. G. Sokolov, A. V. Piskunov, V. M. Makarov, E. V. Baranov, G. A. Abakumov, *Chem. Commun.* **2014**, *50*, 10108-10111.
[44] (a) I. L. Fedushkin, A. S. Nikipelov, K. A. Lyssenko, *J. Am. Chem. Soc.* **2010**, *132*, 7874-7875; (b) I. L. Fedushkin, O. V. Kazarina, A. N. Lukoyanov, A. A. Skatova, N. L. Bazyakina, A. V. Cherkasov, E. Palamidis, *Organometallics* **2015**, *34*, 1498-1506.
[45] I. L. Fedushkin, A. S. Nikipelov, A. G. Morozov, A. A. Skatova, A. V. Cherkasov, G. A. Abakumov, *Chem. Eur. J.* **2012**, *18*, 255-266.
[46] (a) S. L. Dabb, B. A. Messerle, *Dalton Trans.* **2008**, 6368-6371; (b) A. R. Shaffer, J. A. R. Schmidt, *Organometallics* **2008**, *27*, 1259-1266.
[47] N. J. Hill, G. Reeske, J. A. Moore, A. H. Cowley, *Dalton Trans.* **2006**, 4838-4844.
[48] J. C. Peters, S. B. Harkins, S. D. Brown, M. W. Day, *Inorg. Chem.* **2001**, *40*, 5083-5091.
[49] I. L. Fedushkin, A. A. Skatova, V. A. Chudakova, N. M. Khvoinova, A. Y. Baurin, S. Dechert, M. Hummert, H. Schumann, *Organometallics* **2004**, *23*, 3714-3718.

[50] I. L. Fedushkin, N. M. Khvoinova, A. Y. Baurin, G. K. Fukin, V. K. Cherkasov, M. P. Bubnov, *Inorg. Chem.* **2004**, *43*, 7807-7815.
[51] I. L. Fedushkin, N. M. Khvoinova, A. Y. Baurin, V. A. Chudakova, A. A. Skatova, V. K. Cherkasov, G. K. Fukin, E. V. Baranov, *Russ. Chem. Bull.* **2006**, *55*, 74-83.
[52] N. J. Hill, K. Vasudevan, A. H. Cowley, *Jordan J. Chem.* **2006**, *1*, 47-54.
[53] G. Reeske, C. R. Hoberg, N. J. Hill, A. H. Cowley, *J. Am. Chem. Soc.* **2006**, *128*, 2800-2801.
[54] A. Schmidpeter, S. Lochschmidt, W. S. Sheldrick, *Angew. Chem. Int. Ed. Engl.* **1982**, *21*, 63-64.
[55] A. H. Cowley, R. A. Kemp, *Chem. Rev.* **1985**, *85*, 367-382.
[56] D. Gudat, T. Gans-Eichler, M. Nieger, *Chem. Commun.* **2004**, 2434-2435.
[57] A. Lipka, H. Wunderlich, Z. Naturforsch, *Z. Naturforsch., B: Anorg. Chem., Org. Chem.* **1980**, *35*, 1548.
[58] S. Adonin, M. E. Rakhmanova, D. G. Samsonenko, M. Sokolov, V. Fedin, *Hybrid salts of binuclear Bi(III) halide complexes with 1,2-bis(pyridinium)ethane cation: Synthesis, structure and luminescent behavior, Vol. 450*, **2016**.
[59] A. W. A. D. McNaught, *IUPAC. Compendium of Chemical Terminology, 2nd ed. (the "Gold Book").* Blackwell Scientific Publications, Oxford **1997**.
[60] A. J. a. R. Lynch, Chester A. , *The History of Grinding*, Society of Mining, Metallurgy and Exploration, Inc., Littleton, **2005**.
[61] M. C. Lea, *Am. J. Sci.* **1892**, *43*, 527-531.
[62] L. Takacs, *Bull. Hist. Chem.* **2003**, *28*, 26-34.
[63] E. Boldyreva, *Chem. Soc. Rev.* **2013**, *42*, 7719-7738.
[64] A. L. Garay, A. Pichon, S. L. James, *Chem. Soc. Rev.* **2007**, *36*, 846-855.
[65] T. K. Achar, A. Bose, P. Mal, *Beilstein J. Org. Chem.* **2017**, *13*, 1907–1931.
[66] N. R. Rightmire, T. P. Hanusa, *Dalton Trans.* **2016**, *45*, 2352-2362.
[67] (a) J. Sohma, *Prog. Polym. Sci.* **1989**, *14*, 451-596; (b) P. A. May, J. S. Moore, *Chem. Soc. Rev.* **2013**, *42*, 7497-7506; (c) J. Li, C. Nagamani, J. S. Moore, *Acc. Chem. Res.* **2015**, *48*, 2181-2190.
[68] P. Balaz, M. Achimovicova, M. Balaz, P. Billik, Z. Cherkezova-Zheleva, J. M. Criado, F. Delogu, E. Dutkova, E. Gaffet, F. J. Gotor, R. Kumar, I. Mitov, T. Rojac, M. Senna, A. Streletskii, K. Wieczorek-Ciurowa, *Chem. Soc. Rev.* **2013**, *42*, 7571-7637.
[69] C. Suryanarayana, *Prog. Mater Sci.* **2001**, *46*, 1-184.
[70] (a) D. Hasa, W. Jones, *Adv. Drug Delivery Rev.* **2017**, *117*, 147-161; (b) S. Andini, A. Bolognese, D. Formisano, M. Manfra, F. Montagnaro, L. Santoro, *Chemosphere* **2012**, *88*, 548-553.
[71] (a) B. Kubias, M. J. G. Fait, R. Schlögl, in *Handbook of Heterogeneous Catalysis*, Wiley-VCH Verlag GmbH & Co. KGaA, **2008**; (b) J.-L. Do, T. Friščić, *ACS Cent. Sci.* **2017**, *3*, 13-19.
[72] (a) I. J. Lin, *J. Therm. Anal. Calorim.* **1998**, *52*, 453-461; (b) P. Baláž, L. Takacs, M. Luxová, E. Godočíková, J. Ficeriová, *Int. J. Miner. Process.* **2004**, *74*, S365-S371.
[73] T. Hirono, W. Tanikawa, G. Honda, J. Kameda, J.-i. Fukuda, T. Ishikawa, *Geophys. Res. Lett.* **2013**, *40*, 2988-2992.
[74] (a) L. Takacs, *Chem. Soc. Rev.* **2013**, *42*, 7649-7659; (b) S. L. James, C. J. Adams, C. Bolm, D. Braga, P. Collier, T. Friščić, F. Grepioni, K. D. M. Harris, G. Hyett, W. Jones, A. Krebs, J. Mack, L. Maini, A. G. Orpen, I. P. Parkin, W. C. Shearouse, J. W. Steed, D. C. Waddell, *Chem. Soc. Rev.* **2012**, *41*, 413-447; (c) S. L. James, T. Friščić, *Chem. Soc. Rev.* **2013**, *42*, 7494-7496; (d) S. L. James, T. Friščić, *Chem. Commun.* **2013**, *49*, 5349-5350; (e) A. A Gečiauskaitė, F. García, *Beilstein J. Org. Chem.* **2017**, *13*, 2068-2077.
[75] V. D. Makhaev, A. P. Borisov, L. A. Petrova, *J. Organomet. Chem.* **1999**, *590*, 222-226.
[76] (a) M. R. Fructos, T. R. Belderrain, P. de Frémont, N. M. Scott, S. P. Nolan, M. M. Díaz-Requejo, P. J. Pérez, *Angew. Chem. Int. Ed.* **2005**, *44*, 5284-5288; (b) A. Collado, A. Gomez-Suarez, A. R.

Martin, A. M. Z. Slawin, S. P. Nolan, *Chem. Commun.* **2013**, *49*, 5541-5543; (c) S. Gaillard, A. M. Z. Slawin, S. P. Nolan, *Chem. Commun.* **2010**, *46*, 2742-2744.
[77] A. Zhdanko, M. Ströbele, M. E. Maier, *Chem. Eur. J.* **2012**, *18*, 14732-14744.
[78] J. D. Egbert, A. M. Z. Slawin, S. P. Nolan, *Organometallics* **2013**, *32*, 2271-2274.
[79] J. G. Hernandez, N. A. J. Macdonald, C. Mottillo, I. S. Butler, T. Friščić, *Green Chem.* **2014**, *16*, 1087-1092.
[80] J. G. Hernandez, I. S. Butler, T. Friščić, *Chem. Sci.* **2014**, *5*, 3576-3582.
[81] P. J. Nichols, C. L. Raston, J. W. Steed, *Chem. Commun.* **2001**, 1062-1063.
[82] C. S. B. Gomes, P. T. Gomes, M. T. Duarte, *J. Organomet. Chem.* **2014**, *760*, 101-107.
[83] V. P. Balema, J. W. Wiench, M. Pruski, V. K. Pecharsky, *Chem. Commun.* **2002**, 1606-1607.
[84] J.-L. Do, C. Mottillo, D. Tan, V. Štrukil, T. Friščić, *J. Am. Chem. Soc.* **2015**, *137*, 2476-2479.
[85] V. Declerck, E. Colacino, X. Bantreil, J. Martinez, F. Lamaty, *Chem. Commun.* **2012**, *48*, 11778-11780.
[86] G. N. Hermann, P. Becker, C. Bolm, *Angew. Chem. Int. Ed.* **2015**, *54*, 7414-7417.
[87] J. G. Hernandez, C. Bolm, *Chem. Commun.* **2015**, *51*, 12582-12584.
[88] G. N. Hermann, C. Bolm, *ACS Catal.* **2017**, *7*, 4592-4596.
[89] G. N. Hermann, P. Becker, C. Bolm, *Angew. Chem. Int. Ed.* **2016**, *55*, 3781-3784.
[90] M. Juribasic, K. Uzarevic, D. Gracin, M. Curic, *Chem. Commun.* **2014**, *50*, 10287-10290.
[91] (a) D. A. Fulmer, W. C. Shearouse, S. T. Medonza, J. Mack, *Green Chem.* **2009**, *11*, 1821-1825; (b) R. Thorwirth, A. Stolle, B. Ondruschka, *Green Chem.* **2010**, *12*, 985-991.
[92] (a) F. Schneider, T. Szuppa, A. Stolle, B. Ondruschka, H. Hopf, *Green Chem.* **2009**, *11*, 1894-1899; (b) G. Cravotto, D. Garella, S. Tagliapietra, A. Stolle, Schu, S. E. S. Leonhardt, B. Ondruschka, *New J. Chem.* **2012**, *36*, 1304-1307.
[93] (a) L. Chen, B. E. Lemma, J. S. Rich, J. Mack, *Green Chem.* **2014**, *16*, 1101-1103; (b) R. Schmidt, R. Thorwirth, T. Szuppa, A. Stolle, B. Ondruschka, H. Hopf, *Chem. Eur. J.* **2011**, *17*, 8129-8138.
[94] (a) W. Su, J. Yu, Z. Li, Z. Jiang, *J. Org. Chem.* **2011**, *76*, 9144-9150; (b) J. Yu, Z. Li, K. Jia, Z. Jiang, M. Liu, W. Su, *Tetrahedron Lett.* **2013**, *54*, 2006-2009.
[95] (a) D. Tan, C. Mottillo, A. D. Katsenis, V. Štrukil, T. Friščić, *Angew. Chem. Int. Ed.* **2014**, *53*, 9321-9324; (b) D. Tan, V. Strukil, C. Mottillo, T. Friščić, *Chem. Commun.* **2014**, *50*, 5248-5250.
[96] (a) D. V. Aleksanyan, S. G. Churusova, R. R. Aysin, Z. S. Klemenkova, Y. V. Nelyubina, V. A. Kozlov, *Inorg. Chem. Commun.* **2017**, *76*, 33-35; (b) T. J. Ajayi, M. N. Pillay, W. E. van Zyl, *Phosphorus, Sulfur Silicon Relat. Elem.* **2017**, *192*, 1205-1211.
[97] N. R. Rightmire, T. P. Hanusa, A. L. Rheingold, *Organometallics* **2014**, *33*, 5952-5955.
[98] D. W. Peters, R. G. Blair, *Faraday Discuss.* **2014**, *170*, 83-91.
[99] M. Glavinović, M. Krause, L. Yang, J. A. McLeod, L. Liu, K. M. Baines, T. Friščić, J.-P. Lumb, *Sci. Adv.* **2017**, *3*.
[100] (a) K. Kalyanasundaram, *Coord. Chem. Rev.* **1982**, *46*, 159-244; (b) C. K. Prier, D. A. Rankic, D. W. C. MacMillan, *Chem. Rev.* **2013**, *113*, 5322-5363; (c) J. F. Endicott, H. B. Schlegel, M. J. Uddin, D. S. Seniveratne, *Coord. Chem. Rev.* **2002**, *229*, 95-106.
[101] J. C. Koziar, D. O. Cowan, *Acc. Chem. Res.* **1978**, *11*, 334-341.
[102] (a) P. Cintas, *Synlett* **1995**, *1995*, 1087-1096; (b) T.-P. Loh, G.-L. Chua, *Chem. Commun.* **2006**, 2739-2749.
[103] (a) U. Schneider, S. Kobayashi, *Acc. Chem. Res.* **2012**, *45*, 1331-1344; (b) H. T. Dao, U. Schneider, S. Kobayashi, *Chem. Commun.* **2011**, *47*, 692-694; (c) K. K. Chauhan, C. G. Frost, *J. Chem. Soc., Perkin Trans. 1* **2000**, 3015-3019.
[104] C. J. Allan, B. F. T. Cooper, H. J. Cowley, J. M. Rawson, C. L. B. Macdonald, *Chem. Eur. J.* **2013**, *19*, 14470-14483.

[105] A. Juris, V. Balzani, F. Barigelletti, S. Campagna, P. Belser, A. von Zelewsky, *Coord. Chem. Rev.* **1988**, *84*, 85-277.
[106] R. L. Wells, S. S. Kher, R. A. Baldwin, P. S. White, *Polyhedron* **1994**, *13*, 2731-2735.
[107] A. Gavriluta, G. E. Büchel, L. Freitag, G. Novitchi, J. B. Tommasino, E. Jeanneau, P.-S. Kuhn, L. González, V. B. Arion, D. Luneau, *Inorg. Chem.* **2013**, *52*, 6260-6272.
[108] (a) V. Rosa, C. I. M. Santos, R. Welter, G. Aullón, C. Lodeiro, T. Avilés, *Inorg. Chem.* **2010**, *49*, 8699-8708; (b) V. Rosa, T. Avilés, G. Aullon, B. Covelo, C. Lodeiro, *Inorg. Chem.* **2008**, *47*, 7734-7744.
[109] (a) I. L. Fedushkin, A. A. Skatova, V. A. Chudakova, V. K. Cherkasov, G. K. Fukin, M. A. Lopatin, *Eur. J. Inorg. Chem.* **2004**, *2004*, 388-393; (b) I. L. Fedushkin, V. A. Chudakova, A. A. Skatova, N. M. Khvoinova, Y. A. Kurskii, T. A. Glukhova, G. K. Fukin, S. Dechert, M. Hummert, H. Schumann, *Z. Anorg. Allg. Chem.* **2004**, *630*, 501-507.
[110] T. Tu, Z. Sun, W. Fang, M. Xu, Y. Zhou, *Org. Lett.* **2012**, *14*, 4250-4253.
[111] A. L. Gottumukkala, J. F. Teichert, D. Heijnen, N. Eisink, S. van Dijk, C. Ferrer, A. van den Hoogenband, A. J. Minnaard, *J. Org. Chem.* **2011**, *76*, 3498-3501.
[112] K. V. Vasudevan, A. H. Cowley, *New J. Chem.* **2011**, *35*, 2043-2046.
[113] B. R. Spencer, B. J. Kraft, C. G. Hughes, M. Pink, J. M. Zaleski, *Inorg. Chem.* **2010**, *49*, 11333-11345.
[114] N. G. Connelly, W. E. Geiger, *Chem. Rev.* **1996**, *96*, 877-910.
[115] R. A. Klein, C. J. Elsevier, F. Hartl, *Organometallics* **1997**, *16*, 1284-1291.
[116] T. Jurca, J. Lummiss, T. J. Burchell, S. I. Gorelsky, D. S. Richeson, *J. Am. Chem. Soc.* **2009**, *131*, 4608-4609.
[117] M. K. Nazeeruddin, A. Kay, I. Rodicio, R. Humphry-Baker, E. Mueller, P. Liska, N. Vlachopoulos, M. Graetzel, *J. Am. Chem. Soc.* **1993**, *115*, 6382-6390.
[118] A. Yella, H.-W. Lee, H. N. Tsao, C. Yi, A. K. Chandiran, M. K. Nazeeruddin, E. W.-G. Diau, C.-Y. Yeh, S. M. Zakeeruddin, M. Grätzel, *Science* **2011**, *334*, 629.
[119] E. I. Mayo, K. Kilsa, T. Tirrell, P. I. Djurovich, A. Tamayo, M. E. Thompson, N. S. Lewis, H. B. Gray, *Photochem. Photobiol. Sci.* **2006**, *5*, 871-873.
[120] (a) C.-F. Chang, Y.-M. Cheng, Y. Chi, Y.-C. Chiu, C.-C. Lin, G.-H. Lee, P.-T. Chou, C.-C. Chen, C.-H. Chang, C.-C. Wu, *Angew. Chem. Int. Ed.* **2008**, *47*, 4542-4545; (b) H. Sasabe, J.-i. Takamatsu, T. Motoyama, S. Watanabe, G. Wagenblast, N. Langer, O. Molt, E. Fuchs, C. Lennartz, J. Kido, *Adv. Mater.* **2010**, *22*, 5003-5007; (c) A. F. Henwood, A. K. Pal, D. B. Cordes, A. M. Z. Slawin, T. W. Rees, C. Momblona, A. Babaei, A. Pertegas, E. Orti, H. J. Bolink, E. Baranoff, E. Zysman-Colman, *J. Mater. Chem. C* **2017**, *5*, 9638-9650.
[121] (a) L. Wang, P. Cui, S. Kilina, W. Sun, *J. Phys. Chem. C* **2017**, *121*, 5719-5730; (b) F. Monti, A. Baschieri, I. Gualandi, J. J. Serrano-Pérez, J. M. Junquera-Hernández, D. Tonelli, A. Mazzanti, S. Muzzioli, S. Stagni, C. Roldan-Carmona, A. Pertegás, H. J. Bolink, E. Ortí, L. Sambri, N. Armaroli, *Inorg. Chem.* **2014**, *53*, 7709-7721; (c) Q. Zhang, Y. Li, X. Wang, L. Wang, J. Zhang, *Mater. Chem. Phys.* **2016**, *177*, 179-189; (d) E. Baranoff, S. Fantacci, F. De Angelis, X. Zhang, R. Scopelliti, M. Grätzel, M. K. Nazeeruddin, *Inorg. Chem.* **2011**, *50*, 451-462; (e) A. F. Henwood, E. Zysman-Colman, *Chem. Commun.* **2017**, *53*, 807-826.
[122] P. A. Papanikolaou, N. V. Tkachenko, *PCCP* **2013**, *15*, 13128-13136.
[123] M. W. Perkovic, J. F. Endicott, *J. Phys. Chem.* **1990**, *94*, 1217-1219.
[124] H. Masuhara, in *Photophysical and Photochemical Tools in Polymer Science: Conformation, Dynamics, Morphology* (Ed.: M. A. Winnik), Springer Netherlands, Dordrecht, **1986**, pp. 43-63.
[125] R. Berera, R. van Grondelle, J. T. M. Kennis, *Photosynth. Res.* **2009**, *101*, 105-118.
[126] L. Zhang, J. M. Cole, *ACS Appl. Mater. Interfaces* **2015**, *7*, 3427-3455.

[127] I. Fondriest Environmental, *Solar Radiation and Photosynethically Active Radiation* can be found under http://www.fondriest.com/environmental-measurements/parameters/weather/solar-radiation/ **2014**.
[128] A. T. R. Williams, S. A. Winfield, J. N. Miller, *Analyst* **1983**, *108*, 1067-1071.
[129] N. Matsuo, *Bull. Chem. Soc. Jpn.* **1974**, *47*, 767-768.
[130] A. D. McLean, G. S. Chandler, *J. Chem. Phys.* **1980**, *72*, 5639-5648.
[131] J. S. Binkley, J. A. Pople, W. J. Hehre, *J. Am. Chem. Soc.* **1980**, *102*, 939-947.
[132] (a) M. E. Casida, C. Jamorski, K. C. Casida, D. R. Salahub, *J. Chem. Phys.* **1998**, *108*, 4439-4449; (b) R. E. Stratmann, G. E. Scuseria, M. J. Frisch, *J. Chem. Phys.* **1998**, *109*, 8218-8224.
[133] (a) M. Cossi, N. Rega, G. Scalmani, V. Barone, *J. Comput. Chem.* **2003**, *24*, 669-681; (b) V. B. M. Cossi, *J. Chem. Phys.* **2001**, *115*, 4708-4717; (c) V. Barone, M. Cossi, *J. Phys. Chem. A* **1998**, *102*, 1995-2001.
[134] W. R. Browne, N. M. O'Boyle, J. J. McGarvey, J. G. Vos, *Chem. Soc. Rev.* **2005**, *34*, 641-663.
[135] A. A. Grigoriy, *ChemCraft 1.5* can be found under https://www.chemcraftprog.com.
[136] H. Gilman, W. Langham, F. W. Moore, *J. Am. Chem. Soc.* **1940**, *62*, 2327-2335.
[137] B. D. Hosangadi, R. H. Dave, *Tetrahedron Lett.* **1996**, *37*, 6375-6378.
[138] L. Ding, H.-Z. Ying, Y. Zhou, T. Lei, J. Pei, *Org. Lett.* **2010**, *12*, 5522-5525.
[139] R. J. Lundgren, M. Stradiotto, in *Ligand Design in Metal Chemistry*, John Wiley & Sons, Ltd, **2016**, pp. 1-14.
[140] (a) V. Lyaskovskyy, B. de Bruin, *ACS Catal.* **2012**, *2*, 270-279; (b) O. R. Luca, R. H. Crabtree, *Chem. Soc. Rev.* **2013**, *42*, 1440-1459.
[141] H. Yamamoto, in *Lewis Acids in Organic Synthesis*, Wiley-VCH Verlag GmbH, **2008**, pp. 1-7.
[142] A. B. Ferreira, L. C. Abiney, J. d. S. Márcio, *ISRN Renewable Energy* **2012**, *2012*, 13.
[143] (a) O. Dechy-Cabaret, B. Martin-Vaca, D. Bourissou, *Chem. Rev.* **2004**, *104*, 6147-6176; (b) Y. Nakayama, S. Kosaka, K. Yamaguchi, G. Yamazaki, R. Tanaka, T. Shiono, *J. Polym. Sci., Part A: Polym. Chem.* **2017**, *55*, 297-303.
[144] J. Guo, P. Haquette, J. Martin, K. Salim, C. M. Thomas, *Angew. Chem. Int. Ed.* **2013**, *52*, 13584-13587.
[145] (a) F. A. G. Mercier, M. Biesemans, R. Altmann, R. Willem, R. Pintelon, J. Schoukens, B. Delmond, G. Dumartin, *Organometallics* **2001**, *20*, 958-962; (b) Y. Zhang, S. Wang, Z. Xiao, T. Chen, G. Wang, *Res. Chem. Intermed.* **2016**, *42*, 7213-7222; (c) T. Toupance, L. Renard, B. Jousseaume, C. Olivier, V. Pinoie, I. Verbruggen, R. Willem, *Dalton Trans.* **2013**, *42*, 9764-9770.
[146] S. Kaihara, S. Matsumura, A. G. Mikos, J. P. Fisher, *Nat. Protoc.* **2007**, *2*, 2767.
[147] R. L. Melen, *Chem. Soc. Rev.* **2016**, *45*, 775-788.
[148] V. Naseri, R. J. Less, R. E. Mulvey, M. McPartlin, D. S. Wright, *Chem. Commun.* **2010**, *46*, 5000-5002.

Publication list

1. J. Wang, R. Ganguly, Y. X. Li, J. Díaz, H. S. Soo,* and F. García,* *Dalton Trans.*, 2016, **45**, 7941-7946.

2. J. Wang, R. Ganguly, Y. X. Li, J. Díaz, H. S. Soo,* and F. García,* *Inorg. Chem.*, 2017, **56**, 7811–7820.

3. K. Hasan, J. Wang, K. P. Amlan, H. S. Soo,* F. García,* and E. Zysman-Colman,* *Sci. Rep.*, 2017,**7**, 15520.